Involvement of RNA-based regulatory pathways in T cell – cancer cell communication

DISSERTATION

Michaela Eva Bauer

Regensburg 2023

Involvement of RNA-based regulatory pathways in T cell – cancer cell communication

DISSERTATION ZUR ERLANGUNG DES DOKTORGRADES DER NATURWISSENSCHAFTEN (DR. RER. NAT.) DER FAKULTÄT FÜR BIOLOGIE UND VORKLINISCHE MEDIZIN DER UNIVERSITÄT REGENSBURG

vorgelegt von

Michaela Eva Bauer

Aus Hutthurm

Oktober 2023

Promotionsgesuch eingereicht am: 25.10.2023

Die Arbeit wurde angeleitet von: Prof. Dr. Gunter Meister

_____

(Michaela Eva Bauer)

„Man merkt nie, was schon getan wurde,

man sieht immer nur, was noch getan werden muss“

-Marie Curie-

Contents

Declaration

Die vorgelegten Druckexemplare und die vorgelegte elektronische Version der Arbeit sind identisch. Ich habe die Arbeit selbst verfasst, keine anderen als die angegebenen Quellen und Hilfsmittel benutzt und die Arbeit nicht bereits an einer anderen Hochschule zur Erlangung eines akademischen Grades eingereicht. Weiterhin bestätige ich, dass ich von den in § 26 Abs. 6 der geltenden Prüfungsordnung vorgesehenen Rechtsfolgen Kenntnis habe.

Regensburg, den 25.10.2023

_____

Michaela Eva Bauer

1 Abstract

The cancer-immunity cycle describes a stepwise process of highly regulated events, the so-called immune checkpoints. This cycle needs to be initiated and completed for an effective anti-cancer immune response. One crucial step is the infiltration of T cells into tumours which is often prevented due to a repulsive tumour microenvironment (TME). This does not only inhibit the spontaneous killing of cancer cells but also impairs therapeutic strategies. Infiltration of T cells is mediated by endothelial adhesion molecules like ICAM-1 and integrins like LFA-1 expressed on T cells.

RNA-binding proteins (RBPs) are key factors regulating gene expression on a posttranscriptional level. The expression and activity of RBPs is often dysregulated in cancer cells. In this way, tumours utilize this regulatory machinery to adjust protein levels in a quick and stable manner. Being drivers of tumorigenesis, RBPs turned out to be promising targets for drug development to treat cancer. We hypothesize that RNA-based regulatory pathways contribute to the generation of soluble molecules secreted into the TME and therefore support the exclusion of T cells with interfering in the interaction of ICAM-1 and LFA-1.

To identify such molecules, we designed a RNAi screening approach targeting RNA-based regulatory pathways like RBPs, RNA-modifying enzymes and components of the microRNA (miRNA) pathway. For the screening experiment, the recombinant human ICAM-1 protein was purified from mammalian cells and cell adhesion assays were performed using T cells treated with cancer cell tissue culture supernatants. Especially, supernatant of the colorectal cancer cell line HCT 116 significantly reduced T cell binding to the immobilized ligand ICAM-1. The siRNA knockdown of β-catenin (CTNNB1), one of the main actors of the Wnt/ β-catenin pathway, restored T cell binding in cell adhesion assays to some extent. In a preliminary screening approach, the RNA-binding proteins PUF60 and XPO1 were identified to significantly affect T cell binding in our assays. Moreover, our results indicate that PUF60 increases CTNNB1 protein levels by inducing alternative splicing of its 3' UTR and hence reduce T cell binding to ICAM-1. By performing the complete RNAi screening, endogenous targets and target pathways leading to an enhanced T cell adhesion will be identified,

further validated and functionally characterized. These molecules will potentially serve as highly valuable targets for novel RNA-based immunotherapy in the future.

2 Zusammenfassung

Der Krebs- Immun- Zyklus beschreibt einen schrittweisen Prozess von streng regulierten Vorgängen, die so genannten Immun- Checkpoints. Dieser Zyklus muss für eine effektive Immunantwort gegen Krebs gestartet und durchgeführt werden. Einer der wesentlichen Schritte ist das Eindringen von T Zellen in Tumore, welches häufig durch eine abstoßende Mikroumgebung der Tumore blockiert wird. Dies verhindert nicht nur das initiative Töten von Krebszellen, sondern beeinträchtigt auch therapeutische Ansätze. Die Infiltration von T Zellen wird durch die Interaktion von Endothel- Adhäsionsmolekülen wie zum Beispiel ICAM-1 und Integrinen wie LFA-1, die von T Zellen exprimiert und präsentiert werden, vermittelt.

RNA Bindeproteine (RBPs) sind Hauptfaktoren, die Genexpression auf einem post-transkriptionellem Level regulieren. Die Expression und Aktivität von RBPs wird oft in Krebszellen dysreguliert. So nutzen Tumore diesen Regulationsmechanismus, um Proteinlevel in einer schnellen und beständigen Art und Weise anzupassen. Weil diese Proteine die Tumorentstehung vorantreiben, erweisen sie sich als vielversprechende Zielmoleküle für die Wirkstoffentwicklung, um Krebs zu behandeln. Wir gehen davon aus, dass auf RNA- basierende, regulatorische Signalwege zur Entstehung von löslichen Molekülen, die in die Mikroumgebung von Tumoren sekretiert werden, beitragen und somit den Ausschluss von T Zellen unterstützen, indem sie die Interaktion zwischen ICAM-1 und LFA-1 beeinträchtigen.

Um solche Moleküle zu identifizieren, haben wir einen RNAi Screening-Ansatz entwickelt, der RNA regulierende Signalwege als Zielgruppen hat, wie beispielsweise RBPs, RNA-modifizierende Enzyme und Moleküle, die in den microRNA (miRNA) Signalweg involviert sind. Für das Screening-Experiment wurde das humane Endothel-Adhäsionsmolekül ICAM-1 rekombinant aus Säugetierzellen aufgereinigt und Zell-Adhäsionsanalyse durchgeführt, in denen T Zellen, die mit den Überständen von Krebszellen aus humaner Zellkultur behandelt wurden, genutzt wurden. Insbesondere, der Überstand der Darmkrebs-Zelllinie HCT 116 verringerte die Bindung von T Zellen an den immobilisierten Liganden ICAM-1 signifikant. Der siRNA Knockdown von β-Catenin (CTNNB1), einer der Hauptfaktoren des Wnt/ β-Catenin Signalweges, stellte T Zellbindung in Zell-Adhäsionsanalysen zum Teil wieder her. In

einem vorläufigen Screening-Versuch wurden die RNA Bindeproteine PUF60 und XPO1 als Faktoren identifiziert, die T Zellbindung in unseren Analysen signifikant beeinflussen. Zudem deuten unsere Ergebnisse darauf hin, dass PUF60 das Proteinlevel von CTNNB1 hochreguliert, indem alternatives Splicing der CTNNB1 3‘ UTR induziert und als Folge dessen T Zellbindung an ICAM-1 herunter reguliert wird. Durch die Durchführung des kompletten RNAi Screenings, werden endogene Zielgene und Signalwege, die zu einer erhöhten T Zelladhäsion führen, identifiziert, weiter validiert und funktionell charakterisiert werden. Diese Moleküle werden potenziell als sehr wertvolle Zielgene dienen, um in der Zukunft neuartige RNA-basierende Immuntherapie zu entwickeln.

3 Introduction

3.1 Cancer and Immunity

Tumour immunology combines the fields of oncology and immunology. It describes the close connection of the immune system, especially the local immune landscape in the tumour microenvironment (TME), and the progression and control of cancer (Galon and Bruni 2020; Hiam-Galvez et al. 2021). Over the past decades, researchers achieved great innovations in the so-called cancer immunotherapy, which is modifying and utilizing the endogenous immune system for the treatment of cancer (Oiseth and Aziz 2017). For the great progress of cancer immunotherapy in the last years, the understanding of the basic molecular mechanisms of tumour immunology has been essential enabling the specific activation of the immune system for therapeutic usage (Mellman et al. 2011; Ribas and Wolchok 2018).

3.1.1 The cancer-immunity cycle and the regulation of immune checkpoints

The activation of the immune system and the killing of cancer cells by effector T cells are just two of seven steps needed for an effective anti-cancer immune response. The cancer-immunity cycle summarises the stepwise events, which have to be initiated and allowed to progress and develop for a successful elimination of cancer cells (**Figure 3-1**) (Chen and Mellman 2013).

Firstly, oncogenesis generates neoantigens, which are released and taken up by dendritic cells (DCs) (**step 1**). While migrating to the lymph nodes, DCs maturate to antigen-presenting cells (APCs) which process these antigens and present them on major histocompatibility complex (MHC) class I and class II molecules (**step 2**). This induces the priming and activation of tumour-specific effector T cells (**step 3**) in the lymph nodes. The activated effector cells migrate (**step 4**) and infiltrate the tumour (**step 5**) where they are able to specifically recognize and bind cancer cells by their T cell receptors (TCRs) (**step 6**). After killing the target cell, new antigens are released which restart the cycle and further enhance the immune response (**step 7**) (Chen and Mellman 2013; Pio et al. 2019). Each step of the cancer-immunity cycle, the so-called immune checkpoints (ICPs), are highly regulated by immunostimulatory (**Figure 3-1**,

green) and immunosuppressive factors (**Figure 3-1**, **red**). Tumours are certainly able to intervene at almost every step and thereby deregulate and diminish an effective immune response (Motz and Coukos 2013).

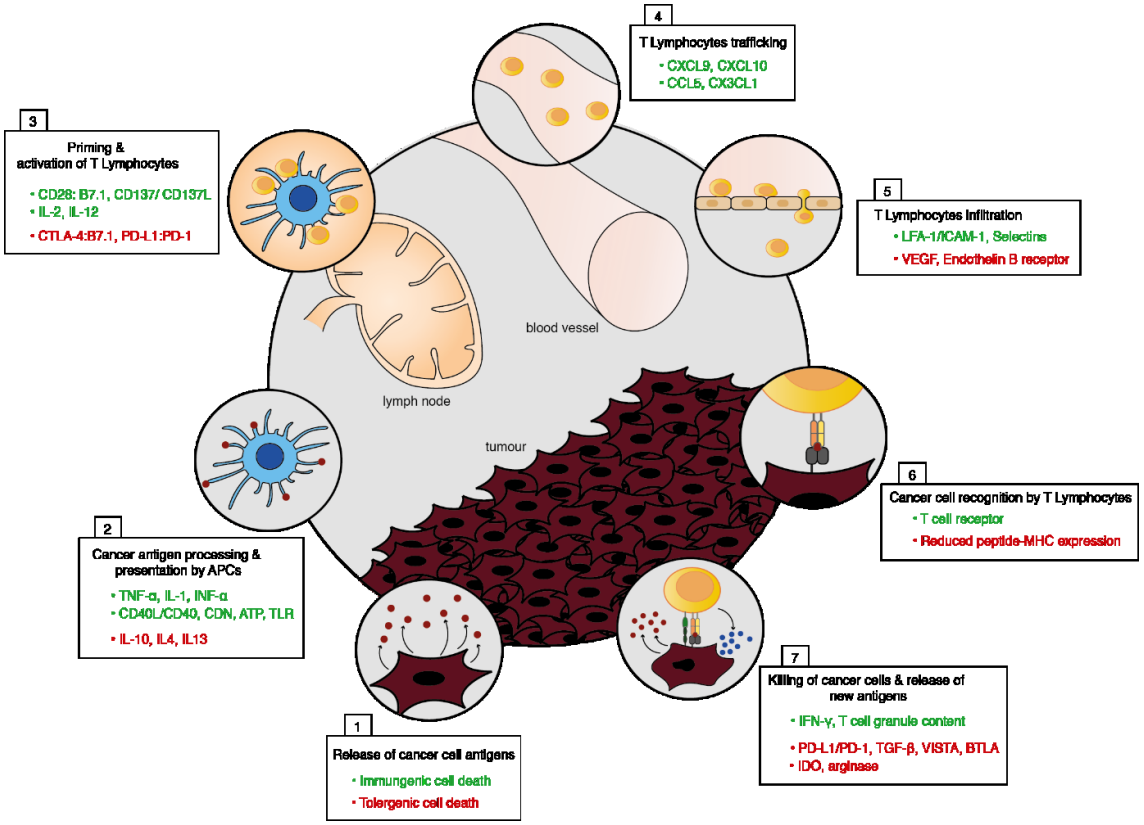

Figure 3-1: The cancer-immunity cycle. *To generate immunity and an effective anti-cancer immune response, a cyclic process of different steps is initiated and leads to T cell response. After releasing cancer cell specific antigens (**1**), these neoantigens are captured by dendritic cells and presented on MHCI or MHCII molecules (**2**) which leads to the priming and activation of effector T lymphocytes in the lymph nodes (**3**). The activated T lymphocytes traffic to the tumour bed (**4**), infiltrate it (**5**), precisely recognize and bind to cancer cells (**6**) and kill their target (**7**). The single steps of the cycle are highly regulated by immunosuppressive (**red**) and immunostimulatory (**green**) factors (modified from Chen and Mellman 2013).*

The goal of cancer immunotherapy is the specific targeting and blocking of immunosuppressive factors and the activation of immunostimulatory factors at certain immune checkpoints to enhance an effective anti-cancer immune response (Shi et al. 2018). Until now, the most promising immunotherapy approaches are immune checkpoint inhibitors, chimeric antigen receptor T cells (CAR-T) and bispecific antibodies (Yi et al. 2018; Zhou et al. 2022; Wu et al. 2021). Well-known examples of immune checkpoint molecules are the programmed cell death 1 (PD-1) and the cytotoxic T lymphocyte-associated protein 4 (CTLA-4), which were already

discovered in the 1990s (Ishida et al. 1992; Krummel and Allison 1995). The PD-1 and CTLA-4 receptors are expressed on T cells. Upon activation, both receptors bind to their corresponding ligands (PD-1 ligands: PD-L1 or PD-L2; CTLA-4 ligands: CD80 and CD86) and induce inhibitory effects on T cell response. In the absence of malignancy, they prevent autoimmunity and support immune tolerance. Cancer cells utilize these functions to suppress T cell response and support tumour growth (Martins et al. 2019). Using antibodies against these targets resulted in great therapeutic relevance, either alone or in combination (Farkona et al. 2016; Ribas and Wolchok 2018). The work on these two factors was honoured with the Nobel prize in physiology and medicine in 2018 (Smyth and Teng 2018). However, the field of identifying new immune checkpoint molecules with therapeutic potential is growing ever since (Qin et al. 2019). Although the outstanding achievements of cancer immunotherapy so far, there are still a lot of limitations, which need to be addressed and overcome. One challenge is the absence of active T cells in the tumour microenvironment, the so-called "cold tumours". In contrast to "hot tumours", which are highly infiltrated with immune cells, cold tumours lack effector immune cells in the tumour microenvironment causing low response rates or at all resistance to cancer immunotherapy (Bonaventura et al. 2019). The challenges and characteristics of the different tumour types are described in more detail in the next chapter.

3.1.2 Challenges of immunotherapy - cold versus hot tumours

As already stated above, cancer immunotherapy has emerged and grown rapidly in the last years and is now already considered the "fifth pillar" of cancer therapy besides surgery, radiation, chemotherapy and targeted therapy (Oiseth and Aziz 2017). But the success of immunotherapy, especially of immune checkpoint inhibitors (ICIs), highly depends on the infiltration of activated T cells which are able to induce killing of cancer cells. Therefore, the distribution, density and diversity of immune cells in the tumour microenvironment is the key characteristic dividing tumours in three different categories: the immune-desert, the immune-excluded and the immune-inflamed phenotype (**Figure 3-2**) (Liu and Sun 2021; Duan et al. 2020). These categories were first described in studies by Camus et al. in primary colorectal cancer

cells where the importance of the balance between tumour escape and immune coordination was emphasized (Camus et al. 2009).

The immune-inflamed phenotype, the so-called “hot tumour”, shows a pre-existing immune response, high rates of immune cell infiltration along with an increase in interferon-γ (IFN-γ) signalling induced by a high density of cytotoxic T cells modulating immune response. Moreover, they are characterized by the expression of the PD-1 ligand PD-L1 in infiltrating immune cells, genomic instability and therefore high tumour mutational burden (TMB) (**Figure 3-2**, **right**). Based on these specific features, hot tumours are likely to respond well when treated with immune checkpoint inhibitors (Herbst et al. 2014; Hegde et al. 2016). The other two phenotypes are referred to as “cold tumours”. In the immune-excluded phenotype, T cells are prevented from efficient infiltration and are only able to gather in the tumour stroma and at the invasion margins which are surrounding tumour cells and keeping immune cells in distance (**Figure 3-2**, **middle**). Other specific features are myeloid inflammation, angiogenesis and high transforming growth factor β (TGFβ) signalling (Mariathasan et al. 2018; Galon and Bruni 2019).

In contrast to this, in immune-desert tumours immune infiltration is almost completely prevented and no T cells are found in the tumour or its surrounding (**Figure 3-2, left**). Moreover, they are characterized by immunological ignorance due to low PD-L1 expression, reduced antigen presentation based on low MHC class I expression, the presence of immunosuppressive cell populations like T-regulatory cells (Tregs), myeloid-derived suppressor cells (MDSCs) and a low tumour mutational burden indicating genomic stability (Hegde and Chen 2020). Because of the non-inflamed state of cold tumours the immunological treatment is a great challenge and immune checkpoint inhibitor monotherapy is barely effective (Hegde et al. 2016; Hegde and Chen 2020; Church and Galon 2017). Thus, turning cold into hot tumours is a major goal in immunotherapy.

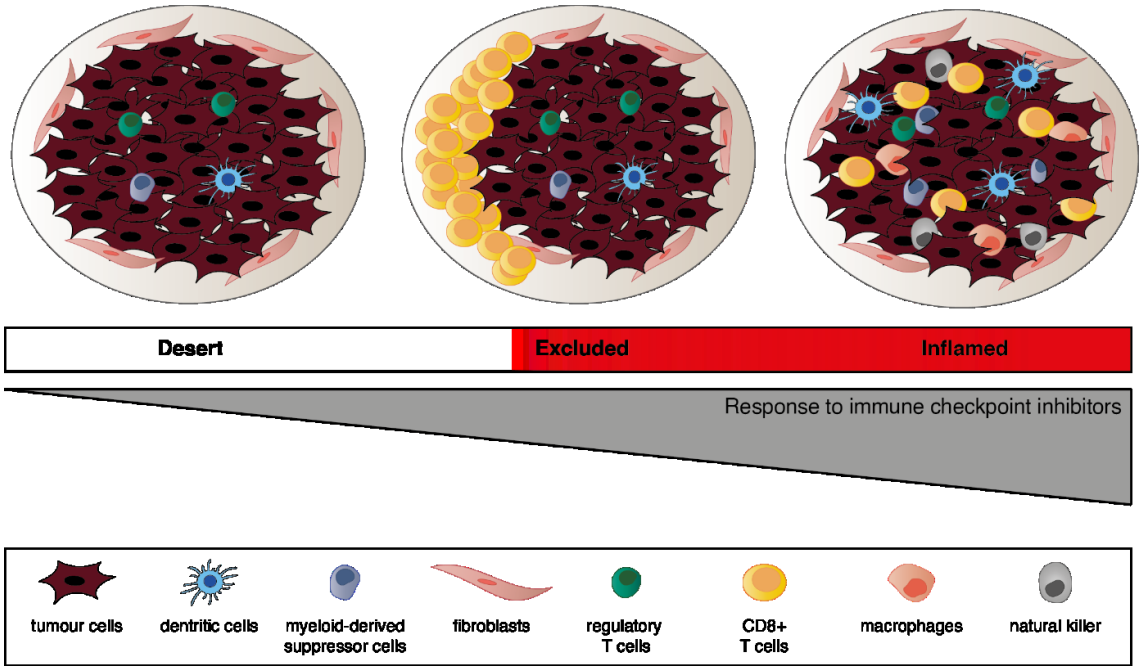

Figure 3-2: The three different tumour immunophenotypes. *Based on the distribution of cytotoxic immune cells in the TME, tumours can be characterized in three different immunophenotypes: (**Left**) The immune-desert phenotype shows no immune cells in the TME or the surroundings. (**Middle**) In the immune-excluded type, infiltration is still prevented although activated immune cells accumulate around the tumour. (**Right**) The immune-inflamed phenotype is highly infiltrated with immune cells, but their effects are inhibited by immune suppressors. In correlation with the gradient of T cell distribution, the response rate to ICIs is increasing with the number of infiltrated immune cells (modified from Liu and Sun 2021).*

Current research focuses on boosting immunotherapy approaches by moving from monotherapy towards combined strategies. The combination of approved immune checkpoint inhibitors with the conversion of cold tumours into hot tumours, could enhance the immune response against cancer and have great clinical benefit. To be able to turn the immune-desert or -excluded phenotype into an immune-inflamed tumour, it is crucial to understand the mechanism and signalling pathways leading to T cell exclusion (Wei et al. 2022). Some examples of such pathways will be described in the following chapter.

3.1.3 Immune regulatory signalling pathways supporting T cell exclusion from tumours

In the cancer-immunity cycle, the step of T cell infiltration is crucial for the success of currently approved immunotherapy approaches (**3.1.1**). The two major mechanisms of tumour immune escape are on the one hand the decreased infiltration and reduced function of activated immune cells and on the other hand the increased presence of immunosuppressive cells in the tumour microenvironment. These mechanisms are thought to be the result of the differential activation of distinct oncogenic pathways. Therefore, the identification and understanding of these pathways are essential for further development and extension of cancer immunotherapy (reviewed in (Spranger and Gajewski 2016); (Yang et al. 2019).

Migration and infiltration of immune cells is dependent on gradients of secreted molecules, so-called chemokines, which function as chemoattractants. This directed cell migration is also known as chemotaxis (Kohli et al. 2021). Immune activating cell types support the immune response and are guided by anti-tumorigenic chemokines. Examples for these cell types are cytotoxic T cells ($CD8^+$), natural killer cells (NK) and dendritic cells (DCs; $CD103^+$). In contrast, the migration of immune suppressive types, for example tumour-associated macrophages and MDSCs, is mediated by pro-tumorigenic chemokines and support tumour escape and progression (Kohli et al. 2021; Aleksandra J. Ozga et al. 2021).

The differential expression of chemokines and activation of distinct oncogenic signalling pathways in tumours are closely connected with each other. Some examples of signalling mechanisms and their effects are explained in more detailed in the following (**Figure 3-3**; **Table 3-1**).

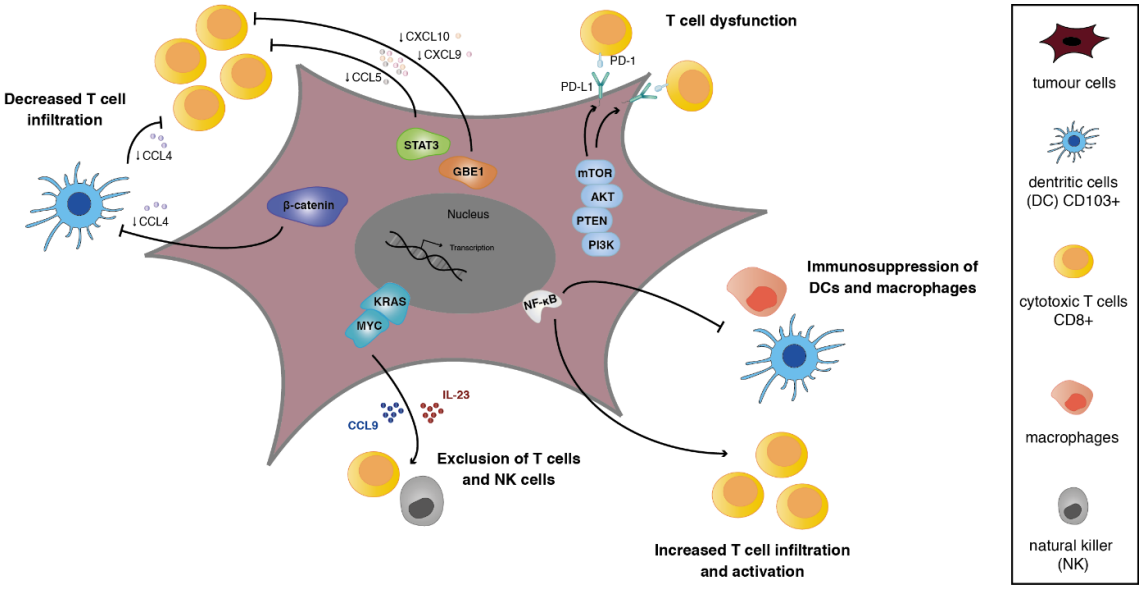

Figure 3-3: Immune regulatory pathways supporting T cell exclusion from tumours. *Oncogenic signalling pathways are activated in the tumour microenvironment, like β-catenin, STAT3, NF-κB, KRAS and PI3K/PTEN/AKT/mTOR. These do not only decrease chemokine production which leads to reduced immune cell infiltration, but are also able to induce T cell dysfunction by for example increased PD-L1 expression (modified from Yang et al. 2019).*

Table 3-1*: Overview of different oncogenic signalling pathways involved in tumour immune escape*

Signalling	Affected target/ chemokine	tumorigenic	Effect
β-catenin	ATF3	pro-	High levels of the ATF3 reduce transcription of CCL4
	CCL4	anti-	Reduced levels lead to reduced recruitment of dendritic cells

	CXCL10/11	anti-	Reduced levels cause lower T cell infiltration
STAT3	CCL5 (RANTES) CXCL10 (IP-10)	anti- anti-	Reduced levels lead to less T cell infiltration
NF-κB	TNFα IL-1	pro- por-	High levels support tumour progression and cell proliferation
	IL-6 IL-8	por- por-	High levels cause suppression of immune activating dendritic cells and macrophages
	CXCL10/11	anti-	High levels increase T cell infiltration and activation
PI3K/PTEN/AKT/mTOR	PD-L1	pro-	High levels of surface molecule PD-L1 cause dysfunction of T cells
GBE1	CCL5 CXCL10	anti- anti-	Reduced levels lead to less T cell infiltration
KRAS/MYC	CCL9 IL-23	pro- por-	High levels cause exclusion of T cells and natural killer cells

3.1.3.1 The Wnt/β-catenin signalling pathway

A first example of an oncogenic driver inducing T cell exclusion is the Wnt/β-catenin signalling pathway (**Figure 3-3**). In both, colorectal cancer and melanoma, studies showed that an upregulation of this pathway correlates with a non-T cell-inflamed phenotype (Xue et al. 2019; Spranger et al. 2015). The activation of this pathway leads to an increase in the expression of the transcription repressor ATF3, which then blocks transcription of the CC-chemokine ligand 4 (CCL4). CCL4 functions as chemoattractant for immune activating dendritic cells. Based on the reduced levels of CCL4 and hence decreased recruitment of dendritic cells, activation of cytotoxic T cells is diminished. Moreover, by RNAi knockdown of CTNNB1 (β-catenin), not only the CCL4 expression is increased but also the total number of immune activating cells, like cytotoxic T cells and dendritic cells, together with the PD-1 T cell checkpoint expression. The same study showed additionally that knockdown of CTNNB1 is linked to increased expression of the CXC-chemokine (CXC) ligands CXCL10 and CXCL11 in a NF-κB dependent manner (Ganesh et al. 2018). Both chemokines regulate the migration of cytotoxic T cells and natural killer (NK) cells which are essential for an effective immune response (Kohli et al. 2021). Moreover, it is postulated that the oncogenic function of CTNNB1 is caused by alternative splicing of its 3' UTR (Chan et al. 2022), which will be described in more detail later on (**3.2.2.2**). All in all, it can be hypothesized that the combined targeting of β-catenin signalling together with anti-PD-1 or anti-CTLA-4 checkpoint blockade could enhance the response rates to cancer immunotherapy and is worth further investigations.

3.1.3.2 The STAT3 signalling pathway

Another essential oncogenic pathway involved in T cell exclusion is the signal transducer and activator of transcription 3 (STAT3) signalling (**Figure 3-3**). In the cytoplasm, STAT3 functions as signal transducer and in the nucleus as transcription factor. There, it is involved in the regulation of genes essential for tumour proliferation, survival, angiogenesis and invasion (Yu et al. 2009). An important activator of STAT3 expression is the pro-tumorigenic cytokine interleukin 6 (IL-6), which is known to promote tumorigenesis - similar to STAT3 - via the regulation of apoptosis, survival, proliferation and angiogenesis (Yang et al. 2007; Kumari et al.

2016). Several studies have shown a close connection of STAT3 levels with reduced expression of proinflammatory mediators (Yu et al. 2009). Active STAT3 signalling in tumours was found to downregulate T cell infiltration and actual T cell number (Wang et al. 2004; Burdelya et al. 2005). By inhibition of STAT3, the expression of critical cell proliferation and survival genes in tumours is downregulated. Whereas the levels of essential chemokines like CCL5 (RANTES) and CXCL10 (IP-10) are increased. Both, CCL5 and CXCL10 are important chemoattractants for immune activating cell types like effector T cells and natural killer cells (Burdelya et al. 2005). Moreover, Ihara et al. found that in STAT3 knockout mice urethane-induced tumorigenesis was reduced. At the same time, antitumour inflammation and natural killer cell immunity was increased. These effects were linked on the one hand to an increased proinflammatory chemokine production of for instance CCL5 and CXCL10. On the other hand, higher sensitivity to NK cell-mediated cytotoxicity was explained by the downregulation of antigen presenting molecules (MHC class I) expressed on tumour cells. These surface molecules on malignant cells are known to be specifically targeted by natural killer cells (Dunn et al. 2002; Ihara et al. 2012).

3.1.3.3 Other important oncogenic signalling pathways

Besides the already described signalling pathways, the effect of T cell exclusion can also be dependent on many others (**Figure 3-3**).

The NF-κB (κ-light chain of enhancer-activated B cells) signalling pathway shows variable effects in cancer, dependent on the cellular context. The activation of NF-κB is upregulated in most cancers leading to high levels of proinflammatory cytokines like TNFα, IL-1, IL-6 and IL-8 in the tumour microenvironment, which are known to play a crucial role in tumour progression and tumour cell proliferation. Additionally, IL-6 and IL-8 may induce immunosuppression of dendritic cells and macrophages. On the contrary, activation of NF-κB signalling shows tumour-suppressing functions by increasing the production of chemokines, which are able to recruit activated T cells to the tumour microenvironment (Zhang et al. 2021).

Besides NF-κB, the PI3K/PTEN/AKT/mTOR signalling was also found to negatively regulate T cell function by reducing T cell infiltration. The upregulation of PD-L1

expression, which is known to be an immunosuppressive factor causing T cell exhausting (Martins et al. 2019), indicates immune escape mechanisms (Xu et al. 2014; Mittendorf et al. 2014).

Similar to STAT3, also the glycogen branching enzyme (GBE1) was shown to be involved in downregulating expression of anti-tumorigenic chemokines CCL5 and CXCL10, and thereby reducing T cell infiltration into the tumour microenvironment (Li et al. 2019a).

Lastly, the oncogenes KRAS and MYC are co-activated and cause elevated levels of pro-tumorigenic cytokines CCL9 and IL-23 in the tumour microenvironment, which are known to exclude immune activating cells, especially effector T cells and natural killer cells from tumours (Kortlever et al. 2017).

In summary, targeting oncogenic signalling pathways in the tumour is a promising approach to improve cancer therapy success rates. Because the absence of activated T cells in the tumour microenvironment is still a major challenge of currently approved cancer immunotherapy approaches, cold tumours are less likely to respond to these treatments. By increasing the infiltration of T cells via targeting the before explained oncogenic pathways, cold tumours could be converted into hot ones. In these immune checkpoint inhibitors for example are already well working. Oncogenic pathway blockade can be performed for example by targeting RNAs or by using RNA-based approaches such as antisense RNA (RNAi). “RNA therapeutics” is an extremely fast-growing field with promising observations and will be described in detail below.

3.2 RNA-targeting therapy and RNA therapeutics

Most current therapies are focused on small-molecule-based targeting agents against proteins and particularly enzymes and receptors that bind lipids with high specificity. These were thought to be the only promising cellular targets. The term “druggable genome” was introduced to summarize exactly this subset of the human genome able to be targeted by small chemical compounds. This assumption was limiting therapy to only 10-14 % of druggable proteins with active binding sites for small-molecule drugs. These binding sites of the proteins correspond to the ligand binding sites of endogenous small molecules. The drug has to compete with these for binding to

guarantee successful treatment outcomes (Hopkins and Groom 2002). Missing such binding sites, a major part of the human genome was thought to be "undruggable". In the last years, research rapidly progressed and developed new approaches to overcome these limitations. Essential breakthroughs were first the approval of recombinant proteins, peptides or drug-antibody conjugates (Mullard 2020). These conjugates are composed of monoclonal antibodies covalently bound to small molecule drugs and are mostly used for treating cancer (Pettinato 2021). Secondly, in May 2019 the first DNA-based therapeutic Zolgensma was approved for the treatment of spinal muscular atrophy (Malone et al. 2019). DNA drugs are used in gene therapy to treat disease either by transferring nucleic acids to patient cells to generate therapeutic proteins or by correcting defective genes via gene editing (Kumar et al. 2016). Further on, the usage of RNAs as drugs revolutionized the treatment possibilities in the clinic. RNA-based therapeutics opened the way for personalized treatments by being able to alter and adapt sequences rapidly based on the intended use. Moreover, they expanded the subset of the druggable genome by the ability to now also target proteins, transcripts and genes which were considered undruggable so far (Damase et al. 2021). Therefore, the developed strategies and promising targets of RNA-based drugs are described in more detail below.

3.2.1 Development and application of RNA therapeutics

The growing field of RNA therapeutics can be divided in two different approaches (**Figure 3-4**). It started with the development of antisense RNAs (RNAi) which are able to recognize and hybridize with endogenous target RNAs via complementary sequences and therefore change expression patterns. This approach can again be divided in using antisense oligonucleotides (ASO) which were already introduced in the 1980s (Stephenson and Zamecnik 1978) or silencing RNAs (siRNAs) (Elbashir et al. 2001) or microRNAs (miRNAs) (Lee et al. 1993) identified two decades later (**Figure 3-4 A** and **B**).

The second approach was developed approximately ten years later and is using messenger RNAs (mRNAs), which encode and express certain proteins for example to

replace defect ones or to produce antigens for vaccination (Sahin et al. 2014) (**Figure 3-4 C**).

The different classes of RNA-based therapy are further explained below.

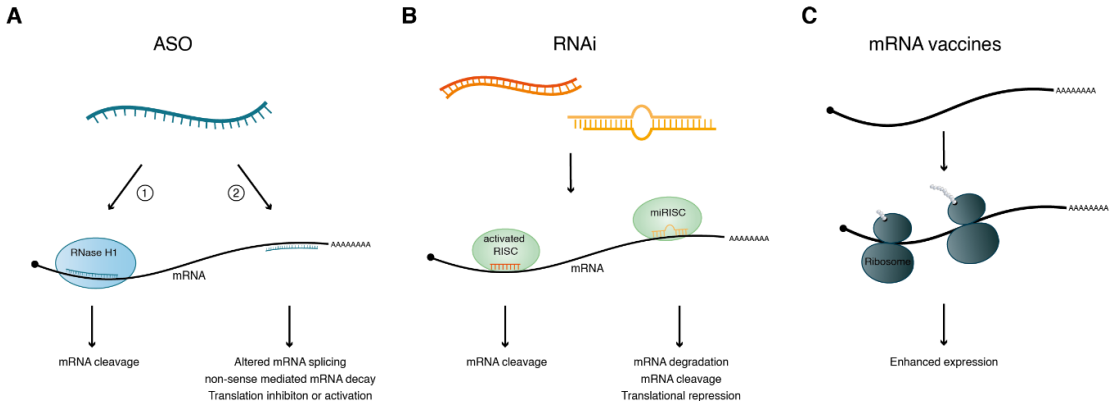

Figure 3-4: Overview of common RNA-based therapeutics. *The field of RNA-based therapeutics can be divided in three subclasses. (**A**) Antisense oligonucleotides (ASO) modulate their target expression either in an occupancy-mediated way introducing target cleavage by RNaseH1 or ribozymes (**1**). Or ASOs act in an occupancy-only mechanism (**2**). In this case, instead of degrading the target, they cause altered splicing events, non-sense mediated mRNA decay (NMD) or translation inhibition or activation. (**B**) RNAi-mediated therapeutics are based on long, double-stranded RNAs (dsRNAs, **orange**) or precursor miRNAs (**yellow**) which are fully processed, and the antisense strand (indicated in lighter colours) is loaded into the RNA-induced silencing complex (RISC) introducing RNA cleavage followed by degradation or translational repression. (**C**) mRNA vaccines are delivered by lipid nanoparticles (LNPs) and released into the cytoplasm. There, the mRNA gets translated by the ribosomes to antigen proteins which then support the endogenous immune system by priming and activating effector T cells and B cells.*

3.2.1.1 Antisense oligonucleotides (ASOs)

ASOs are synthetic, short, single-stranded (ss) oligonucleotides (DNA or RNA) with a length of 12 – 24 nucleotides (nt) which recognize target RNAs via base-complementarity and bind by Watson-Crick base-pairing. After binding, ASOs alter their targets and are able to reduce, modify or restore protein expression (Crooke et al. 2021). Many medicinal chemistry efforts were taken to introduce drug properties. Most effective were modifications in the phosphodiester backbone and the 2' position in the sugar. These modifications are supposed to achieve enhanced target binding of ASOs, increased resistance to degradation by nucleases, reduced pro-inflammatory effects and improved pharmacokinetic features and most importantly an optimized induced response after target binding (Bennett et al. 2017). ASOs function in two

different mechanisms (**Figure 3-4 A**). Firstly, downregulation of the target transcripts is induced by the cleavage at the ASO binding site mediated by specific enzymes. Examples are RNase H1 or ribozymes, which are able to cleave RNA/DNA hybrids (Liang et al. 2017; Mulhbacher et al. 2010). Secondly, in contrast to this, up- or downregulation of target transcripts is achieved without the help of specific enzymes. In this way, altered splicing or splice switching can be introduced leading to exon skipping or inclusion. Moreover, ASOs can bind to pre-mRNAs and introduce a premature termination codon resulting in non-sense mediated mRNA decay (NMD) or modulate polyadenylation sites. Additionally, target binding can result in activation or inhibition of translation (Crooke et al. 2021).

Until now, three ASOs are approved by the US Food and Drug Administration (FDA) and one other (Eteplirsen) is cleared for the therapeutic use in Europe. Nusinersen, Inotersen and Volanesorsen were developed by Ionis Pharmaceuticals and are used for the treatment of different diseases. Nusinersen is used against spinal muscular atrophy (SMA) caused by the mutation or deletion of the survival motor neuron 1 gene (SMN1) (Neil and Bisaccia 2019). Inotersen is applied for the treatment of familial amyloid polyneuropathy which is resulting from a mutation in the transthyretin (TTR) gene (Mathew and Wang 2019). The third one, Volanesorsen, was recently approved in Europe and targets the apolipoprotein CIII which causes the familial chylomicronemia syndrome when it is expressed in high levels (Paik and Duggan 2019). Lastly, the therapeutic Eteplirsen was generated by Sarpeta Therapeutics and is applied in the treatment of Duchenne muscular dystrophy (DMD) where a premature stop codon in the DMD gene produces a non-functional protein (Lim et al. 2017).

3.2.1.2 RNA interference (RNAi)

When the mechanism of RNAi was discovered in the late 1990s (Fire et al. 1998), the basis for novel RNA-utilizing therapies was established. Compared to other antisense-based strategies, RNAi as therapeutic approach benefits from using the cellular machinery which leads to efficient targeting of complementary sequences and thereby downregulating and silencing gene expression (Traber and Yu 2023; Meister

and Tuschl 2004). RNAi can function by using noncoding RNAs (ncRNAs) like small interfering RNAs (siRNAs) which are highly specific to one mRNA target or by miRNAs which can bind to multiple targets (Lam et al. 2015) (**Figure 3-4 B**).

In many organisms, siRNAs originate from long double-stranded RNAs (precursor siRNAs) which range from 30 – 100 bp in size. There, siRNAs are transcribed, but they can also be artificially introduced (**Figure 3-5**, **left**) (Lam et al. 2015). After processing by the specialized ribonuclease (RNase) III-like enzyme Dicer, the 20-30 bp long RNA duplex contains a two nucleotide 3' overhang. This siRNA duplex consists of a sense (passenger) strand and an antisense (guide) strand. After binding of the siRNA to the RNA-induced silencing complex (RISC), the passenger strand is cleaved and degraded by the RISC component Argonaute 2 (Ago2), which is an endonuclease, while the guide strand remains bound. Subsequently, the now "loaded" RISC is guided to fully complementary regions in the 3' untranslated regions (3'UTR) of target mRNAs, where Ago2 cleaves sequence-specifically (Martinez et al. 2002; Meister et al. 2004).

On the other hand, miRNAs are encoded in the genome individually or as clusters and are transcribed as Polymerase II (Pol II) transcripts (**Figure 3-5, right**). These primary miRNAs (pri-miRNAs) contain a 5' cap, are 3' polyadenylated and form stem-loop structures (Lee et al. 2004). These nuclear pri-miRNAs are processed into precursor miRNAs (pre-miRNAs) by the so-called microprocessor complex consisting of the RNase III enzyme Drosha, the dsRNA-binding protein DiGeorge critical region 8 (DGCR8) and several auxiliary factors (Lee et al. 2003; Gregory et al. 2004). The single pre-miRNA hairpins are then exported to the cytoplasm by Exportin 5 (Bohnsack et al. 2004). There, they are further processed as already described for siRNAs. In short, the pre-miRNAs are cleaved by a second RNase III-like enzyme Dicer into 20-25 nt long dsRNAs which have a two nucleotide 3' overhang and are loaded into RISC, where the Ago2 protein selects the guide strand and discards the passenger strand (Treiber et al. 2019). The loaded miRISC is then guided to target mRNAs, where it binds via partial complementarity of the miRNA to the target. Binding occurs usually between the 3' UTR of the mRNA and the bases at position 2-7 of the 5' end of the miRNA, the so-called miRNA seed (Ha and Kim 2014).

Gene silencing by miRISC can be induced in different ways (Gebert and MacRae 2019). Translational repression can be initiated via inhibiting the initiation step (Fukao et al. 2014). mRNA decay can be induced through the interaction with glycine-tryptophan protein of 182 kDa (GW182) proteins which mediate deadenylation followed by decapping (Meister et al. 2005; Rehwinkel et al. 2005). Lastly, based on full base complementarity, miRISC can directly cleave target mRNAs via the endonuclease activity of Ago2 (Meister et al. 2004).

The function of siRNAs and miRNAs to specifically downregulate gene expression of multiple mRNA targets has high therapeutic potential based on the fact, that many diseases arise from expression of undesired or mutated genes or by overexpression of normal genes (Lam et al. 2015). Although unmodified siRNAs can induce gene silencing, siRNA drugs are highly chemically modified. This ensures the suppression of immunostimulatory siRNA-derived activation of the innate immune response, it improves the chemical stability and efficacy and decreases off-target induced toxicity (Khvorova and Watts 2017).

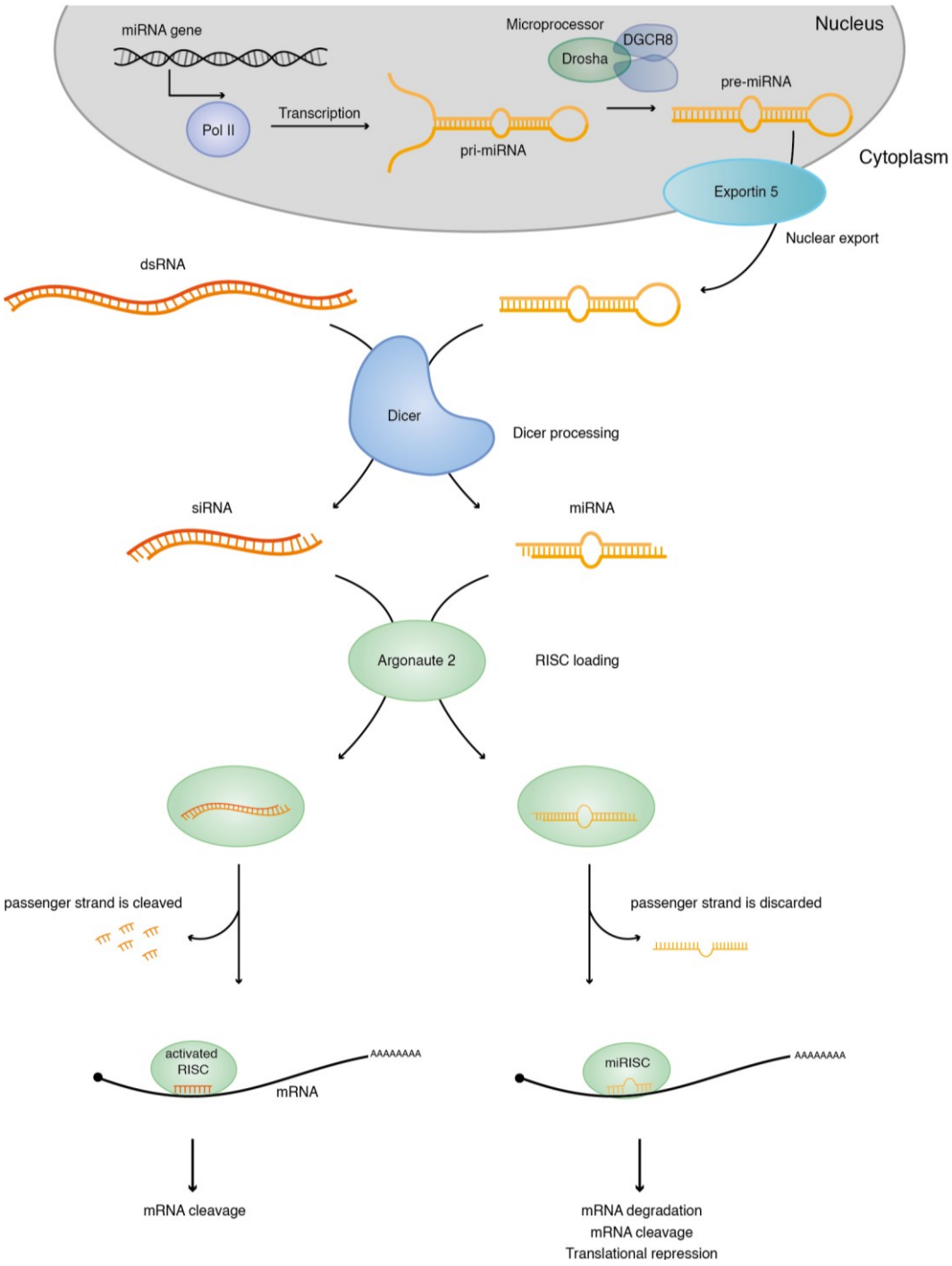

Figure 3-5: siRNA and miRNA biogenesis and mechanism. ***(Left)*** *siRNAs originate from long dsRNAs (transcribed or artificially introduced) and are processed by Dicer into siRNAs. siRNAs are loaded into Argonaute 2 (Ago2) building the activated RISC. Ago2 cleaves the passenger strand and RISC is guided by the bound guide RNA to the mRNA target which is then cleaved and degraded. (**Right**) miRNAs are transcribed by Polymerase II (Pol II) in the nucleus. These pri-miRNAs are processed by the microprocessor complex Drosha and DGCR8 into pre-miRNAs which are exported to the cytoplasm by Exportin 5. There, Dicer further processes the pre-miRNA and mature miRNAs are loaded into RISC in which Argonaute 2 selects the guide strand and discards the passenger strand. Binding the target mRNA, the miRISC induces translational repression, RNA cleavage and degradation (modified from Lam et al. 2015).*

Although siRNAs and miRNAs are very similar, the therapeutic approaches differ. In the case of siRNAs, RNAi is initiated to inhibit the expression of one specific mRNA (Behlke 2006). On the other hand, miRNA-based therapy is focused on miRNA inhibition or replacement. Inhibition is induced by synthetic miRNA antagonists (antagomirs) to block endogenous miRNA function (van Rooij et al. 2012). Replacement is mediated by synthetic miRNAs mimicking endogenous miRNA function (Bader et al. 2010).

So far, four siRNA drugs are approved by the FDA of which three were generated by Alnylam Pharmaceuticals. The first one, Patisiran (Onpattro) is used for the treatment of polyneuropathy in adult patients which is caused by hereditary transthyretin-mediated amyloidosis (Kristen et al. 2019). Secondly, Givosiran (Givlaari) is applied for treating acute hepatic porphyria which is induced by high levels of neurotoxic intermediates (Syed 2021). The third one, Lumasiran is used for the treatment of primary hyperoxaluria type 1 which is a rare autosomal recessive disorder occurring when the levels of the alanine-glycolate aminotransferase are decreased (Garrelfs et al. 2021). The last and most recently approved siRNA drug Inclisiran was developed by Novartis and is used for the treatment of homozygous familial hypercholesterolemia and elevated low-density lipoprotein cholesterol (LDL-C) (Dyrbuś et al. 2020).

Besides these approved siRNA therapeutics, several other potential candidates are already in early or late-stage clinical trials. One example would be Vutrisiran which is momentarily in phase III clinical trials. It was also developed by Alnylam Pharmaceuticals and has the same application as patisiran treating hereditary transthyretin-mediated amyloidosis. The difference between these two siRNA drugs is that vutrisiran is designed with enhanced stabilization chemistry and the third-generation siRNA delivery platform of Alnylam (Habtemariam et al. 2021). These optimizations are essential to enhance potency and activity in tissues other than the liver which was generally targeted based on the until then available of delivery systems (Smith et al. 2022).

As stated above, the use of miRNAs in the clinic, is divided into two categories. miRNA mimics are dsRNAs which mimic mature sequences of particular miRNAs to increase their abundance. On the other hand, miRNA inhibitors are ssRNA oligos, so-called

antagomirs, designed to inhibit miRNA function by preventing target binding (Crooke et al. 2018). So far, no miRNA therapeutics are officially approved, but several are tested in clinical trials for several disease types including anti-cancer treatment (Smith et al. 2022). To name some examples, the antagomirs CDR132L and MRG-110 are in clinical trials for the treatment of cardiovascular disease. CDR132L is an inhibitor of miR-132 which is involved in cardiac remodelling, transformation and hypertrophy. MRG-110 is planned to promote angiogenesis by blocking the regulatory functions of miR-92a (Traber and Yu 2023).

3.2.1.3 mRNA vaccines and therapeutics

The ability to use mRNA for therapy was first proved by the successful transcription and expression of an *in vitro* transcribed mRNA in mouse skeletal muscle cells and set the basis for the promising mRNA-based therapeutics with several advantages but also challenges (Sahin et al. 2014). In theory by using mRNA, any desired protein/ peptide can be produced by the translation machinery and the transfection efficiency is quite high. Moreover, the toxicity is low because full functionality of the RNA is already achieved without the need to enter the nucleus (Deal et al. 2021). Manufacturing of mRNA therapeutics is simple and cost-effective. Additionally, a personalized therapy is now feasible based on the ability of easily modifying the RNA (Damase et al. 2021). But knowledge about the structure instability and immunogenicity of mRNA drugs is still lacking, hence it is important to address these challenges for the further development and optimization of mRNA-based therapeutics (Qin et al. 2022). To modulate translation efficiency and decay rate, a functional synthetic mRNA is mimicking natural occurring ones (**Figure 3-4 C**). Therefore, the RNA is designed and engineered with the 5' cap structure, the 3' Poly(A) tail and the open reading frame (ORF) flanked by the 5' and 3' untranslated regions (UTRs) (Shin et al. 2018). To improve the stability and translation of the mRNA, researchers set focus on optimizing these specific RNA features. The 5' cap was optimized to have higher translation efficiency by recruiting the eukaryotic translation initiation factor 4E (eIF4E) and increasing the resistance to decapping. Additionally, the coding region was optimized via codon optimization to boost translation (Sahin et al. 2014). To further increase stability and protein production,

incorporating highly stable UTRs, like for the example from the β-globin gene, is crucial together with the optimal size of the Poly(A) tail (Linares-Fernández et al. 2021). Lastly, the delivery of RNA drugs, not only mRNA but in general, has to be highly efficient. Therefore, research is especially focusing on optimizing the available delivery methods which are the use of lipid nanoparticles (LNPs) and *in vitro* nanoparticles which are vehicles enabling efficient delivery of therapeutics (Paunovska et al. 2018; Lokugamage et al. 2021). The currently applied approaches for mRNA drugs are replacement therapy to compensate defect genes or proteins, vaccination to produce specific antigens and cell therapy where *ex vivo* modified cells with specific functions or phenotypes are transplanted into patients (Damase et al. 2021).

One very important example for the therapeutic use of mRNAs are the two COVID-19 vaccines from Pfizer-BioNTech (BTN162b2) and Moderna (mRNA-1273) encoding the SARS-CoV-2 spike protein to boost antigen production. The vaccination provided approximately 90 % effectiveness for full vaccination and helped to halt the worldwide pandemic (reviewed in (Kumar et al. 2023). The foundation and optimizations in the field of mRNA vaccines were honoured with the Nobel prize in physiology and medicine this year (Karikó et al. 2005).

3.2.2 RNA-binding proteins as targets for cancer treatment

Eukaryotic gene expression is tightly regulated at a transcriptional but also at a posttranscriptional level like splicing, RNA export to the cytoplasm, mRNA turnover and storage or translation. One of the main regulators of this “mRNA life cycle” are RNA-binding proteins (RBPs) which form together with RNA different regulatory ribonucleoprotein (RNP) complexes (Coppin et al. 2018). Tumour cells utilize these post-transcriptional regulatory mechanisms to adjust protein levels in a quick and stable manner in response to intrinsic or extracellular signals. Additionally, it was shown that the expression and activity of RBPs are dysregulated in cancer (Pereira et al. 2017). Therefore, knowing that RBPs are drivers of tumorigenesis, makes them promising targets for drug discovery to treat cancer. However, until recently, RBPs were considered “undruggable” based on their often non-catalytic activity and their

integration into large protein-RNA complexes, which makes it difficult to generate specific inhibitors able to access and bind these targets (Bertoldo et al. 2023). Hence, it is of major interest to deeply understand the structure and interactome of different RBPs and the processes they regulate to identify suitable therapeutic targets.

3.2.2.1 RNA-binding domains and RNA binding motifs

Using high-throughput screens in diverse cell types, a catalogue of 1542 RBPs was determined which is representing approximately 7,5 % of all protein-coding genes in humans (Gerstberger et al. 2014). This high number of proteins, which were shown to be evolutionally conserved across species, proves the important role of RBPs in the regulation of gene expression (Matia-González et al. 2015). The binding of RBPs to their target RNA is mediated by individual RNA-binding domains (RBDs) recognizing sequence-specific motifs, secondary structures or a combination of sequence and structure. Moreover, the combination of different RBDs can provide higher specificity and affinity. Classical RBDs are for example K-homology domain (KH), RNA recognition motif (RRM), Zinc finger domain (ZNF), Pumilio homology domain (PUM), dsRNA binding domain (dsRBD) and some others (Lunde et al. 2007; Corley et al. 2020). Strikingly, only a subset of the identified RBPs contain these classical binding motifs. A large group of RBPs was identified to contain non-canonical RBDs which are characterized by intrinsically disordered regions adapting their structure upon contact with RNA and subsequently regulating cell cycle, metabolism and signal transduction (Baltz et al. 2012; Hentze et al. 2018). RBPs assemble on nascent and mature mRNA, packing and modifying the target throughout its life cycle, from transcription and processing, which includes RNA splicing, polyadenylation and capping, up to nuclear export, localization, translation and mRNA stability. Based on genome-wide studies and research, it is generally agreed that mRNAs are bound by multiple RBPs whereas individual RBPs have hundreds or thousands of RNA targets (Müller-McNicoll and Neugebauer 2013). Moreover, detailed studies revealed that the recognition of specific binding sequences or motives by RBPs is evolutionally conserved and helps to associate distinct functions in the diverse types of post-transcriptional regulation (Ray et al. 2013). The identification and understanding of functional elements encoded by the human genome which are only recognized on

RNA level is further supporting the idea that specific binding motifs can help mapping and classifying specific functions of different RBPs (van Nostrand et al. 2020).

3.2.2.2 Therapeutic targeting of dysregulated RBPs in cancer

Because RBPs are controlling gene expression on the post-transcriptional level, it is not surprising that a malfunction of these proteins can cause various disorders including cancer. The dysregulation of RBPs is suggested to mediate cancer initiation and progression based on their crucial involvement in several important cellular mechanisms like proliferation, differentiation, metastases, angiogenesis and apoptosis which can cause a cancer phenotype (Neelamraju et al. 2018). The dysregulation of RBPs in cancer is not only caused by altered gene expression, but also by alterations in protein activity which can be induced by post-translational modifications (PTMs). PTMs like methylation, phosphorylation or ubiquitination can change the binding properties, function and subcellular localization of RBPs. Because the RBD of the proteins are very likely to be modified, these modification are presumably one of the main mechanisms resulting in the RBP dysregulation in cancer (Pereira et al. 2017).

RBPs display a functional diversity in cancer. Firstly, they are involved in alternative splicing events by the dysregulation of hnRNPs or serine/arginine-rich (SR) proteins (Lee and Abdel-Wahab 2016). For example, the overexpression of the splicing factor hnRNPA2 in human glioblastoma induces exon skipping and inclusion of various targets causing the synthesis of antiapoptotic isoforms of tumour suppressor genes. Moreover, the upregulation of hnRNPA1 supports alternative splicing of RON which generates the oncogenic isoform of this tyrosine kinase receptor and hence modulates invasiveness and motility of tumour cells (Golan-Gerstl et al. 2011). Interestingly, it is postulated that CTNNB1, key factor of Wnt/ β-catenin signalling pathway (**3.1.3.1**), is a target for alternative 3' UTR splicing and dependent on the cellular context specific splice variants are upregulated (Thiele et al. 2006). The shorter 3'UTR splice variant of CTNNB1 is suggested to be the dominant isoform in tumours and might be responsible for an increased protein expression and its tumorigenic functions (Chan et al. 2022).

Secondly, RBPs can induce alternative polyadenylation (APA) generating shorter 3' UTRs which appears to be a common feature in cancer cells. This global 3' UTR shortening seems to be controlled by the subunits of the cleavage factor Im (CFIm) complex and can increase protein production of targets (Martin et al. 2012).

A third example for altered molecular mechanisms in cancer cells would be the regulation of subcellular localization of specific targets which is essential for establishing and maintaining cell polarity. The insulin-like growth factor-2 mRNA binding proteins 1,2 and 3 (IGF2BP1/2/3) are required for proper nerve cell migration and for the control of cytoskeletal remodelling and dynamics during development. In tumour-derived cells, they modulate cell polarization, adhesion and migration and are highly associated with cancer metastasis and expression of oncogenic factors like KRAS or MYC (Bell et al. 2013). Lastly it is worth to mention that mRNA stability and translation can also be altered in cancer cells by the dysregulation of RBPs (Pereira et al. 2017).

All in all, RBPs are the key players in the post-transcriptional gene regulation by binding to RNA targets and building RNP complexes. Malfunctions or dysregulation of these RBPs can cause several disorders and are most likely involved in cancer initiation and progression. Therefore, it is clear that RBPs are promising therapeutic targets for the development of anti-cancer drugs. Although they were considered "undruggable" due to their non-catalytic function and the formation of large protein-RNA complexes, with the development and improvements of new therapeutic tools, like the RNA-based therapeutics, RBPs can now be considered druggable targets (Bell et al. 2013; Mohibi et al. 2019).

3.3 Mechanism and regulation of T cells infiltration

One crucial step of the previously introduced cancer-immunity cycle is the efficient infiltration of T cells into the tumours which is essential for an effective anti-cancer immune response (**3.1.1; Figure 3-1**). However, T cells are often prevented to invade tumours successfully due to the repulsive TME. This does not only preclude spontaneous cancer cell killing but also interferes with therapeutic strategies of cancer immunotherapy like immune checkpoint blockade (**3.1.2**). The ability of leukocytes to transition from circulation to infiltration is regulated by a cascade of events enabling the recognition of the vascular endothelium in inflamed tissues or tumours and the interaction with the blood vessel wall. These events are summarized in the so-called leukocyte adhesion cascade (Ley et al. 2007; Vestweber 2015).

3.3.1 The leukocyte adhesion cascade

The leukocyte adhesion cascade describes the multi-step process which explains und summarizes the recruitment of leukocyte subsets to specific tissues essential for eliminating the inflammation trigger and contributing to tissue repair (Nourshargh and Alon 2014) (**Figure 3-6**).

To initiate the cascade, inflammatory reactions which are caused by tissue damage or infectious agents induce the release of pathogen-associated molecular patterns (PAMPs) from microorganism or damage-associated molecular patterns (DAMPs) from injured tissue cells. These danger signals first activate the cells of the innate immune system, like DCs, macrophages or mast cells which then release cytokines and pro-inflammatory stimuli causing the activation of endothelial cells (Medzhitov 2008). This activation of the endothelium can occur in a fast (type I) and slow manner (type II). The rapid activation can be caused by histamine and the platelet activating factor (PAF), whereas the slow activation is dependent on cytokines like interleukin 1 β (IL-1β) or tumour necrosis factor α (TNF-α) (Pober and Sessa 2007). Activated endothelial cells express high levels of cell-surface adhesion molecules which initiated the capture and tethering of leukocytes (**Figure 3-6**, **step 1**).

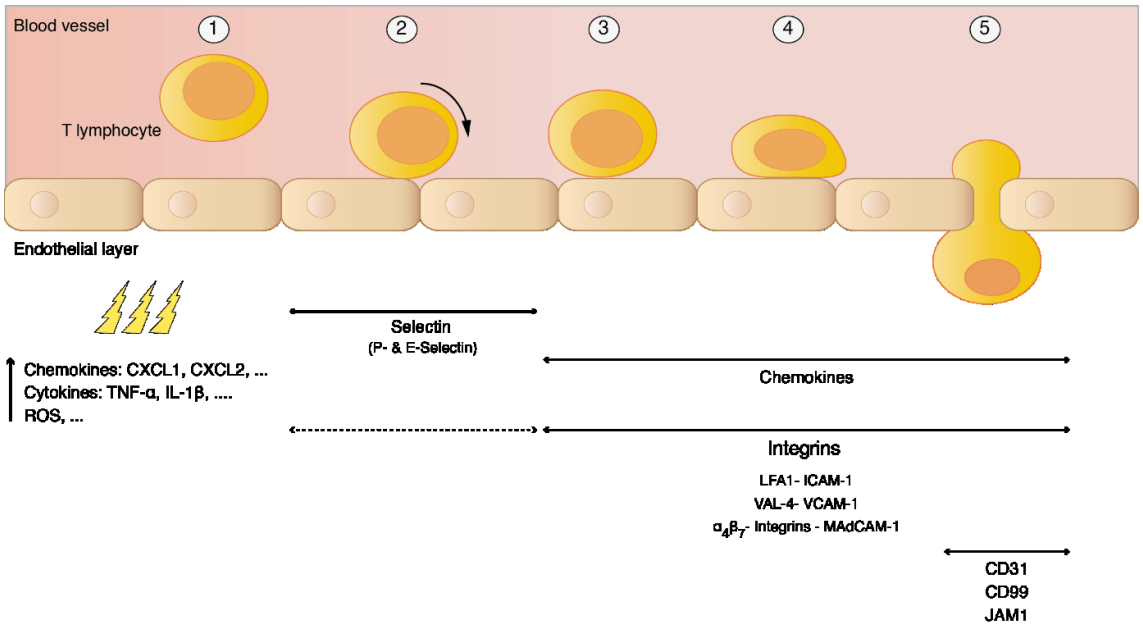

Figure 3-6: The leukocyte adhesion cascade. *Leukocyte capture and tethering is initiated by inflammatory stimuli, like pathogen-associated molecular patterns (PAMPs), damage-associated molecular patterns (DAMPs), inflammatory cytokines or cellular stress (**1**). After the capture of leukocytes, selectin-mediated rolling is induced (**2**). Chemokine signals cause activation which leads to leukocytes arrest on the endothelium stimulated by integrins (**3**). Attached lymphocytes start to migrate along the endothelial surface (**4**) until they migrate through the endothelium, by the so-called diapedesis which is mediated by the accumulation of junctional adhesion molecules (**5**) (modified from Kinashi 2005).*

Capture and tethering is mainly mediated by E-selectin and P-selectin via the interaction with their ligands P-selectin glycoprotein ligand 1 (PSGL1) and other glycosylated ligands like CD44 or E-selectin ligand 1 (ESL1) expressed on immune cells (Ley et al. 2007). The interaction of selectins with their ligands depends on shear stress and the blood flow (Beste and Hammer 2008). Afterwards, the next step of the adhesion cascade, the rolling of leukocytes on the activated endothelium is initiated (**step 2**) (Marshall et al. 2003). Rolling is also supported by integrins which then mediate firm adhesion of leukocytes (**step 3**). Integrins are expressed on leukocytes and interact with endothelial adhesion molecules like intercellular adhesion molecule 1 (ICAM-1) and vascular cell adhesion molecule 1 (VCAM-1) which are expressed upon pro-inflammatory cytokine signalling on the activated endothelium (van Buul et al. 2007). Integrin interactions cause the firm adhesion and spreading of leukocytes enabling the immune cells to crawl on the luminal surface (**step 4**) and after finding suitable exit sites, transmigrate through the endothelial barrier (**step 5**). The

transmigration, also called diapedesis, can be achieved through a paracellular or a transcellular mechanism in which junction adhesion molecules (JAMs), CD99, CD31, which is also known as platelet endothelial cell adhesion molecule 1 (PECAM1), and several others participate (Schenkel et al. 2002; Vestweber 2015).

The transition from rolling to firm adhesion followed by the transmigration and infiltration of leukocytes into the inflamed tissue is mainly mediated by cell adhesion molecules (CAMs), including receptors as ICAM-1 and integrins as LFA-1. Because cell adhesion is not only important for leukocyte trafficking but also plays a role in many other biological processes, researchers developed great interest in studying this event *in vitro* and utilize the strong interaction of LFA-1 with its ligand ICAM-1 for so-called cell adhesion assays. In this assay, the adhesion of differently treated T cells to its target molecules can be measured using a plate reader (Strazza et al. 2014; Weitz-Schmidt and Chreng 2012). The interaction between LFA-1 and ICAM-1 was also used in this work to establish a cell adhesion assay protocol. Therefore, these two key molecules for T cell adhesion are described in more detail in the next chapter.

3.3.2 Adhesion molecules and integrins as key players of T cell adhesion

3.3.2.1 Intercellular adhesion molecule 1 (ICAM-1)

The Intercellular adhesion molecule 1 (ICAM-1; CD54) is a protein of the immunoglobulin (Ig) superfamily, which are type I transmembrane proteins. ICAM-1 has approximately 76 – 144 kilodaltons (kDa) and is expressed on different cell types like endothelial cells, fibroblast and also leukocytes (Dustin et al. 1986). These cells show basal expression levels of ICAM-1 and its production is highly upregulated upon inflammatory signalling by for example the cytokines TNF-α, IL-1β and IFN-γ or by reactive oxygen species and shear stress (Morigi et al. 1995; Hubbard and Rothlein 2000). Transcription of ICAM-1 is regulated by many different transcription factors like NF-κB or yes-associated protein 1 (YAP1) (Hou et al. 1994; Lv et al. 2018).

Characteristically for a member of the Ig-supergene family, the full-length isoform of the protein consists of five extracellular Ig-like domains (D1 – D5), a transmembrane domain and a short cytoplasmic tail which contains multiple threonine residues and interacts with the actin cytoskeleton (**Figure 3-7**, **left**). In the membrane-bound

ICAM-1 isoform, the Ig domains are arranged end to end and stabilized by disulfide bonds at conserved cysteine residues (Staunton et al. 1988; Staunton et al. 1990). ICAM-1 is glycosylated at eight different N-glycosylation sites in human and at ten different sites in mice which are involved in ligand binding and specificity (Jiménez et al. 2005; Scott and Patel 2013). Moreover, it was shown that ICAM-1 can form a homodimer at the D4 – Ig domain which results in a stiff D4 - D5 stem and a bending at the junction between D3 and D4. The dimerization was shown to highly increase the affinity to its ligands (Yang et al. 2004). The main ligands of ICAM-1 are β_2 integrins like the integrins lymphocyte function-associated antigen 1 (LFA-1) and macrophage-1 antigen (MAC-1). Interestingly, LFA-1 is mainly bound by the D1 – Ig domain, whereas MAC-1 binding occurs at the D3 domain (Haydinger et al. 2023).

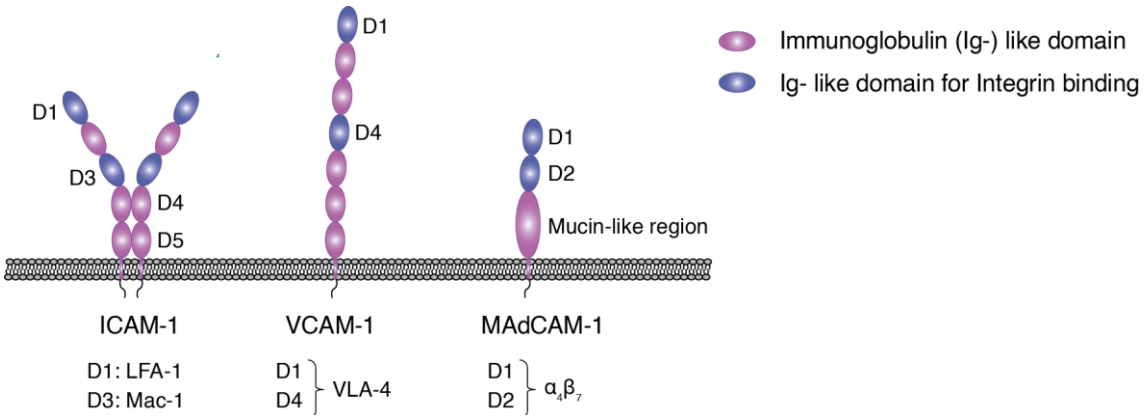

Figure 3-7: Schematic representation of endothelial adhesion molecules. *The Ig-supergene family proteins are type I transmembrane proteins, containing extracellular Ig-like domains, a transmembrane domain and a short cytoplasmic tail. (**Left**) The ICAM-1 protein consists of five Ig-like domains. The D1 domain binds the integrin LFA-1 and the D3 domain binds MAC-1. The protein can form homodimers mediated by the D4 domain which increases ligand binding affinity. (**Middle**) VCAM-1 consists of seven (d7) or six (d6) Ig domains. D1 is the ligand binding domain and in the d7 isoform additionally D4. (**Right**) MAdCAM-1 contains two Ig – like domains which binds the α4β2 integrin and a mucin – like region binding L-selectin.*

3.3.2.2 Vascular adhesion molecule 1 (VCAM-1)

There are several other adhesion molecules besides ICAM-1 mediating leukocyte rolling and firm adhesion in different cell types. The vascular cell adhesion molecule 1 (VCAM-1; CD106) is expressed on the luminal and lateral side of endothelial cells under inflammatory signals mediating leukocyte recruitment to sides of inflammation like ICAM-1 (Ley et al. 2007). VCAM-1 belongs also to the Ig superfamily and consist

of six (d6) or seven (d7) Ig - like domains depending on the splice variant which is missing or including the D4 domain. Ligand binding is mediated by the D1 or D4 domain (**Figure 3-7**; **middle**). Several different integrins are binding to VCAM-1 but the very late activation antigen-4 (VLA-4) is the one best investigated. The d6 isoforms shows higher affinity to VLA-4 under soluble conditions and the d7 VCAM-1 is more efficient in cell adhesion and spreading (Osborn et al. 1992; Schlesinger and Bendas 2015).

3.3.2.3 Mucosal addressin cell adhesion molecule 1 (MAdCAM-1)

A third example of an important cell adhesion molecule of the Ig superfamily is the mucosal addressin cell adhesion molecule 1 (MAdCAM-1) which is expressed on high-endothelial venules of Peyer's patches, other gut associated lymphoid tissues and venules of the lamina propria regulating the trafficking of a subset of leukocytes into mucosal tissues (Briskin et al. 1993; Tan et al. 1998). Typical for this class of molecules, expression is upregulated upon pro-inflammatory signals by cytokines as TNF-α and depends besides NF-κB also on PI3-K/Akt (Ogawa et al. 2005). MAdCAM-1 contains two Ig - like domains (D1-D2) and an additional mucin - like region, together with the transmembrane domain and the short cytoplasmic tail (**Figure 3-7**, **right**). Similar to ICAM-1, the protein was reported to be able to form dimers which gave rise to the idea that it functions as an oligomer (Dando et al. 2002). MAdCAM-1 is considered a unique dual function protein in the class of adhesion molecules. The main ligands are the α4β7 integrin which is binding to D1 and D2 and L-selectin which is regulated by suitable O-glycosylation and binds the mucin – like domain. L-selectin mediates transient adhesion of leukocytes whereas the α4β7 integrin induces upon activation firm adhesion (Tan et al. 1998).

3.3.2.4 Lymphocyte function-associated antigen 1 (LFA-1)

Integrins are the main ligands binding adhesion molecules to induce firm adhesion in the leukocyte adhesion cascade. They are large heterodimers and can combine 18 different types of α-chains and 8 types of β-chains forming in total a family of 24 different integrins (Kinashi 2005). Leukocytes express a variety of integrins, which

bind various different ligands like soluble proteins, proteins on the surface of other cells or ligands in the extracellular matrix. Most important for immune cells are the integrins β1 (e.g. α4β1), β2 (e.g. αLβ2 (LFA-1; CD11a/CD18), αMβ2 (MAC-1), αXβ2 (CD4), αDβ2) and the β7 (α4β7) whereby the β2-integrins (CD18) are predominantly expressed on leukocytes. Upon activation, integrins undergo conformational changes to efficiently bind to their ligands which will be described in a later chapter (**3.3.3**) (Harjunpää et al. 2019). In the following, the focus will be set on LFA-1 as the main ligand of ICAM-1.

Integrins in general belong to the group of type I transmembrane glycoproteins, which are characterized by a long extracellular domain, a single-spanning transmembrane domain and short cytoplasmic tail (**Figure 3-8 A**). The α-subunit comprises of a leg with three β-sandwich domains. The lower leg has the calf-1 and calf-2 domain and is linked to the thigh domain of the upper leg via a small calcium (Ca^{2+})- binding loop, the so-called genu (knee) domain. The genu is essential for conformational extension and bending of the α-subunit. The leg is linked to the headpiece of the α-chain by the β-propeller domain. For nine integrins, an α – I domain is integrated in the β-propeller, which is the main and exclusive ligand binding domain of these integrins (Luo et al. 2007). The β-subunit is more complex. The lower part of the leg consists of four integrin epidermal growth-factor-like (I-EGF) domains and a β-tail, which facilitate β-leg bending. The lower leg is inserted in the plexin/semaphorin/integrin (PSI) domain, which comprises two segments and is closely linked to the upper I-EGF domain. The head part is built by the hybrid domain followed the β - I domain. The hybrid domain is the connection of the lower and upper part of the subunit and critical for conformational changes. The β - I domain is a homolog to the α – I domain and is essential for determining ligand specificity (Nishida et al. 2006; Luo et al. 2007).

LFA-1 belongs to the I-domain containing integrins which bind their ligands via the α - I domain inserted in the β-propeller domain as already mentioned above. Crucial in this domain is the metal ion – dependent adhesion site (MIDAS). There, a divalent magnesium ion (Mg^{2+}) is coordinated, which is crucial for ligand binding. Moreover, two additional sides were shown to be essential for the conformational change. These

two domains are called ligand-induced metal-binding site (LIMBS) and adjacent to MIDAS (ADMIDAS) (Shimaoka et al. 2003; Walling and Kim 2018).

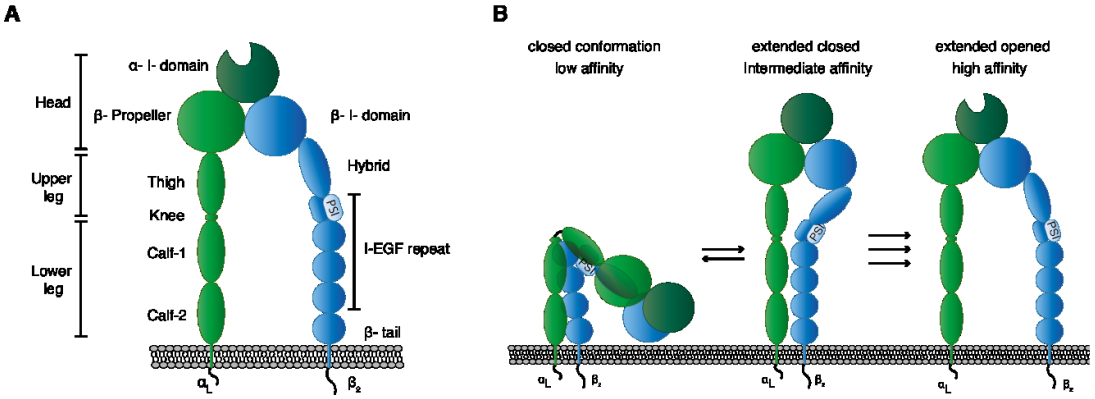

Figure 3-8: Schematic representation of the LFA-1 integrin structure and conformational change upon activation. *(**A**) Integrins are heterodimers with an α – and β -chain comprising of an extracellular domain, a transmembrane domain and a short cytoplasmic tail. The α subunit consist of two calf-domains linked via a small genu (knee) domain to the thigh followed by the β-propeller with an inserted α – I – domain. The β subunit has a β-tail inserted in I-EGF repeats and the PSI domain. The following hybrid domain is linked to the β - I – domain. (**B**) LFA-1 can occur in three different conformations which are regulating affinity. The closed conformation with a bent headpiece has low affinity to ligand binding. The extended closed state shows intermediate affinity, and the extended open conformation is the fully active form (modified from Luo et al. 2007).*

As stated above, LFA-1 can have at least three different conformational states which can remodel into each other via the movement of the extracellular and cytoplasmic domains (**Figure 3-8 B**). The closed conformation shows a bent headpiece which makes the integrin unavailable for ligand binding because of the close proximity of the binding site to the plasma membrane. In the extended closed state, the integrin is already extended but the cytosolic tails stay closed which allows only weak interaction with the ligand. The extended open conformation is the fully active form and has high binding affinity to ligands (Shimaoka et al. 2003).

To achieve this conformational change and generate the fully active LFA-1 state, a number of structural modifications occur, which are induced by mechanisms called “inside-out” and “outside-in” signalling (Walling and Kim 2018). These two integrin - activation mechanisms will be described in the following chapter.

3.3.3 Outside-in and inside-out signalling mechanism for LFA-1 activation

Integrins are typically expressed in their closed, inactive conformation. Thereby, leukocytes are able to freely circulate in the blood vessels because of minimal aggregation or interaction with vessel walls. Upon activation signalling, the integrins rapidly change their conformation into the active state for ligand binding. The conformational switch can be induced either by an outside-in or an inside-out signalling mechanism (Gahmberg et al. 2009; Arnaout 2016).

In outside-in signalling, ligand binding to extracellular integrin domains induces conformational change. Binding occurs at the β - I domain, which is accessible for external ligands, and induces a swinging-out of the hybrid domain. The change in the hybrid domain weakens the interaction between the head- and tailpiece and also between the α- and β-subunit. Thereupon, internal ligands, especially cytoskeletal molecules talin and kindlin, bind to the cytoplasmic tails resulting in the extension of the integrin and leg separation. Moreover, intracellular signals are activated, which can cause for instance integrin clustering (Mao et al. 2020).

For inside-out signalling, non-integrin external receptors induce internal signalling cascades which activate intracellular pathways leading to the conformational change and ligand binding of integrins (**Figure 3-9**) (Gahmberg et al. 2009).

The binding of PSGL-1 to selectins expressed on the endothelium can initiate the internal signalling cascade needed for LFA-1 activation. Moreover, the binding of various chemokines to their respective chemokine receptors can also trigger integrin activation. Examples for such arrest chemokines are the CXCL8 binding to the CXC-chemokine receptor CXCR1 or CXCR2 or the chemokines CCL21, CXCL12 and CXCL13 and many more (Thelen 2001; Ley 2014). Moreover, integrins itself can influence the activation of other integrins in a process called integrin transregulation (Rose et al. 2003). All these interactions initiate a signalling cascade which leads to the activation of Rap1-GDP to Rap1-GTP which is a key player in integrin activation (Shimonaka et al. 2003). Active Rap1 either directly or via the Rap1-interacting adaptor molecule (RIAM), plays a central role in talin activation (especially talin-1) which then binds to the cytoplasmic tail of the β-subunit of LFA-1. Binding of talin leads to the extended-closed conformation and intermediate interaction with the ligand ICAM-1

(**Figure 3-9**, **step 1**). For the full activation and the high affinity conformation of LFA-1, additional binding of kindlin (especially kindlin-3) to the cytoplasmic tail of the β-chain is needed. The activation of kindlin-3 is not really understood yet but there might be a connection to Rap1 signalling. The binding of both, talin-1 and kindlin-3, keeps LFA-1 in the open conformation and binding to its ligand ICAM-1 (**Figure 3-9**, **step 2**) (Wen et al. 2022).

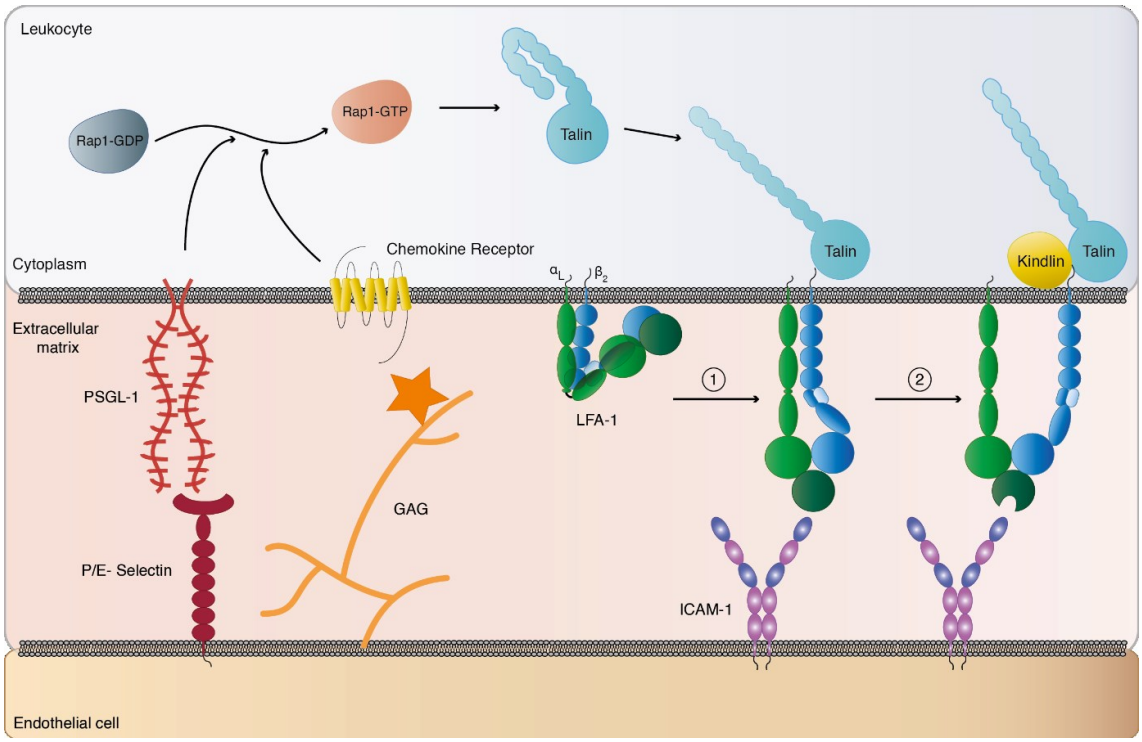

Figure 3-9: Schematic representation of the activation of LFA-1 via inside-out signalling mechanism. *Binding of different ligands to their receptors, like PSGL-1 to P- or E-selectin and by glycosaminoglycan (GAG) presented chemokines to their respective chemokine receptors, induce cell signalling. These signals lead to the activation of Rap1-GDP to Gap1-GTP. Rap1-GTP is able to active talin which then binds to the cytoplasmic tail of the β-subunit inducing extension of LFA-1 (**1**). Next, kindlin is also binding to the cytoplasmic tail of the β chain, which triggers the separation of the legs and activation of the ligand-binding domain (**2**). LFA-1 remains in the extended open conformation while talin and kindlin are stably bound (modified from Harjunpää et al. 2019).*

In summary, to ensure efficient infiltration of T cells into inflamed tissue or tumours, the firm adhesion to the endothelium is a crucial step in the leukocyte adhesion cascade. The major molecules involved in this process are the adhesion molecule ICAM-1 expressed on endothelial cells and the integrin LFA-1, expressed on T cells. Binding to ICAM-1 is only able when LFA-1 is activated and alters its conformation from the closed into the extended high affinity conformation. This conformational

change is initiated by outside-in or inside-out signalling. Crucial for both mechanisms are the internal ligands talin-1 and kindlin-3. Both molecules stay in an autoinhibitory state to keep LFA-1 in an inactive form. Upon induced signalling cascades by for example ligand or chemokine binding, the autoinhibition is relieved, talin and kindlin are recruited to the plasma membrane and activate LFA-1 which ensures binding to ICAM-1 and firm adhesion of T cells.

3.4 Aims of this work

One important step of the cancer-immunity cycle is the infiltration of activated T cells into the tumours. However, T cells are often prevented to invade successfully due to the repulsive tumour microenvironment. This does not only preclude spontaneous cancer cell killing but also interferes with therapeutic strategies of cancer immunotherapy. Infiltration of T cells is mediated by the interaction of endothelial adhesion molecules such as ICAM-1 and integrins like LFA-1 expressed on T cells. We hypothesize that regulatory RNA pathways contribute to the generation of soluble molecules that are secreted by cancer cells and modulate the LFA-1 – ICAM-1 interaction and thus exclude T cells from tumours. In this work we aim to identify RNA binding proteins (RBPs) contributing to T cell exclusion and preventing efficient T cell infiltration.

Therefore, an RNAi screening approach will be designed and optimized to investigate regulatory events originating from cancer cells interfering in the interaction of ICAM-1 and LFA-1. Firstly, a protocol for the purification of recombinant human ICAM-1-Fc (hICAM-1-Fc) protein from mammalian cells will be established. The purified protein will then be used for the so-called cell adhesion assay, which will be created and optimized to enable the monitoring of T cell binding to ICAM-1 *in vitro*. Next, T cells will be treated with cell culture supernatants to identify cancer cell lines downregulating the T cell binding in these assays. Subsequently, RNAi knockdown experiments in the verified cancer cell lines will be performed to identify potential RNA-based regulatory pathways including RBPs or RNA-modifying enzymes, restoring and enhancing T cell binding in cell adhesion assays. Lastly, identified targets will be further validated and functionally characterized in detail. These identified molecules will potentially serve as highly valuable targets for RNA-based immunotherapy in the future.

4 Results

4.1 Purification of recombinant hICAM-1-Fc protein from mammalian cells

4.1.1 Establishing of purification protocol for hICAM-1-Fc

In order to purify the human ICAM-1 protein (hICAM-1/ hICAM-1-Fc) from adherent HEK 293T cells, a purification protocol was established and optimized (**Figure 4-1**). The recombinant protein consisted of the extracellular part of the protein which corresponds to all five immunoglobulin domains and is essential for ligand binding (**3.3.2**). Additionally, it was expressed with a N-terminal signal sequence which led to the secretion of the protein into the supernatant. The C-terminal immunoglobulin tag, which is the Fc-fragment of antibodies (containing aminoacids P100 to K330), was a suitable purification tag because of its high affinity to Protein A and Protein G beads (**Figure 4-1 A**). Additionally, the Fc-fragment supports dimerization and generation of the V-shaped structure, which both are essential for fully functional ICAM-1 protein (Yang et al. 2004; Gattinger et al. 2021).

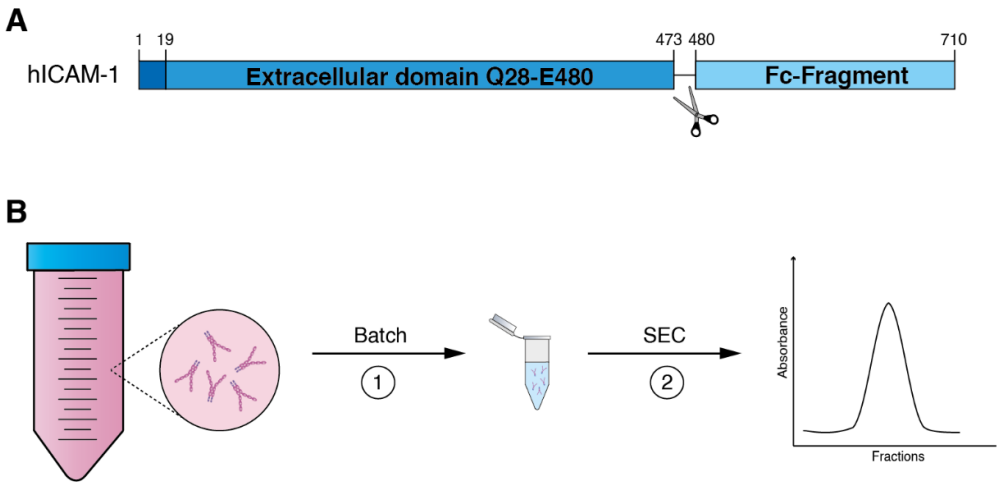

***Figure 4-1: Schematic overview of purification strategy for hICAM-1 protein**. (**A**) The recombinant hICAM-1 protein consists of an N-terminal signal sequence, the extracellular part of the protein and a C-terminal immunoglobulin tag which can be cleaved off using an inserted FactorX site. (**B**) For the purification of hICAM-1, first a batch purification using Protein A affinity purification beads was performed (**1**) and after acidic elution from the beads, the protein was further purified by a size exclusion chromatography (SEC) (**2**).*

To optimize purification conditions, the Protein A and Protein G affinity purification beads were tested together with different wash buffers and different elution buffers

(data not shown). In the end, using the following two-step protocol yielded the highest amounts of purified protein. After transient transfection of adherent HEK293T cells for 48 h, supernatants were collected and batch purification was performed. To recover bound protein from the beads, acidic elution at pH 3,0 was performed (**step 1**). As second purification step a gel filtration was used (**step 2**) to remove possible contaminants which could be copurified with the protein of interest (**Figure 4-1 B**).

The success of the protein purification was checked via SDS-PAGE (**Figure 4-2**). The acidic elution step was repeated four times to ensure high recovery of the protein from the beads. Although the predicted size of the protein was 78 kDa, the single elution fractions showed each a band at approximately 120 kDa. This corresponded to the predicted running behaviour of the hICAM-1-Fc protein based on post-translational modifications of the protein, especially glycosylation (Scott and Patel 2013). The elution was very efficient with only a small amount of remaining protein which was still bound to the beads (**Figure 4-2 A**, lane 8). Additional unspecific fragments running at 180 kDa and 55 kDa were co-purified in the batch purification.

The protein-containing fractions were pooled and concentrated before the gel filtration was performed. Based on the obtained chromatogram, fractions A13 to B15 were checked via SDS-PAGE (**Figure 4-2 B** and **C**). The fractions A14 to B5 showed enrichment of the protein with the same band running at 120 kDa (**Figure 4-2 C**, lane 3 – lane 9) which was already seen after the batch purification. These fractions also corresponded to the first peak of the gel filtration chromatogram (**Figure 4-2 B**). The other fractions, especially from B6 to B10, still contained some amount of hICAM-1-Fc protein but also the additional non-specific fragments at 55 kDa and 180 kDa (**Figure 4-2 C**, lane 11 – lane 15). Based on these results, protein containing fractions A14 to B5 were pooled and concentrated.

To ensure specific purification, the protein was analysed and validated by Western Blot and mass spectrometry, which proved that the detected bands of the SDS-PAGE corresponded to the hICAM-1-Fc protein (data not shown.).

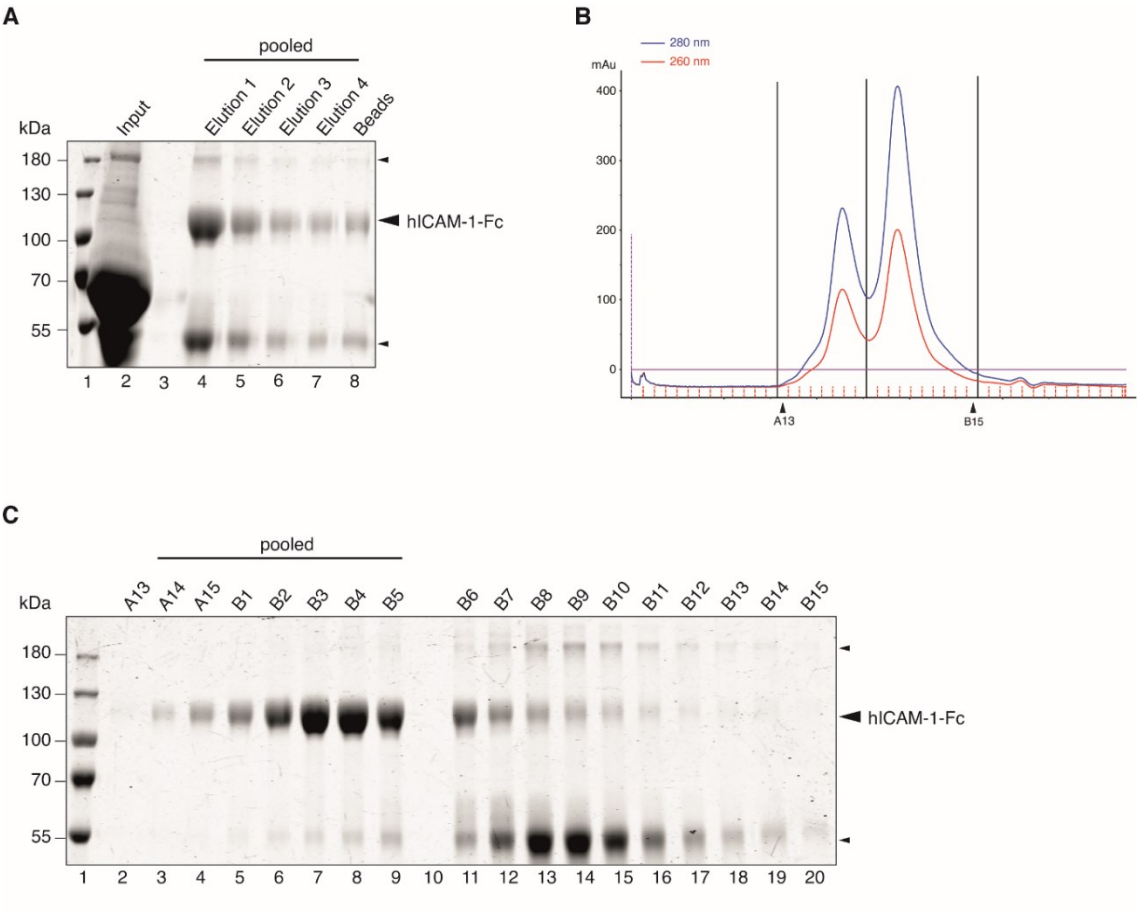

Figure 4-2: Purification of recombinant hICAM-1-Fc protein. *(**A**) Batch purification of hICAM-1 protein shows high yield of protein in each of the four elution fractions running at approximately 120 kDa. Additional bands appear at 180 kDa and 55 kDa. (**B**) The gel filtration shows two peaks starting with fraction A13 and ending with fraction B15. (**C**) SDS-PAGE of the gel filtration shows enrichment of hICAM-1-Fc protein in fraction A14 to B5. The other fractions B6 to B15 contain the non-specific fragments. (hICAM-1-Fc = 78 kDa)*

4.1.2 Generation of stable hICAM-1-Fc Flp-In™ TREx™ 293 cell line

In order to simplify protein purification, a stable cell line was generated using the Flp-In™ TREx™ 293 cell line, which was supposed to express the hICAM-1-Fc protein after induction with tetracycline. To validate positive clones, 24 h after induction with tetracycline, supernatants were collected and immunoprecipitation (IP) was performed using Protein A affinity purification beads to enrich for the protein of interest followed by Western Blot analysis (**Figure 4-3**). Induction for 24 h yielded sufficient amounts of the hICAM-1-Fc protein, which was detected at the expected weight of 120 kDa using a specific α-human IgG-HRP antibody binding the Fc-tag of

the protein. For clone 1.7 (cl. 1.7) more protein was detected compared to clone 1.9 (cl. 1.9) and was therefore picked for further experiments (**Figure 4-3**, lane 5 and 7). The wildtype (WT) did not show any expression (**Figure 4-3**, lane 2-3) as well as all non-induced samples (**Figure 4-3**, lane 10-15). As loading control, an α-Fibronectin antibody was used detecting rather weak but equal levels of the protein in the all input lanes.

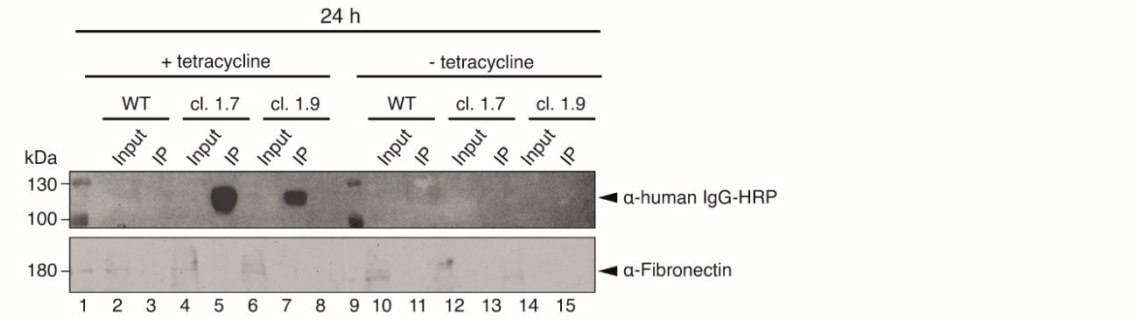

Figure 4-3: Generation of stable Flp-In™ TREx™ 293 cell line. *Induction with tetracycline for 24 h induces expression of hICAM-1-Fc protein. Expression is higher in clone 1.7 compared to clone 1.9. The used antibody is detecting the Fc-tag of the protein. (hICAM-1-Fc = 78 kDa).*

The positive clone 1.7 was used in order to test the established purification protocol and determine the protein yield after purification. Therefore, cells were induced for 24 h, 48 h and 72 h using tetracycline and batch purification was performed using Protein A affinity purification beads as it was established before (**4.1.1**). Success of purification was check by SDS-PAGE and Western Blot (**Figure 4-4**).

After 24 h and 48 h of induction, only weak expression of ICAM-1 was detected at the expected weight of 120 kDa (**Figure 4-4 A**). The induction for 72 h yielded sufficient levels of the ICAM-1 protein. However, also the levels of the unspecific band at 55 kDa were increased. The Western Blot indicated similar results using a specific α-ICAM-1 antibody for detection. With longer induction times, the yield of the protein increased significantly (**Figure 4-4 B**). But, at 72 h induction the recovery of the beads was not as successful as for shorter induction times. Although four elution steps were performed, a strong band was detected indicating remaining protein which was still bound to the beads (**Figure 4-4 B**, lane 21). After induction of the stable cell line, the amount of generated protein was lower compared to the transient transfection, which

was used for the establishing of the purification protocol. Moreover, the induction caused higher levels of unspecific contaminants.

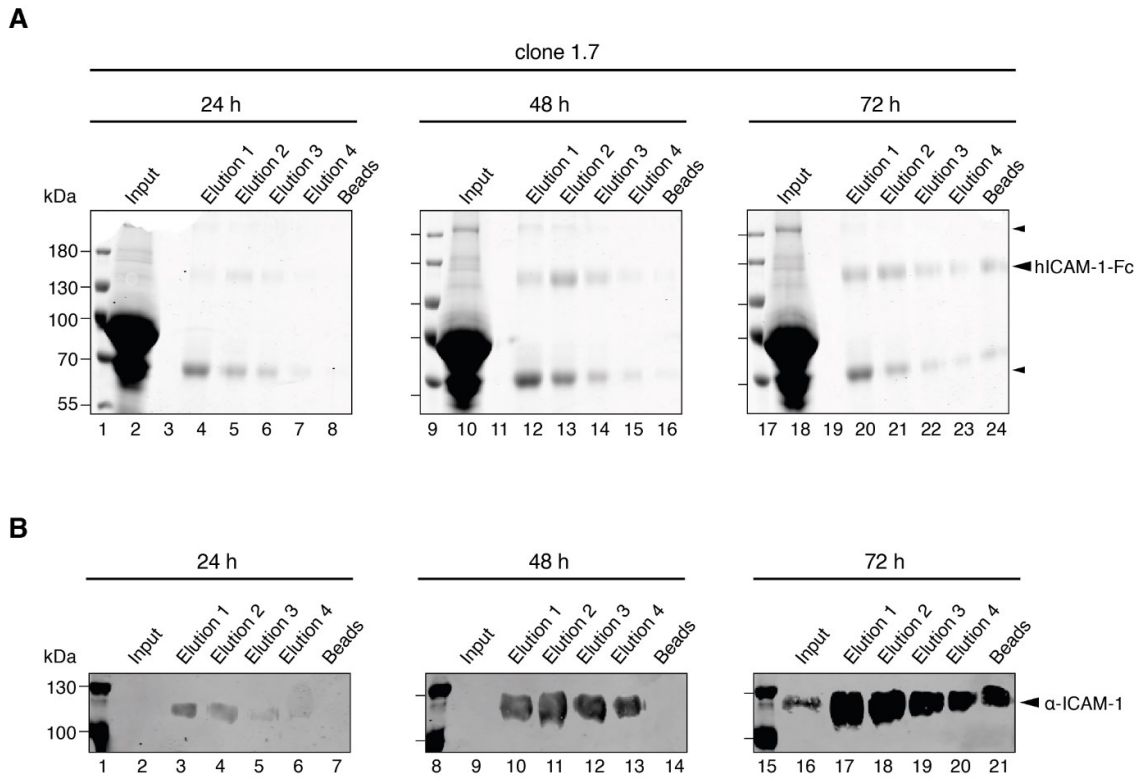

Figure 4-4: Test purification of hICAM-1-Fc protein in inducable stable Flp-In™ TREx™ 293 cell line. ***(I.)*** *SDS-PAGE shows for clone 1.7 increased protein levels with increasing time of induction. For purification, 72 h induction was chosen.* ***(II.)*** *Also, the Western Blot shows increased ICAM-1 levels over time of induction. The used antibody is specific for ICAM-1. (hICAM-1-Fc = 78 kDa)*

Therefore, for protein purification transient transfection of hICAM-1-Fc was used because of higher yield in the purification and shorter incubation time of only 48 h instead of 72 h. Functional analysis or other experiments regarding hICAM-1-Fc could be performed with the stable cell line when induced for 72 h with tetracycline. The recombinant purified hICAM-1-Fc protein was further used for cell adhesion assays which will be described in more detail below.

4.2 Establishment and optimization of *in vitro* cell adhesion assay to mimic T cell binding

In order to monitor T cell binding *in vitro*, cell adhesion assays were established and optimized. The strong interaction between the adhesion molecule ICAM-1 and the integrin LFA-1 expressed on T cells was used in this assay.

4.2.1 Establishment of *in vitro* cell adhesion assay

For investigation of the binding affinity of T cells to the hICAM-1 adhesion molecule at different conditions *in vitro*, a cell adhesion assay was established (**Figure 4-5**). Recombinant purified hICAM-1-Fc protein (**4.1**) was immobilized on 96 well plates directly or mediated by a specific α-human IgG primary antibody which binds the Fc-tag of the protein. This step will be called "coating" from now on. Primary T cells, which have been fluorescently labelled using the CellTracker™ Green CMFDA reagent beforehand, were added to the coated wells. Unbound cells were removed by performing several washing steps. The binding of the cells was measured by a plate reader. As background, wells without coated protein were used ("uncoated").

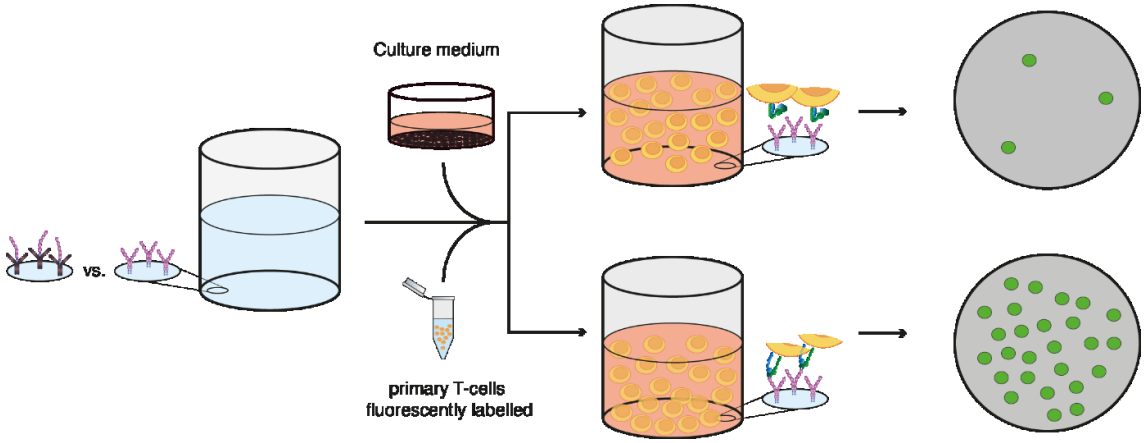

Figure 4-5: Overview of in vitro cell adhesion assay. *For in vitro cell adhesion assay, 96 well plates were coated with hICAM-1-Fc protein, either directly or mediated by an α-human IgG antibody. Then, fluorescently labelled T cells were added. After several washing steps, the fluorescent signal was measured by a plate reader.*

At first, the coating efficiency of the protein to the plate was optimized. Therefore, different buffer conditions were tested and analysed by enzyme-linked immunosorbent assay (ELISA) (**Figure 4-6**). Different amounts of hICAM-1-Fc protein were diluted in carbonate buffer with pH 8,5 and pH 9,5. After incubation with

an α-IgG-HRP antibody (detection antibody), which bound to the Fc-fragment, chemiluminescent signals were developed using Clarity Western ECL substrate and detected by the ChemiDoc Touch Imaging System. The direct coating of hICAM-1-Fc showed low background signal in uncoated wells and nice saturation with a maximum between 100 ng and 500 ng protein per well (**Figure 4-6 A**). Moreover, for the carbonate buffer with a pH of 9,5, the detected signals were higher compared to the buffer at pH 8,5 and thus indicated that coating at higher pH was more effective. In contrast to that, the primary mediated coating showed unspecific binding of the detection antibody to the coating antibody. When only the coating antibody was immobilized, the measured signals were almost as high as for other conditions, which made it difficult to obtain clear results (**Figure 4-6 B**). The signal intensity was not increasing much with increasing amount of hICAM-1-Fc protein. Nevertheless, as already seen for the direct coating, the buffer at pH 9,5 was more efficient compared to the one at pH 8,5. Based on these results, the carbonate buffer with a pH of 9,5 was chosen for further experiments.

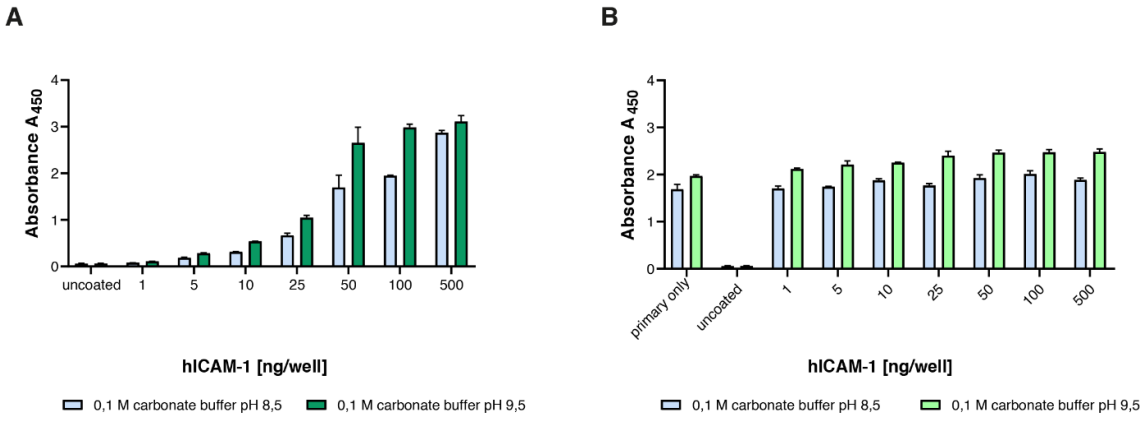

Figure 4-6: Coating buffer optimization of in vitro cell adhesion assay. *(A)* ***Direct hICAM-1 coating****. Direct coating of the hICAM-1 protein is more efficient when carbonate buffer with pH 9,5 is used. (**B**)* ***hICAM-1 coating mediated by a primary antibody.*** *As seen for direct coating, primary mediated hICAM-1 coating is more efficient with carbonate buffer pH 9,5. The background signal of the primary antibody itself is very high in the ELISA assay.*

As a next step, the different coating techniques were compared by ELISA as already described above. Therefore, the hICAM-1-Fc protein was coated to the wells directly or mediated by a primary antibody using increasing protein concentrations. Signals were detected using the α-IgG-HRP detection antibody inducing chemiluminescence (**Figure 4-7 A**).

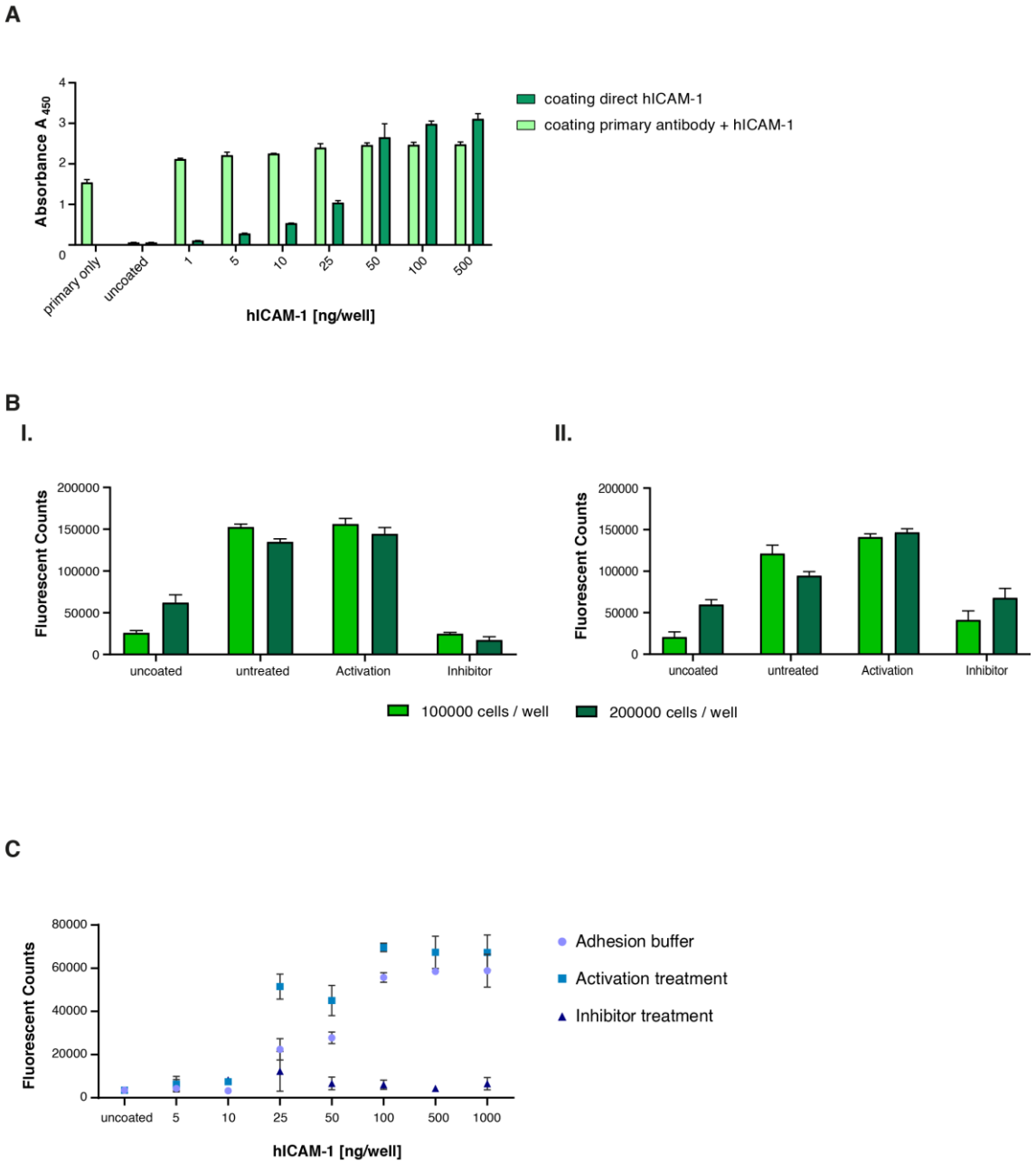

Figure 4-7: Establishing an in vitro cell adhesion assay to monitor T cell binding. *(A)* ***Coating Optimization – primary versus direct coating.*** *Comparing primary antibody mediated and direct coating of hICAM-1 protein, the direct coating shows higher efficiency and lower background signal. (**B**)* ***Optimization of T cell number.*** *The binding efficiency of T cells to immobilized hICAM-1 protein, coated directly (**B I**) or primary antibody mediated (**B II**.), is not dependent on the amount of T cells added. More T cells do not increase the measured signals. (**C**)* ***Correlation of T cell binding on hICAM-1 coating.*** *The T cell binding correlates with increasing concentrations of hICAM-1 protein but shows high standard deviations and variability.*

The efficiency of directly immobilized hICAM-1-Fc protein was higher compared to the primary antibody mediated binding of the protein to the wells. Additionally, the background signal induced by the primary antibody was higher than the one of

directly coated protein, which again made the results less reliable. The background of uncoated wells induced no signal, which proved specificity of the ELISA. Based on the low background and overall higher signals, the direct coating of hICAM-1 seemed to be more efficient and was chosen for further experiments.

Further on, the binding efficiency of labelled T cells was compared (**Figure 4-7 B**). In order to do this, cell adhesion assays were performed as described before, comparing the addition of either 100.000 or 200.000 T cells per well. Additionally, T cells were treated with phorbol myristate actetate (PMA) as activator and BI-1950 as LFA-1 antagonist. PMA activates multiple kinases especially protein-kinase C, which is positively stimulating T cells (Ai et al. 2013). The inhibitor BI-1950 is effectively blocking the interaction between LFA-1 and ICAM-1 by blocking the integrin in the inactive conformation (Kelly et al. 1999).

For both T cell numbers, results of directly (**Figure 4-7 B I.**) and primary antibody mediated coating of the hICAM-1-Fc protein (**Figure 4-7 B II.**) were similar. In case 200.000 T cells were added to each well, the background signal of the uncoated control wells was almost doubled in intensity compared to 100.000 cells per well. In contrast to that, the binding of activated T cells, which were treated with the activator PMA, was not increased by higher cell numbers. For both cell numbers similar signal intensities were observed. Also, the signals for T cells treated with the specific LFA-1 inhibitor BI-1950 were comparable for the two different cell numbers.

Based on these results, direct coating of 500 ng hICAM-1 protein with carbonate buffer of pH 9,5 and adding 100.000 T cells per well were determined as the best conditions for the *in vitro* cell adhesion assay.

As a final validation step and quality control, the correlation between T cell binding and the amount of coated hICAM-1 protein was checked (**Figure 4-7 C**). Therefore, cell adhesion assays were performed with the optimized conditions. Before labelled T cells were added to the wells, they were treated with PMA for activation, with BI- 1950 for inhibition or with adhesion buffer, which contained divalent magnesium and manganese ions known to activate the LFA-1. With increasing concentration of coated protein, the measured fluorescent signal was increased when T cells were activated by adhesion buffer or additional activation treatment. Saturation was

reached using 500 ng of protein per well, as already seen in the optimization experiments before. If T cells were treated with a specific LFA-1 inhibitor (**Figure 4-7 C**, **dark blue rectangles**), the signal remained low, also at high concentrations of hICAM-1 protein in the well. However, in all conditions the standard deviations were high and measured signals varied to some extent. Hence, further optimization was needed to be able to obtain more reliable results.

4.2.2 Optimization of the *in vitro* cell adhesion assay

In order to further optimize the *in vitro* cell adhesion assay and reduce variability, a different readout was tested. As new readout, the CellTiter Glo® reagent (Promega) was chosen, which is based on inducing a luminescent signal instead of the fluorescent labelling of T cells (**Figure 4-8 A**). After coating the recombinant purified hICAM-1-Fc protein to 96 well plates, the differently treated primary T cells were added to the wells. The binding was then detected via the luminescent signal induced by the CellTiter Glo® reagent based on a luciferase reaction. The reagent induces lysis of the bound cells in the wells, which releases ATP. Free ATP is used by the luciferase and generates the luminescent signal (Alimov et al. 2019).

Using the new readout with the established assay conditions, the binding of activated T cells correlated nicely with the amount of coated hICAM-1 protein in each well (**Figure 4-8 B I**.). With increasing concentration of the protein, the induced luminescent signal also increased and saturated at approximately 500 ng protein per well. When T cells were treated with the a specific LFA-1 antibody (α-CD18), which stalled the integrin in the low affinity state (Neri et al. 2018), almost no binding occurred regardless of the concentration of protein coated per well. With the new optimized readout, also the standard deviations were very low in contrast to the results obtained before (**Figure 4-7 C**). Moreover, using the new readout, a linear correlation between the number of cells added to each well and the luminescent signal was observed (**Figure 4-8 B II**.). The more T cells were added to each well, the higher was the detected signal.

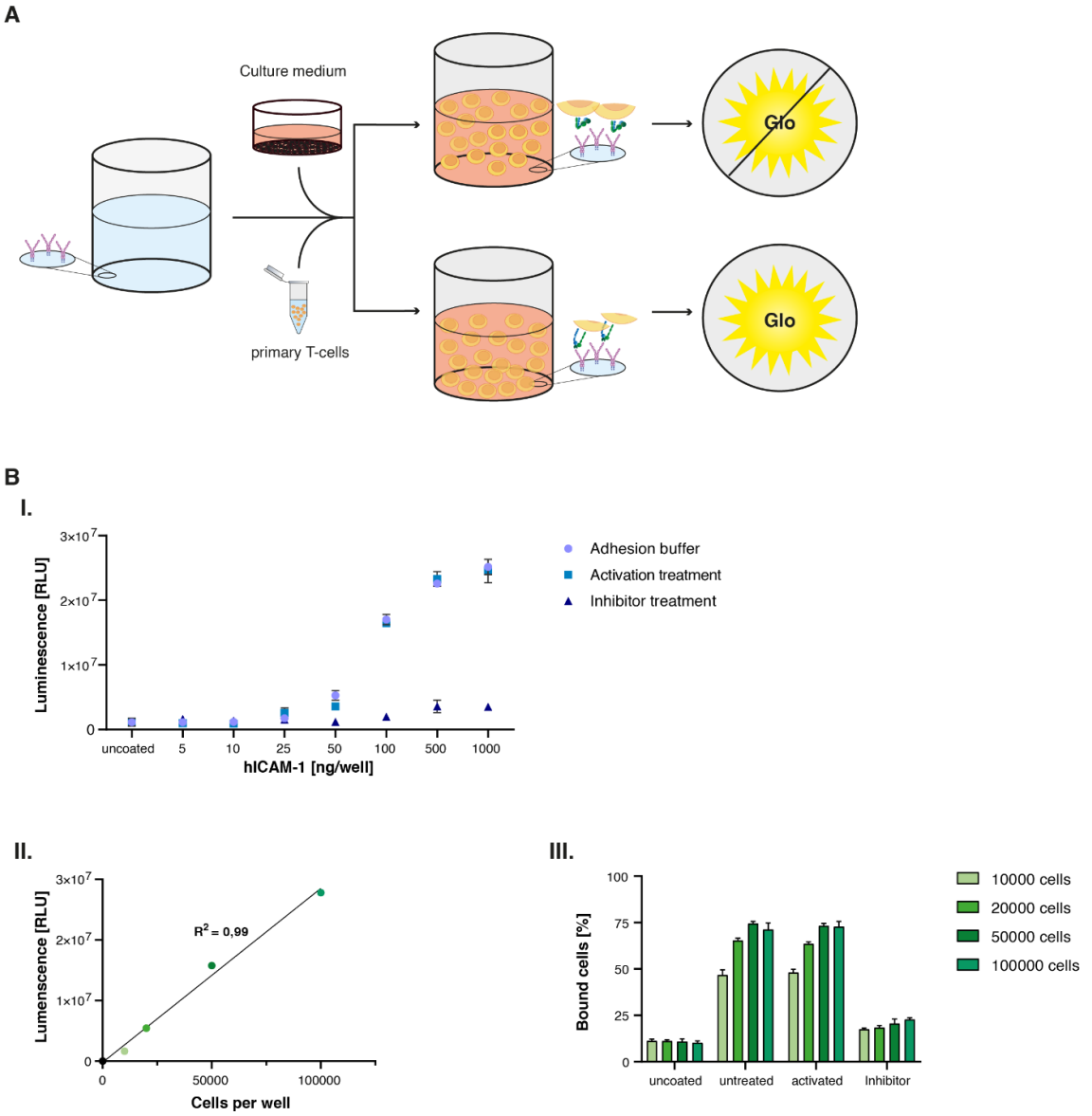

Figure 4-8: Optimization of established in vitro cell adhesion assay. *(**A**) Schematic overview of in vitro cell adhesion assay with new readout. Recombinant hICAM-1-Fc protein is coated on 96 well plates. T cells treated differently are added and after washing steps, the number of bound cells is detected via a luminescent readout induced by the lysis of cells. (**B I.**) **Correlation of T cell binding to hICAM-1 coating.** The T cell binding is dependent on the amount of coated hICAM-1 protein. (**B II.**) **Correlation of luminescence and cell number.** The luminescent signal correlates with the number of T cells added to the wells. (**B III.**) **Quantitative readout of bound cells.** Because of this linear correlation, quantification of bound cells is possible.*

Based on this linear correlation, a quantification of the amount of T cells in each well was possible (**Figure 4-8 B III.**). In the case of activation, when high cell numbers were added, approximately 80 % of the T cells were bound in the well compared to a loading control, which resembled the maximum number of cells added to each well. When T cells were inhibited, the detected signal was comparable to the background

signal, regardless of the number of cells added to each well. There, only 5 – 10 % unspecific binding was detected, which is acceptable compared to the maximum signals obtained. Moreover, the signal of the uncoated background wells did not change with higher numbers of added cells. In general, very low standard deviations were observed in the now optimized *in vitro* cell adhesion assay.

The established and optimized *in vitro* cell adhesion assay was used to investigate the impact of different cancer cell lines on the binding ability of T cells to the hICAM-1 protein, which will be described in the next chapter.

4.3 Downregulation of T cell adhesion induced by different cancer cell lines

Different cancer types generate immunosuppressive tumour microenvironments via, for example, the upregulation of oncogenic signalling pathways and many more mechanisms, which then reduce an effective anti-cancer immune response (**3.1.2**, **3.1.3**). These tumours exclude activated T cells by preventing their infiltration mediated by the interaction of ICAM-1 with LFA-1 (**Figure 4-9**).

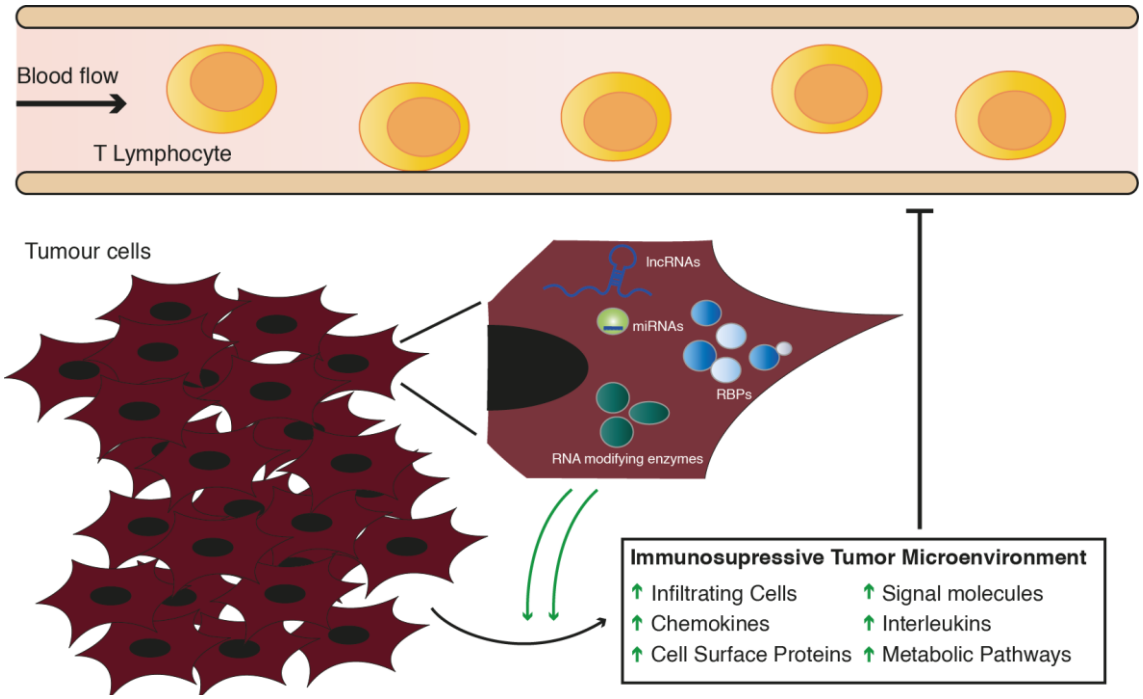

Figure 4-9: Schematic overview of T cell exclusion from tumours. *The immunosuppressive tumour microenvironment (TME) consisting of upregulated signalling pathways, factors like cell surface proteins, chemokines or different immunosuppressive cell types can effectively exclude T cells and prevent infiltration.*

For the investigation whether different cancer cell lines secret molecules that affect T cell adhesion, *in vitro* cell adhesion assays were performed as described above using T cells treated with supernatants of various cell lines. The supernatants of cancer cell lines were tested and compared to their specific growth medium and the supernatant of a non-cancerous control cell line, which both were not expected to contain secreted molecules interfering in T cell binding. Before the primary T cells were added to the wells with immobilized hICAM-1, they were resuspended either in the supernatant of different cell lines cultivated for 48 h or 72 h or in the respective growth medium of the tested cell line. Thereby, T cells were exposed to the conditioned supernatants of

cell lines and medium. This treatment could influence the conformational state of LFA-1, which is the essential parameter for T cell binding (**3.3.2**). As non-cancerous control cell line, the human dermal fibroblast cell line (hDF) was chosen cultured in DMEM medium. The quantification of bound cells was normalized to the specific growth medium of each cell line.

First, the colorectal cancer (CRC) cell lines HCT 116 and HT 29 were tested. Both cell lines were cultured in McCoy medium (**Figure 4-10 A** and **B**).

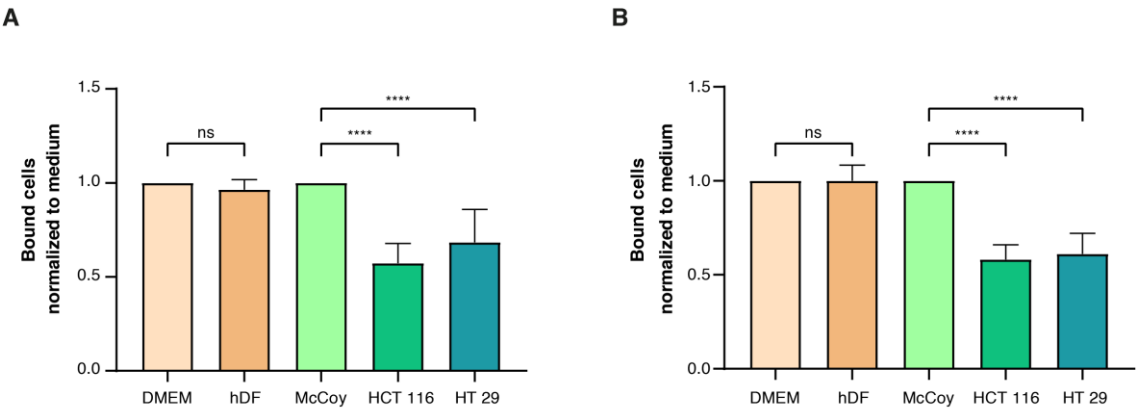

Figure 4-10: Effect of colorectal cancer cell lines on T cell binding. *The supernatants of colorectal cancer cell lines HCT 116 and HT 29 were tested in the in vitro cell adhesion assay and compared to their growth medium McCoy and to the control cell line hDF. (**A**) **Supernatant after 48 h.** Supernatants after culturing cells for 48 h show significant downregulation of T cell binding compared to the control cell line hDF which has no effect on T cell binding. (**B**) **Supernatant after 72 h.** Similar effects are observed with supernatants after 72 h growth. Analyses were performed as biological replicates (n ≥ 10). The mean was calculated and error bars represent the standard deviation.*

The supernatant of both cell lines significantly reduced T cell binding after growing for 48 h and 72 h. The binding efficiency of T cells to the coated hICAM-1 protein was decreased to 50 % compared to the growth medium McCoy. In contrast, the hDF control cell line had no effect on T cell adhesion after normalization to its growth medium DMEM. Standard deviations for all tested conditions were very low, which made the results reliable and reproducible.

As a second cancer type, the three different melanoma cell lines A 375, SK-MEL-28 and MEL-HO were tested in the *in vitro* cell adhesion assay. These cell lines were cultured in DMEM medium without pyruvate referred to as "DMEM ⊖" (**Figure 4-11 A** and **B**).

For the tested cell lines, only the supernatant of A 375 cells showed significant downregulation of T cell adhesion after 48 h and 72 h. After the treatment, only approximately 50 % cells were bound to the coated protein compared to the culture medium DMEM ⊖. No change in the binding efficiency of T cells was detected for the tested cell lines MEL-OH and SK-MEL-28. These showed equal numbers of bound cells compared to DMEM ⊖ medium. The hDF control cell line showed again no change in T cell binding compared to its culture medium as it was expected and already seen before. Also, in these assays the standard deviations are low indicating robust and reliable results.

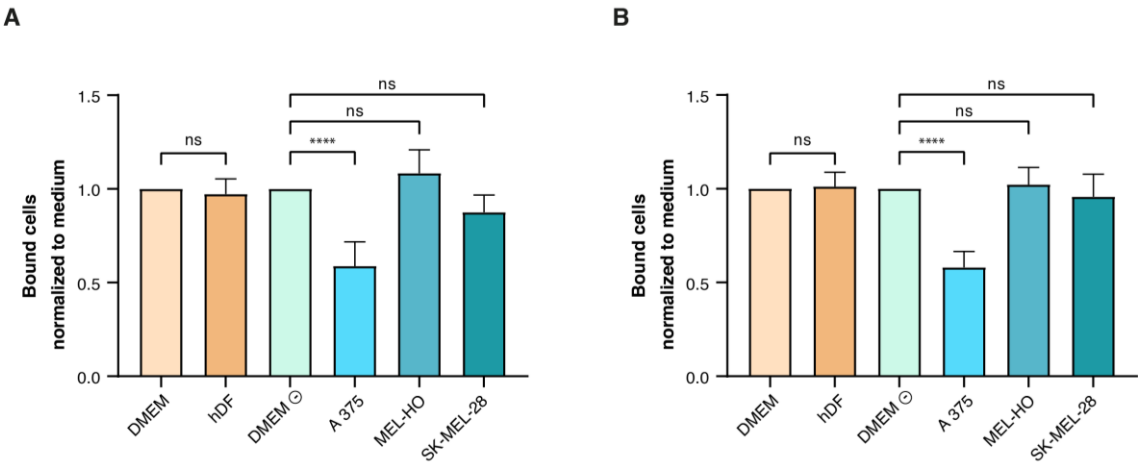

Figure 4-11: Effect of melanoma cell lines on T cell binding. *Supernatants of melanoma cell lines A 375, MEL-HO and SK-MEL-28 were used for in vitro cell adhesion assay and compared to their growth medium DMEM - and to the control cell line hDF. (**A**) **Supernatant after 48 h.** After 48 h, the T cell binding is significantly reduced by the A 375 cell line compared to the controls. The cell lines MEL-HO and SK-MEL-28 show no significant effect in the assay. (**B**) **Supernatant after 72 h.** Similar effects are observed after 72 h in culture. The cell lines hDF, MEL-HO and SK-MEL-28 have no effect on T cell adhesion, whereas A 375 significantly reduces T cell binding. Analyses were performed as biological replicates (n ≥ 3). The mean was calculated and error bars represent the standard deviation.*

Several more cancer cell lines were tested and compared to the control cell line hDF and their growth medium. In this case, the growth medium DMEM was the same for the control and the cancer cell lines. The cell lines A 549 (lung cancer/ NSCLC), PANC-1 (pancreas cancer/ PDAC), Hep G2 (liver cancer/ HCC), HeLa (cervical cancer/ CESC) and MCF7 (breast cancer/ BRCA) were chosen for the experiments (**Figure 4-12 A** and **B**). The supernatants of A 549, PANC-1, Hep G2 and HeLa significantly reduced T cell binding to the coated hICAM-1 protein to different extent. Only the breast cancer

cell line MCF7 showed no significant reduction in the number of bound cells after normalization to the growth medium DMEM. The non-cancerous control cell line hDF had again no effect on T cell binding. As seen for the results before, the very low standard deviations proved reproducibility and reliability of the obtained data.

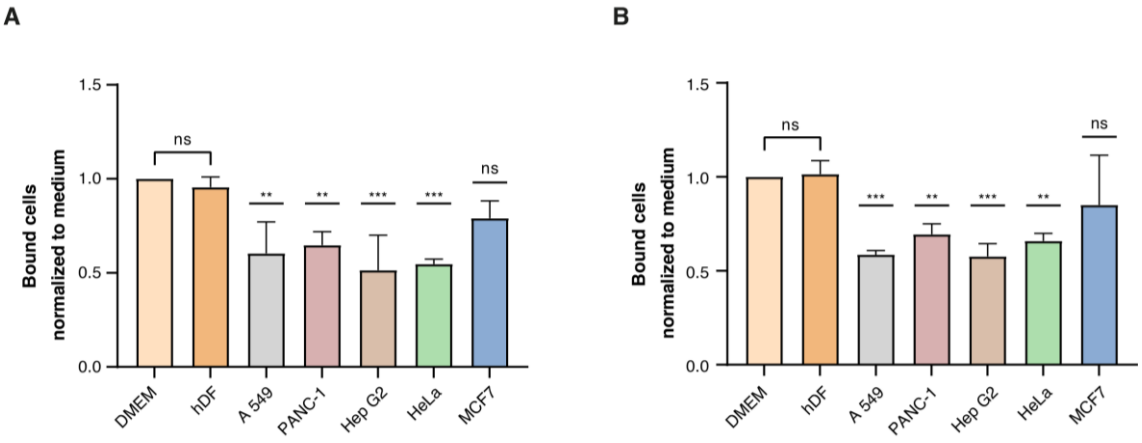

Figure 4-12: Effect of different cancer cell lines on T cell binding. *(A)* ***Supernatant after 48 h.*** *In in vitro cell adhesion assay, the supernatant of A 549 (lung), PANC-1 (pancreas), Hep G2 (liver) and HeLa (cervix) cell lines downregulate T cell binding significantly after growing for 48 h compared to their culture media DMEM and the human hDF control cell line which shows no effect on T cell adhesion. MCF7 cells (breast) have no significant effect on T cell binding (**B**)* ***Supernatant after 72 h.*** *Same effects are observed for the supernatants after culturing cells for 72 h. Analyses were performed as biological replicates (n ≥ 2). The mean was calculated and error bars represent the standard deviation.*

With the established *in vitro* cell adhesion assay, cancer cell line-specific effects on T cell adhesion were detected compared to a non-cancerous control cell line. Most of the tested cell lines showed clear downregulation of T cell binding. For further experiments, the colorectal cancer cell line HCT 116 was chosen. In order to further validate the effects of cancer cell lines detected in *in vitro* cell adhesion assays, the activation state of LFA-1 was analysed by performing LC-AA assays. Results are described in the next chapter.

4.4 Reduced activation of LFA-1 caused by tissue culture supernatants

The previously performed experiments demonstrated that T cell binding could be monitored *in vitro* by cell adhesion assays which are based on the interaction of the integrin LFA-1 and the adhesion molecule ICAM-1 (**4.2**). Moreover, this interaction

could be influenced by tissue culture supernatants, especially by cancer cell supernatants, which downregulated T cell binding in this assay (**4.3**). These results suggest that the supernatants of cancer cell lines effectively impair the binding of LFA-1 to ICAM-1. Because LFA-1 is activated via inside-out signalling inducing a conformational change (**3.3.3**), the question arises if this mechanism is inhibited by cancer cell supernatants, hence keeping LFA-1 in its inactive form and preventing binding to its ligand ICAM-1.

To address this question, LC-AA assays were performed, which were able to specifically determine the conformational state of LFA-1 via fluorescence activated cell sorting (FACS). LFA-1 activation was checked in HCT 116 cells and compared to the growth medium McCoy. Additionally, the cell lines MCF7 and SK-MEL-28 were tested and compared to their growth medium DMEM. These cell lines were chosen as control cell lines because, in previously performed cell adhesion assays, they did not have significant effects on T cell binding (**Figure 4-11**; **Figure 4-12**).

For the LC-AA assay, peripheral blood mononuclear cells (PBMCs) were used, which were isolated from whole blood beforehand and cultured in RPMI medium until further use. In order to distinguish different cell populations by FACS, $CD3^+$ cells, $CD4^+$ cells, $CD8^+$ cells and ICAM-1c protein were labelled with different fluorescent dyes. Labelling dyes were mixed in LC-AA basic buffer and supplemented with 4 mM $MgCl_2$ and TCR activator to ensure complete activation of LFA-1. PBMCs were treated with either growth media or cancer cell supernatants and then mixed in a 1:1 ratio with the labelling mix. After incubation, cells were fixed with 4 % PFA, transferred to a V-bottom plate, washed with 1x PBS and then measured with a flow cytometer. Because the ICAM-1c protein was tagged with a fluorescent dye, only the cells with active LFA-1, which have bound the labelled ICAM-1c, were detected in the measurements as the "mean fluorescence intensity" (MFI) of active LFA-1 (LFA-1a+ [MFI]). In addition to the MFI, the percentage of cells with fully activated LFA-1 was determined (LFA-1a+ [%]).

For HCT 116 cells, only small differences were identified comparing the supernatant to the growth medium (**Figure 4-13**). In the cancer cell supernatant, less cells with activated LFA-1 were detected compared to the growth medium McCoy. For both, $CD8^+$ and $CD4^+$ cells, the MFI was lower which indicated less cells have bound the

labelled ICAM-1c protein (**Figure 4-13 A I.**). Once the counts were normalized to the medium, approximately 20 % less CD4⁺ and CD8⁺ cells were detected in the cancer cell supernatant. This indicated lower activation of LFA-1 in the HCT 116 supernatant than in the growth medium (**Figure 4-13 A II.**).

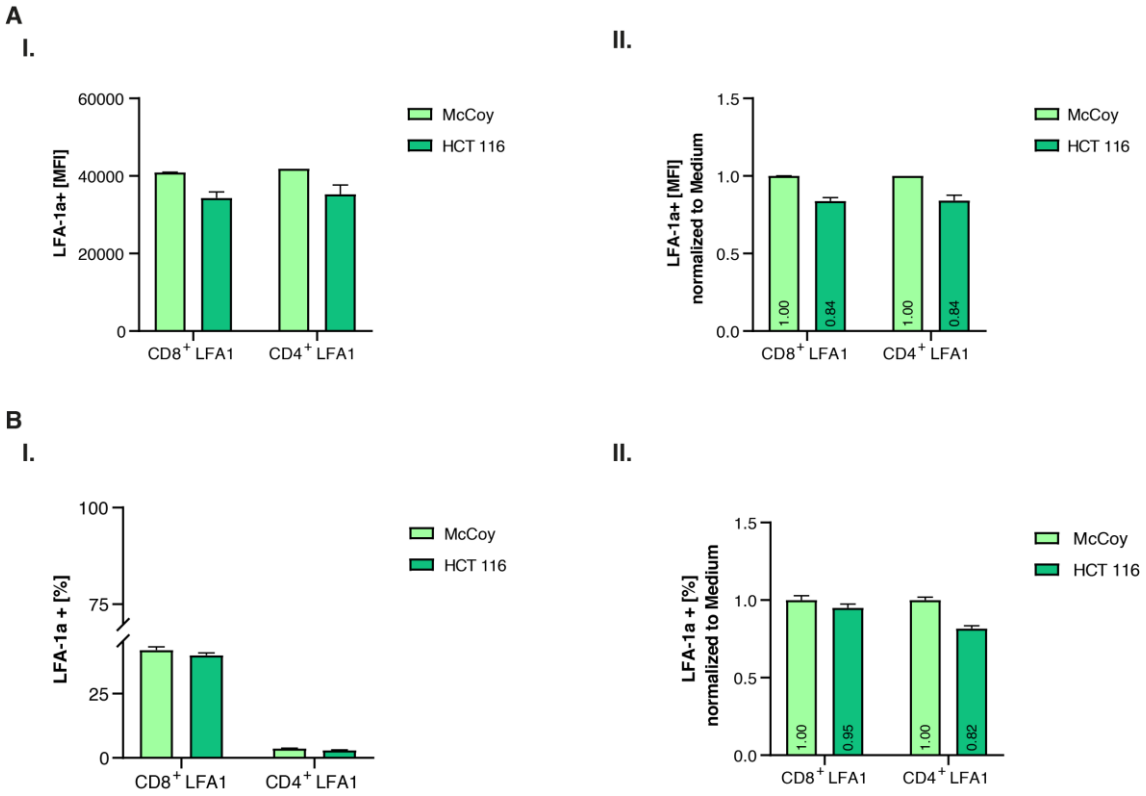

Figure 4-13: Quantification of T cell populations with active LFA-1 in McCoy and HCT 116 by LC-AA assay. *(**A I**) **Effects of McCoy and HCT 116 on active LFA-1.** The MFI indicates lower cell numbers with active LFA-1 in cancer cell supernatant compared to the growth medium. (**A II**) **Normalization of detected signals of McCoy and HCT 116.** After normalization to the McCoy medium, a 20 % decrease is verified in HCT 116 supernatants. (**B I**) **Effects of McCoy and HCT 116 on ratio of active LFA-1.** The ratio of cells with active LFA-1 is way lower for CD4⁺ cells compared to CD8⁺ cells. A maximum of 30 % cells containing active LFA-1 indicates already inhibitory effect of the growth medium. (**B II**) **Normalization of detected ratios for McCoy and HCT 116.** After normalization, a small decrease of LFA-1 activation is detected for the cancer cell supernatant for CD8⁺ cells. An even lower LFA-1 activation level is measured for CD4⁺ cells which is not reliable based on the low cell numbers detected.*

When the ratio of active LFA-1 containing cells was tested, less CD4⁺ cells were detected by FACS than CD8⁺ cells. In only around 4 % of the CD4⁺ T cell population LFA-1 was detected in its active conformation, whereas almost 30 % of the CD8⁺ cells showed LFA-1 activation. But overall, these low cell numbers already indicated major inhibitory effects of the growth medium McCoy, which could make it difficult to detect

differences in LFA-1 activation levels in cancer cell supernatants versus medium. Unfortunately, almost no difference could be seen between medium and HCT 116 supernatant (**Figure 4-13 B I.**). After normalization to the McCoy medium, a 5 % decrease of LFA-1 activation was detected for the $CD8^+$ T cell population in the cancer cell supernatant. For $CD4^+$ cells, this decrease was almost 20 % though this ratio was not reliable based on the low cell number detected (**Figure 4-13 B II.**).

Comparing the chosen control cell lines to their growth medium, the results were similar to the observed effects of HCT 116 cell supernatant (**Figure 4-14**).

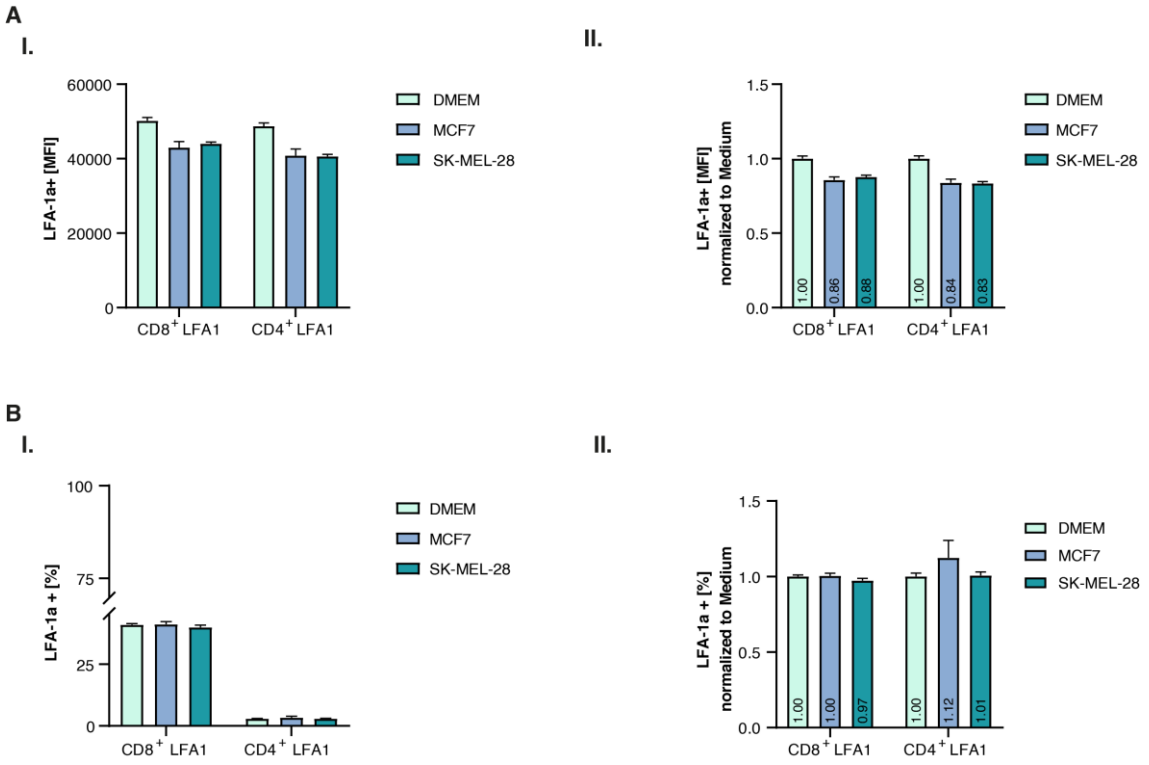

Figure 4-14: Quantification of active LFA-1 T cell populations in DMEM and control cell lines MCF7 and SK-MEL-28 by LC-AA Assay. *(**A I**) **Effect of DMEM and control cell lines on active LFA-1.** The MFI indicates lower cell numbers with activated LFA-1 in the MCF7 and SK-MEL-28 cell supernatant compared to the growth medium DMEM. (**A II**) **Normalization of detected signals of DMEM and control cell lines.** After normalization to the medium, a 20 % decrease is verified in the supernatants of chosen control cell lines. (**B I**) **Effects of DMEM and control cell lines on ratio of active LFA-1.** The ratio of cells with active LFA-1 was with 4 % very low for $CD4^+$ cells compared to $CD8^+$ cells with maximum of 30 % cells containing active LFA-1. This indicates already inhibitory effect of the growth medium. (**B II**) **Normalization of detected ratios for DMEM and control cell lines.** After normalization, no decrease of LFA-1 activation is detected for $CD8^+$ cells and $CD4^+$ cells treated with the cancer cell supernatants.*

Only minor differences were identified between the growth medium DMEM and the control cell lines MCF7 and SK-MEL-28. For the supernatants, the amount of detected $CD4^+$ and $CD8^+$ cells with activated LFA-1 were similar to each other and lower compared to the detected cells in the DMEM growth medium (**Figure 4-14 A I.**). After normalization, 20 % less cells were detected in the cancer cell supernatants containing activated LFA-1 with bound ICAM-1c (**Figure 4-14 A II.**).

As already seen for HCT 116 cells, the ratio of cells showing activated LFA-1 was lower for $CD4^+$ cells than for $CD8^+$ cells. LFA-1 activation was identified for approximately 4 % of the $CD4^+$ cell population in contrast to around 30 % of the $CD8^+$ cell population (**Figure 4-14 B I.**). These low cell numbers indicated major inhibitory effects induced by the DMEM growth medium, which made it difficult to detect lower LFA-1 activation levels in cancer cell supernatants as it was already seen before (**Figure 4-13**). After normalization, there was very low or no difference between control cell line supernatants and growth medium in the $CD8^+$ and $CD4^+$ cell population (**Figure 4-14 B II.**).

In contrast to MCF7 and SK-MEL-28, in the HCT 116 supernatant, at least a small reduction of LFA-1 activation was overserved in both cell populations, $CD4^+$ and $CD8^+$. These results indicated a partial inhibition of LFA-1 activation induced by the HCT 116 cell line compared to the control cell lines MCF7 and SK-MEL-28. But the detected differences were very weak and potentially insignificant.

In conclusion, LC-AA assays did not show inhibition of LFA-1 in cancer cell supernatants compared to growth medium. The very low cell numbers, which could be measured, indicated already inhibitory effects of the DMEM and McCoy growth media, which made it very difficult to observe LFA-1 inhibition in the cancer cell supernatants. The experimental setup and protocol need to be optimized in order to monitor LFA-1 activation in cell culture supernatants and gain reliable results.

Because of the difficulties and inconclusive results obtained by LC-AA measurements using cancer cell supernatants, we did not proceed with this approach. Still, in cell adhesion assays a decreased binding of T cell to ICAM-1was detected using cancer cell supernatants (**4.3**). Therefore, we decided to focus further experiments on this approach.

4.5 Analysis of T cell binding in cancer cell lines after siRNA knockdown experiments

In order to further investigate whether RNA pathway components are involved in the reduced binding affinity of T cells to ICAM-1 after treatment with cancer cell supernatants in cell adhesion assays, RNAi knockdown experiment of such factors was performed. With the knockdown of RPBs, RNA modifying enzymes or miRNA pathway components, we hypothesize that the tumour microenvironment is changed to a less immunosuppressive state and T cell binding and infiltration can be restored to a certain extent (**Figure 4-15**).

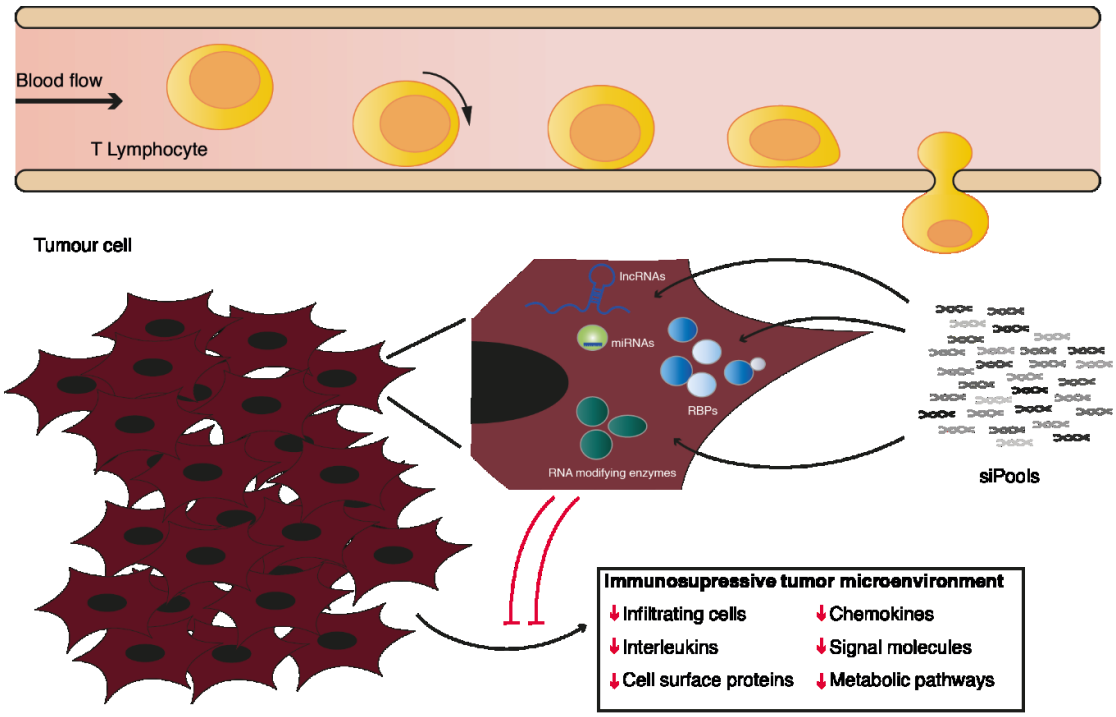

Figure 4-15: Schematic overview of RNAi knockdown approach to restore T cell infiltration. *By performing RNAi knockdown experiments of specific targets in cancer cells, which were identified to downregulate T cell binding in in vitro cell adhesion assays, the immunosuppressive state of the tumour microenvironment could be reduced, and T cell infiltration could be restored to some extent. Potential targets are RBPs, RNA modifying enzymes or factors involved in the miRNA pathway.*

As a general measure, we first tested if T cell binding could be restored by a RNAi knockdown of known oncogenes in the before validated cancer cell lines (**4.3**). For these experiments, the CRC cell lines HCT 116 and HT 29 and the melanoma cell line A 375 were transfected with specific siPOOLs directed against CTNNB1, STAT3 and ATF3 and overexpression constructs of the same targets for 48 h and 72 h. These

molecules are drivers of oncogenic signalling pathways known to be involved in the exclusion of T cells from tumours (**3.1.3**). Used siPOOLs contained 30 different siRNAs targeting the same mRNA and thereby reduce potential off-target effects, often observed when single siRNAs are used. Overexpression constructs were expressed with a Flag/HA (F/HA) tag and a strong promotor to ensure high protein levels. Six hours after transfection, the medium was changed and after incubation for the estimated timepoints, cell adhesion assays were performed with primary T cells treated with the supernatants of transfected cancer cell lines. The effects of the supernatants on T cell binding were analysed and normalized to a scrambled siRNA control (siCtrl). The cancer cells were harvested to check knockdown and transfection efficiency of the siPOOLs and overexpression constructs.

4.5.1 Increase of T cell binding in colorectal cancer cell line HCT 116 by CTNNB1 siRNA knockdown

In HCT 116 cells, the three tested targets CTNNB1, STAT3 and ATF3 induced different effects on T cell binding to hICAM-1 protein upon overexpression and siRNA knockdown (**Figure 4-16**). The control siPOOL (siCtrl) did not impact T cell adhesion compared to wildtype (WT) and therefore was a valid control for normalization. Both, WT and siCtrl showed significant downregulation of T cell binding when compared to the growth medium McCoy. For all tested conditions, the standard deviations were small, although for the 72 h timepoint, they were higher than for 48 h after transfection.The most significant effects were detected for the target CTNNB1 (**Figure 4-16 A**). After 48 h, the overexpression of the protein significantly decreased T cell binding after normalization to the control siCtrl transfection. The knockdown of CTNNB1 on the other hand showed an increase in T cell binding of up to 25 %. A similar effect was seen after 72 h. Although the effects were not significant anymore because of high standard deviations, T cell binding to coated hICAM-1 protein appeared to be block by the overexpression and increased upon siRNA knockdown. These results were expected based on the current knowledge of CTNNB1 (**3.1.3.1**) and underscores the suitability of our assay to identify factors regulating T cell binding.

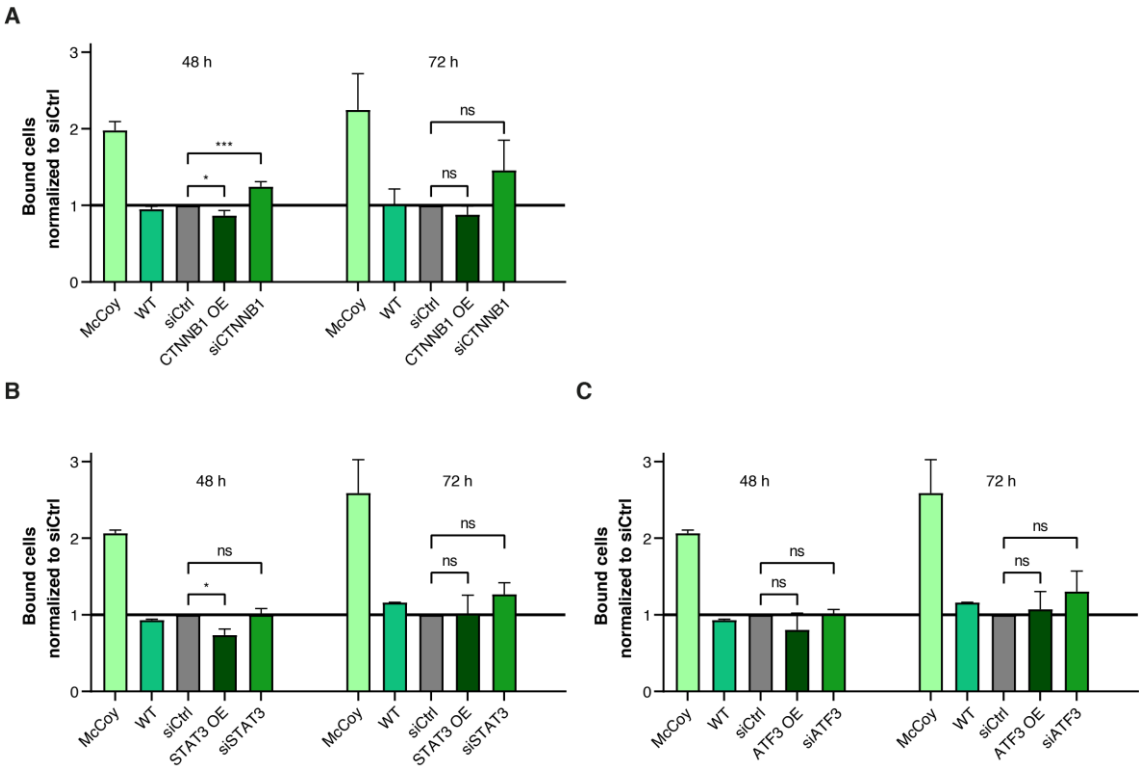

Figure 4-16: Validation of RNAi knockdown approach in HCT 116 cells*. The effects of CTNNB1, STAT3 and ATF3 were tested by overexpression and siRNA knockdown in HCT 116 cells followed by cell adhesion assay. (**A**) **Impact of CTNNB1 on T cell binding.** After 48 h, CTNNB1 (beta catenin) shows significant downregulation of T cell binding by overexpression and significant upregulation of T cell adhesion after siRNA knockdown. The effect is weaker after 72 h but the upregulation is still detected. (**B**) **Impact of STAT3 on T cell binding.** For STAT3, the overexpression decreases T cell binding after 48 h, but not after 72 h. The siRNA knockdown does not show a significant effect. (**C**) **Impact of ATF3 on T cell binding.** The overexpression and siRNA knockdown of ATF3 does not show significant effects on T cell binding. Analyses were performed as biological replicates (n ≥ 3). The mean was calculated, and error bars represent the standard deviation.*

The effects for STAT3 were not as strong as for CTNNB1 (**Figure 4-16 B**). Although after 48 h, the overexpression of the protein decreased T cell adhesion significantly, the knockdown did not induce increased T cell binding. After siRNA knockdown for 72 h, more T cells seemed to have bound after normalizing to the siCtrl, but the effect was not significant. The decrease of T cell binding by overexpression of STAT3 was not detected anymore for the 72 h timepoint.

For ATF3 overexpression and siRNA knockdown, the obtained results were similar to the effects detected for STAT3 (**Figure 4-16 C**). After 48 h, the overexpression of the target decreased T cell binding to some extent, but not significantly due to high

standard deviations. The knockdown did not show any effect. For the 72 h timepoint, the siRNA knockdown slightly increased T cell adhesion, but the effect of the overexpression was not detected anymore. To further validate and confirm detected effects of the differently treated cancer cells in the cell adhesion assays, the siRNA knockdown efficiency was validated by qPCR and the overexpression was checked by Western Blot for all three targets (**Figure 4-17**)

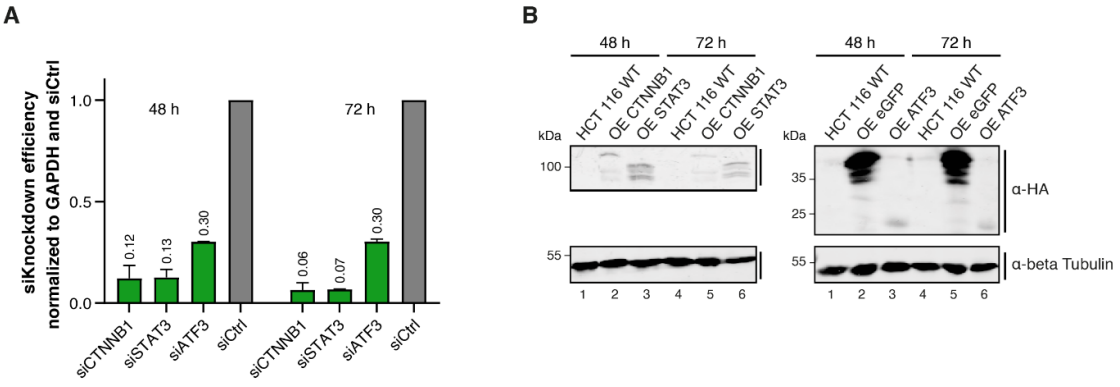

Figure 4-17: Validation of siRNA knockdown and overexpression efficiency. *(A)* ***siKnockdown efficiency.*** *siKnockdown efficiency of tested targets was determined via qPCR and analysed with the $\Delta\Delta C_T$ method. The knockdown after 48 h and 72 h is very efficient which leaves only 10-30 % remaining mRNA. Analyses were performed as biological replicates (n ≥ 3). The mean was calculated and error bars represent the standard deviation. (**B**)* ***Overexpression efficiency.*** *The overexpression of tested targets was checked via Western Blot and detected via an α-HA antibody. Targets are expressed at low levels due to low transfection efficiency in HCT 116 cells. Equal loading is detected with α-beta Tubulin antibody. (CTNNB1 = 92 kDa; STAT3 = 88 kDa; ATF3 = 23 kDa; eGFP = 37 kDa; Tubulin = 50 kDa).*

The siRNA knockdown for 48 h and 72 h was highly efficient (**Figure 4-17 A**). The knockdown of CTNNB1 and STAT3 reduced the amount of mRNA to great extent with approximately 10 % remaining. For ATF3, the siRNA knockdown was not as efficient as for the other targets with 30 % remaining mRNA. The Western Blot for validation of overexpressed constructs indicated only low transfection efficiency for all three targets (**Figure 4-17 B**). For both timepoints, weak signals were detected for CTNNB1, STAT3 and ATF3 using an α-HA antibody against the F/HA tag of the constructs. Moreover, the detected signals got weaker from 48 h to 72 h. Only the control transfection of an eGFP construct showed high expression of the protein. The loading control beta-Tubulin proved equal loading of the samples. Therefore, overexpression effects observed in the adhesion assay could still be unspecific or were in the noise range.

4.5.2 Minor effects on T cell binding in colorectal cancer cell line HT 29 after CTNNB1 siRNA knockdown

In the colorectal cancer cell line HCT 116 the T cell binding appeared to be restored to some extent after knockdown of CTNNB1. To further support these results, the effect of CTNNB1 knockdown and overexpression was validated in the second colorectal cancer cell line HT 29 (**Figure 4-18**). This cell line also showed a downregulation of T cell binding in the previously performed cell adhesion assay (**Figure 4-10**). The siRNA knockdown experiment was performed with the same setup as described above (**4.5**).

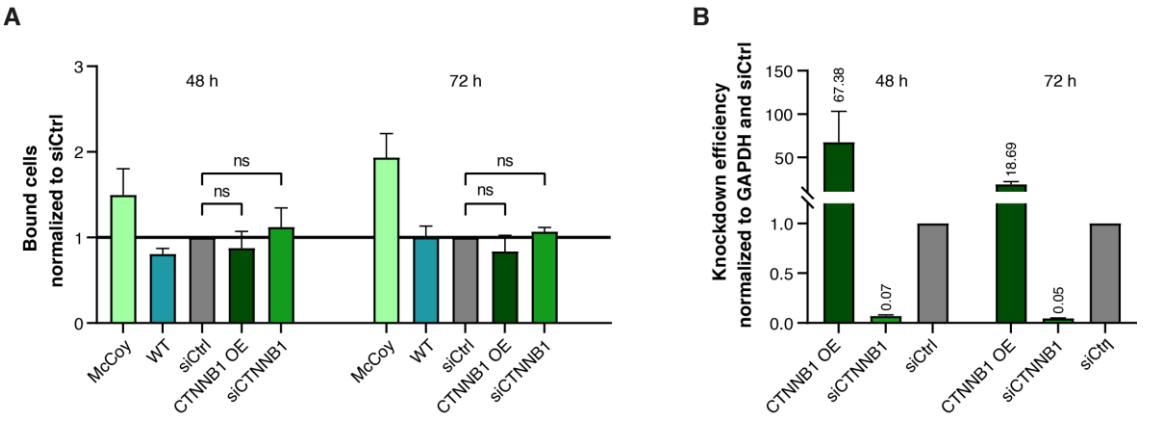

Figure 4-18: Validation of the effect of CTNNB1 on T cell biding in HT 29 cells. *The effect of CTNNB1 was tested by overexpression and siRNA knockdown in HT 29 cells followed by cell adhesion assay.* ***(A) Impact of CTNNB1 on T cell binding.*** *After 48 h, CTNNB1 (beta catenin) shows slight downregulation of T cell binding by overexpression and a small upregulation of T cell adhesion after siRNA knockdown. The same tendency is detected after 72 h but the effects are smaller. All detected effects are not significant.* ***(B) Transfection efficiency.*** *The transfection efficiency was validated via qPCR and analysed by $\Delta\Delta C_T$ method. Overexpression shows increased levels of CTNNB1 after normalization to siCtrl. The siRNA knockdown is highly efficient. Analyses were performed as biological replicates ($n \geq 2$). The mean was calculated, and error bars represent the standard deviation.*

In HT 29 cells, the effects of siRNA knockdown and overexpression indicated the same tendency to the ones detected for HCT 116 cells, but they were not significant (**Figure 4-18 A**). However, already the siCtrl showed higher T cell binding compared to the WT, which made this control less reliable for normalization. The overexpression showed slight downregulation of T cell binding whereas the siRNA knockdown slightly increased the T cell adhesion. Comparing the results to WT instead of the siCtrl, the binding of T cells was significantly increased after

transfection for 48 h. The detected effects at the 72 h timepoint were even weaker. Here, the siCtrl had no effect on T cell binding compared to WT and was a valid control for normalization. Nevertheless, neither knockdown nor overexpression induced a significant effect in the cell adhesion assay.

Because performed Western Blots did not show any signals for successful transfection (data not shown), overexpression as well as knockdown of CTNNB1 were checked via qPCR (**Figure 4-18 B**). The overexpression could be detected by qPCR, but results indicated low transfection efficiency of CTNNB1 after overexpression, which could explain the missing signals in Western Blots. The expression even decreased at the 72 h timepoint. In contrast, the siRNA knockdown for 48 h and 72 h was highly efficient. The CTNNB1 knockdown led to not even 10 % remaining mRNA. The low transfection efficiencies could explain the mild effects detected in the adhesion assay. Still, both colorectal cancer cell lines HCT 116 and HT 29 showed similar effects induced by CTNNB1.

4.5.3 Controversial effects on T cell binding in melanoma cell line A 375 after siRNA knockdown

Because the supernatant of the melanoma cell line A 375 also reduced T cell binding significantly, the effects of all three targets CTNNB1, STAT3 and AFT3 were validated after overexpression and knockdown by performing cell adhesion assays, as described above (**4.5**) (**Figure 4-19**).

In contrast to the colorectal cancer cell lines, none of the checked targets showed significant effects on T cell binding in the cell adhesion assays. For all targets, the siCtrl already increased T cell binding compared to WT. Therefore, the results after 48 h were not reliable. The effect of the siRNA control was lost after 72 h, which made these results more plausible.

Keeping this in mind and considering the results with caution, CTNNB1 could be a promising target in A 375 cell line as seen in HCT 116 cells as well (**Figure 4-19 A**). At 48 h, a clear difference between overexpression and knockdown was detected. Comparing the results to WT, T cell binding upon knockdown was upregulated up to 25 %. The overexpression induced a 15 % decrease in T cell binding after normalizing

to the siCtrl. But because also the signal for WT was lower after normalization, this effect is unspecific. The effects for overexpression and knockdown were not detected anymore after 72 h.

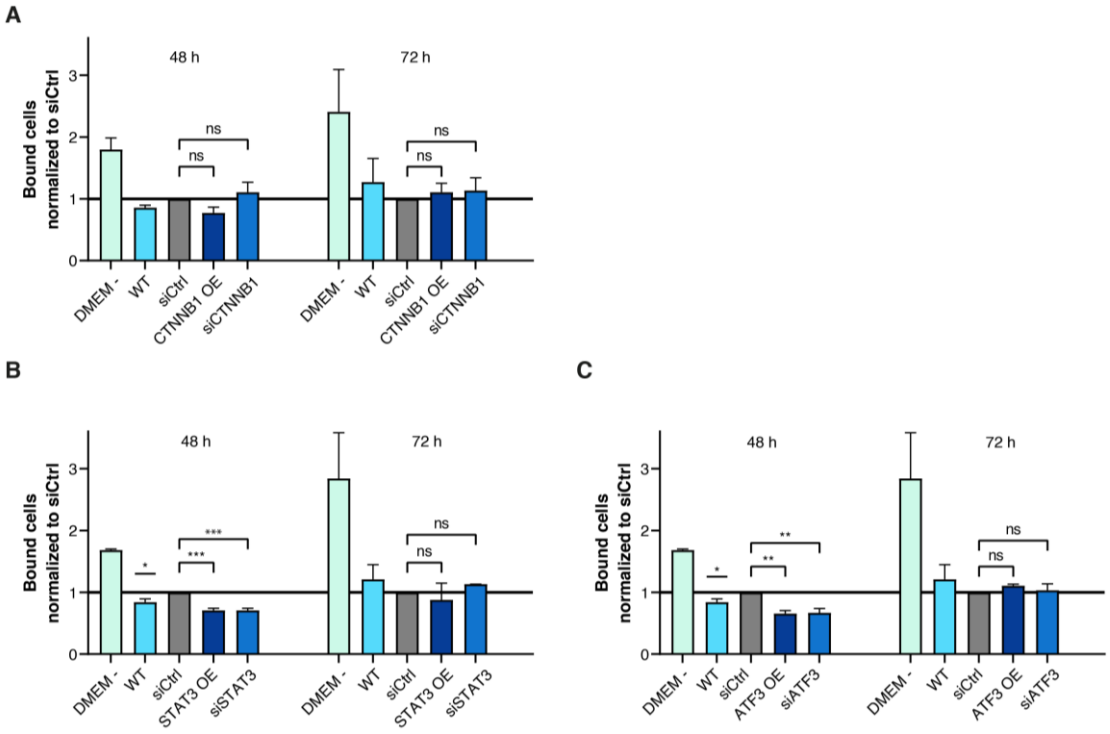

Figure 4-19: Validation of RNAi knockdown approach in A 375 cells. *The effect of different potential controls was tested by overexpression and siRNA knockdown in A 375 cells followed by cell adhesion assay.* ***(A) Impact of CTNNB1 on T cell binding.*** *After 48 h, CTNNB1 (beta catenin) shows downregulation of T cell binding by overexpression and slight upregulation of T cell adhesion after siRNA knockdown, but not significant. The effects are not detected after 72 h.* ***(B) Impact of STAT3 on T cell binding.*** *For STAT3, after 48 h the siRNA knockdown of the control decreases T cell binding significantly. Therefore, measured downregulation after overexpression and siRNA knockdown are not reliable. After 72 h this effect is gone.* ***(C) Impact of ATF3 on T cell binding.*** *For ATF3 similar effects are observed as for STAT3. After 48 h, the obtained results are not reliable, after 72 h no effects are detected. Analyses were performed as biological replicates (n ≥ 3). The mean was calculated, and error bars represent the standard deviation.*

When looking closer at the targets STAT3 and ATF3, for the 48 h timepoint, the knockdown of siCtrl induced a significant increase in T cell binding compared to WT (**Figure 4-19 B** and **C**). Additionally, overexpression and knockdown of both targets had the same effects and seemed to reduce T cell binding. Because of the undependable control, the obtained results for the A 375 cell line were not reliable. The effects detected at 48 h were lost after 72 h. There, the control did not have an impact on T cell binding compared to WT, which made the results more plausible. Still,

neither knockdown nor overexpression showed an effect on T cell adhesion in the assays.

The siRNA knockdown efficiency was validated via qPCR and the transfection efficiency of overexpression constructs was checked by Western Blot (**Figure 4-20**).

After 48 h, the knockdown efficiency of all three targets was low and very variable. Except CTNNB1, there was still up to 50 % remaining mRNA detected. After 72 h, the knockdown was comparable to the results obtained for HCT 116 cells. There, approximately 15-30 % remaining RNA was detected (**Figure 4-20 A**).

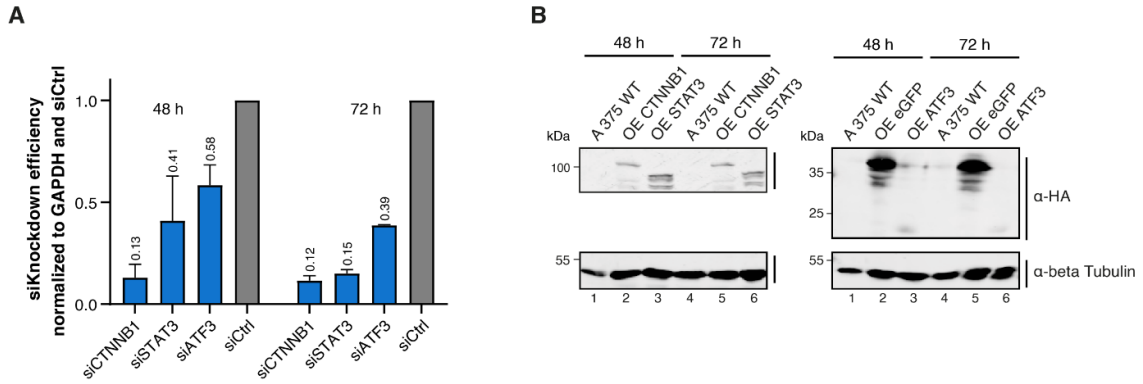

Figure 4-20: Validation of siKnockdown and overexpression efficiency in A 375 cells. *(A)* ***siKnockdown efficiency.*** *siKnockdown efficiency of tested targets was determined via qPCR and analysed with the $\Delta\Delta C_T$ method. The knockdown after 48 h with about 15-50 % is less efficient compared to 72 h which leaves 10-30 % remaining mRNA. Analyses were performed as biological replicates (n ≥ 3). The mean was calculated and error bars represent the standard deviation. (**B**)* ***Overexpression efficiency.*** *Overexpression of tested targets was checked via Western Blot and detected via an α-HA antibody. Targets are expressed at low levels due to low transfection efficiency in A 375 cells. Equal loading is detected with α-beta Tubulin antibody. (CTNNB1 = 92 kDa; STAT3 = 88 kDa; ATF3 = 23 kDa; eGFP = 37 kDa; Tubulin = 50 kDa).*

The Western Blot to check the overexpression of the targets showed a similar pattern as seen for HCT 116 cells (**Figure 4-20 B**). For both timepoints, only weak signals were detected for all targets using an α-HA antibody binding the F/HA tag of the constructs. However, the detected signals did not change from 48 h to 72 h and looked similar. Only for the eGFP control, high expression was induced after overexpression at 48 h and 72 h. Equal loading of all samples was verified by using a beta-Tubulin antibody.

In summary, by performing siRNA knockdown of CTNNB1 in colorectal cancer cell lines HCT 116 and HT 29, the effect of reduced T cell binding affinity to coated hICAM-

1 protein could be restored to some extent. Additionally, for HCT 116, the overexpression of CTNNB1 induced an even higher decrease in T cell adhesion compared to WT. These results were expected based on the current knowledge of CTNNB1 acting as driver of the oncogenic Wnt/β-catenin signalling pathway (**3.1.3.1**). Therefore, CTNNB1 is a valid positive control for our theory that by using siRNAs in order to knockdown specific factors in cancer cells, T cell binding can be restored *in vitro*. Moreover, our data supports the hypothesis that by targeting specific RNA-regulatory pathways in the tumour, the immunosuppressive state of the microenvironment could be changed and T cell binding can be restored as well. As next step, to identify such RNA-regulatory pathways and validate their impact on T cell binding, a RNAi screening was designed and performed. The results for the primary screening of some targets are described in more detail below.

4.6 Design of RNAi screening approach for the identification of potential immune regulators involved in T cell infiltration

After the successful proof that RNAi knockdown of specific targets can restore T cell binding in the *in vitro* cell adhesion assay, an RNAi screening approach was designed. With this screening we aimed to identify RNA-based regulatory pathways, including specific RBPs or RNA modifying enzymes, which might be involved in the reduced binding affinity and hence the exclusion of T cells from tumours. Therefore, siRNA knockdown of several different targets with specifically designed siPOOLs was performed in HCT 116 cells in a 96 well format and 6 h after transfection the medium was changed. 48 h after the transfection, cell adhesion assays were performed with primary T cells treated with the supernatants of the transfected cancer cells. The transfected cancer cells were harvested to validate siRNA knockdown efficiency and viability of cells after transfection. Viability was checked using the CellTiter-Glo® reagent, which was also used as readout of the cell adhesion assay. Both, siRNA knockdown efficiency and viability were essential parameters to determine whether induced effects could be positive hits or false positives. Analyses were performed in biological replicates. For the screening, a RNAi library targeting approximately 700 different RBPs was generated by siTOOLs Biotech GmbH (Planegg, Germany). The

library was arranged on 96 well plates using a specific layout, which resulted in 86 different siPOOLs on one plate with a total number of eight plates.

Nevertheless, to verify and ensure that the idea and the design of this particular RNAi screening approach in the 96 well format is working, as a first step only one library plate was used for transfection followed by the cell adhesion assay. The primary screening of this plate was performed in biological replicates and potential hits were identified and selected for further validation and detailed analyses.

4.6.1 Identification of potential targets in primary RNAi screening

The primary screening of the first library plate was performed in biological replicates and normalized to the siRNA control transfection (**Figure 4-21**). Additionally, the growth medium McCoy and WT were included as control treatments and proved that the cell adhesion assays worked and were reliable. These conditions are not represented in the screening overview figure.

The results of the primary screening clearly showed that after normalization most of the tested targets scattered around the level of the siRNA control (siCtrl) and did not have a specific effect on the binding efficiency of the T cells in the *in vitro* cell adhesion assays (**Figure 4-21 A, grey** and **black**). However, the siRNA knockdown of some of the targets seemed to induce an increase in T cell adhesion compared to siCtrl knockdown (**Figure 4-21 A, red**). It is worth to mention, that LIN28A was one of the targets included on the library plate and had no effect on T cell adhesion. This was expected because the protein is not expressed in HCT 116 cells (Parisi et al. 2021) (**Figure 4-21 A, black**). Interestingly, the knockdown of SRRM4 induced a slight increase of T cell binding in the screening, although this target is most likely not expressed in HCT 116 cells as well (Uhlén et al. 2015) *Human Protein Atlas;* proteinatlas.org) (**Figure 4-21 A, purple**). Hence, the increase in T cell binding caused by this target was used as a threshold to exclude potential false positive hits of the primary screening. When organizing the targets of the siRNA library plate based on their molecular functions, most of the potential hits are involved in mRNA splicing or the nucleocytoplasmic transport (**Figure 4-21 B, red** and **blue star**). But not every splice factor showed an increase in T cell binding. Most of them had no effect at all or

were close to the set threshold. Therefore, these factors were excluded from the list of potential hits.

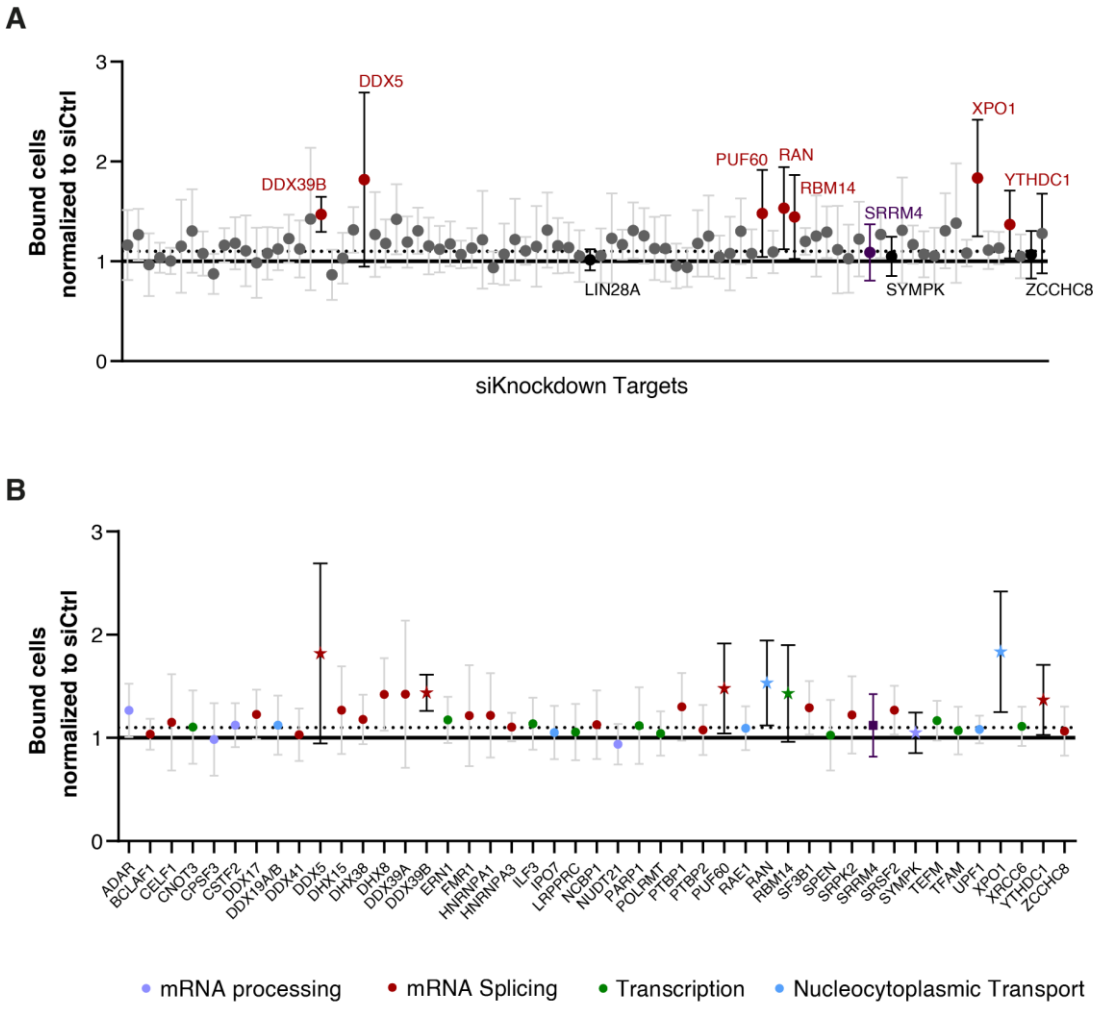

Figure 4-21: Primary screening results of RBP siPOOL library. *(A)* ***Primary screening results of RNAi screening approach.*** *siRNA knockdown of in total 86 different RBPs with specific siPOOLs was performed followed by cell adhesion assay 48 h after transfection. Bound cells were normalized to siCtrl transfection. While most of the targets show no increase (examples in* ***black****), some show clear enrichment in T cell binding (in* ***red****). Because SRRM4 is not expressed in HCT 116 cells, a threshold can be set at the level of this target (in* ***purple****). (B)* ***GO-Term analysis of targets of primary screening.*** *Based on GO-Term analysis, the siRNA knockdown of splicing factors (in* ***red****) and nucleocytoplasmic transport (in* ***blue****) is likely to be able to increase T cell binding. Analyses were performed as biological replicates (n ≥ 3). The mean was calculated, and error bars represent the standard deviation.*

Moreover, some factors of the library plate are known to be involved in other mRNA processing processes and transcription. These seemed to have minor impact on T cell binding (**Figure 4-21 B, lilac**). Only RBM14 induced an increase in T cell binding in the screening (**Figure 4-21 B, green star**). Therefore, the results of the primary

screening indicated that in general siRNA knockdown of factors involved in mRNA localization and processing, but most importantly in RNA splicing, was able to restore T cell binding.

Based on the results of the primary screening, some potential hits could be identified (**Figure 4-22 A**, **red, blue** and **green**). In the screening, the siRNA knockdown of DDX5 and XPO1 significantly increased T cell binding. Some other targets like PUF60 and YTHDC1 had a similar effect, but to a lower extent. On the other hand, some of the tested factors did not have any impact on T cell binding like the polyadenylation factor SYMPK for example (Kolev and Steitz 2005) (**Figure 4-22 A**, **black**). When the viability of the transfected cancer cells was tested 48 h after the siRNA knockdown and normalized to the siCtrl, almost no change was detected for most of the selected potential targets except for DDX39B and RAN (**Figure 4-22 B**).

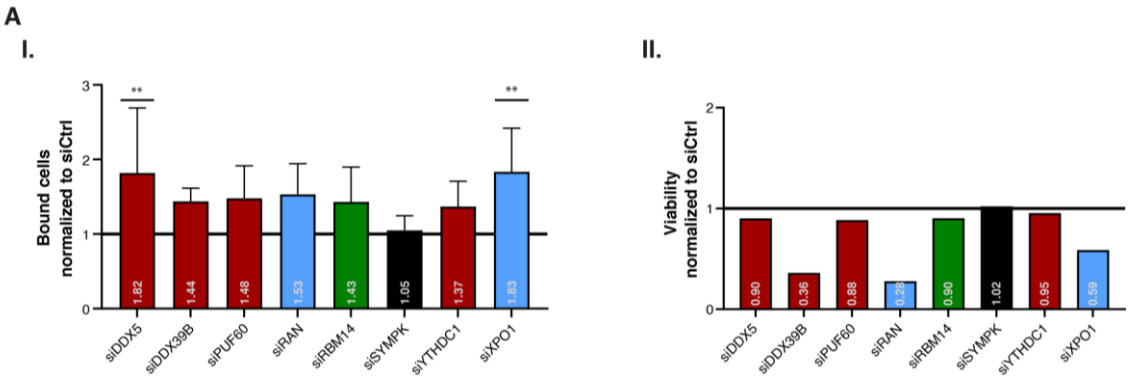

Figure 4-22: Identification of potential targets in primary RNAi screening. *(**A I**) **Identified targets for further validation analyses.** After siRNA knockdown, several splicing factors (in **red**), export factors (in **blue**) and RBM14 as transcription factor (in **green**) show increased T cell binding in cell adhesion assay compared to the siCtrl. Still, most of the targets, e.g. SYMPK (in **black**) show no change in T cell binding. (**A II**) **HCT 116 viability after siRNA knockdown.** Viability of HCT 116 cells was checked 48 h after siRNA knockdown (n = 1). For the chosen targets, viability of cells is not significantly affected compared to siCtrl, expected by siRNA knockdown of RAN, DDX39B and to lower extent for XPO1.*

The reduced viability caused by these two targets could be the reason for the effect identified in the cell adhesion assay. Also, the knockdown of XPO1 showed reduced viability but not as much as DDX39B and RAN. Viability was only tested once during the primary screening, but thereafter included in the detailed validation of potential targets. Therefore, all three targets were still included in the following experiments to obtain more reliable results.

The results of the primary screening indicated that specific RBPs could be involved in reducing the binding ability of T cells when treated with cancer cell supernatants. Especially, the siRNA knockdowns of splicing factors seemed to have a positive impact on T cell binding in the cell adhesion assay. The identified targets, which increased T cell binding compared to the control knockdown were validated in more detail and the results will be described below.

4.6.2 Validation of potential hits identified in primary screening

As a first step to validate the identified hits of the primary screening, individual knockdown experiments, excluded from the screening approach, were performed to reproduce and investigate previously detected effects in detail (**Figure 4-23**). Therefore, siRNA knockdowns were performed in HCT 116 cells for 48 h and 72 h and the supernatants were used for cell adhesion assay (**Figure 4-23 A**) whereas the cells were harvested and checked for knockdown efficiency and viability (**Figure 4-23 B** and **C**). The observed level of bound T cells in the siRNA control (siCtrl) sample was similar to WT (**Figure 4-23 A**, **grey**). Both downregulated T cell binding significantly compared to the medium. Hence, the siCtrl was a valid reference for normalization. For all targets, the standard deviation at 72 h was higher compared to the 48 h timepoint which indicated higher variability of the assay for longer knockdown durations. Based on this, for the following validation experiments the siRNA knockdown was performed for 48 h only. As already seen in the primary screening, SYMPK had no effect on T cell binding after knockdown for 48 h and 72 h (**Figure 4-23 A, black**). Moreover, most of the identified targets, which increased T cell binding in the primary screening, still showed the same effect but to lower extent (**Figure 4-23 A**, **red, blue** and **green**). For example, DDX5 showed significant upregulation of T cell adhesion in the screening, but in the individual knockdown experiments, it induced only mild effects in the assay. On the other hand, for the export factor XPO1 the significant upregulation of T cell binding was reproducible. The highest increase in the assay was detected for the second export factor RAN. The siRNA knockdown of this target doubled the number of bound T cells compared to the siCtrl.

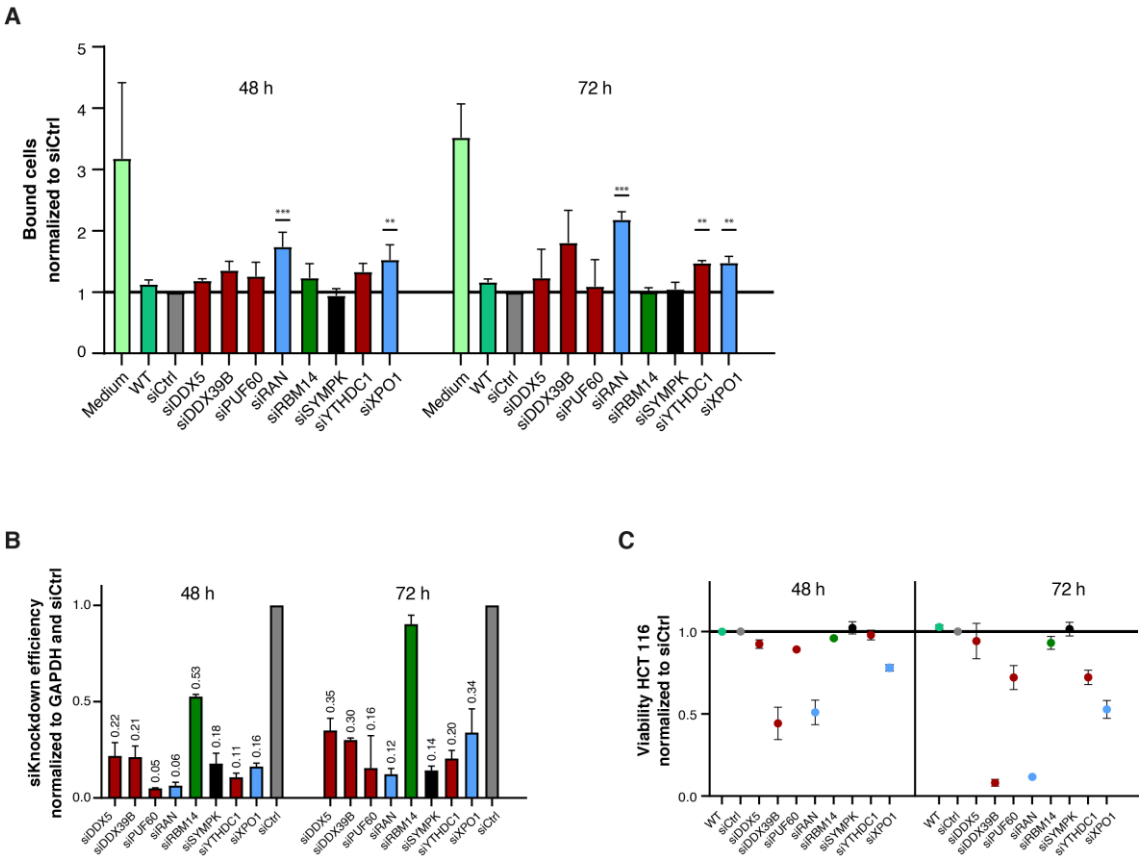

Figure 4-23: Validation of potential hits identified in primary screening. (A) Validation of potential hits of primary screening. *For the validation of identified potential hits, siRNA knockdown of targets and cell adhesion assays were performed after 48 h and 72 h. The previously observed effect of increased T cell binding by the targets is reproducible (**red**, **blue** and **green**). Also, the control SYMPK (**black**) induces no increase, as seen before. (**B**) **siKnockdown efficiency.** The knockdown efficiency was determined by qPCR and analysed with the $\Delta\Delta C_T$ method. The siRNA knockdown is highly efficient except for RBM14. (**C**) **HCT 116 viability after siRNA knockdown.** The viability of HCT 116 cells was checked after siRNA knockdown for 48 h and 72 h. Only the knockdown of DDX39B and RAN decreases viability to great extent. For the other targets, cell viability is almost not affected. Analyses were performed as biological replicates ($n \geq 3$). The mean was calculated and error bars represent the standard deviation.*

To ensure that the effects were induced by an efficient knockdown of the targets, qPCR was performed and normalized to the siRNA control (**Figure 4-23 B**). All siPOOLs used in the screening experiments showed effective downregulation of the target RNAs in the qPCR analyses. Only the knockdown of RBM14 was not as strong as the others with up to 50 % remaining mRNA after knockdown for 48 h. For 72 h, no knockdown was detected anymore (**Figure 4-23 B**, **green**). The efficiency of the siRNA knockdown of all validated targets decreased from 48 h to 72 h which was determined by higher levels of remaining target mRNA. This could explain the higher

variability of the measured effects in the cell adhesion assay (**Figure 4-23 A**). As second validation of the induced effects, the viability of the transfected HCT 116 cells was checked and normalized to the siCtrl (**Figure 4-23 C**). For most of the targets, the viability of the cells was not impaired by the siRNA knockdown, neither for 48 h nor for 72 h. The exceptions were the knockdown of DDX39B and RAN, which decreased cell viability to 50 % 48 h after transfection and to only 10 % living cells after 72 h. Although the knockdown of XPO1 had a negative effect on the viability of HCT 116 cells, it was considered insignificant with approximately 80 % viable cells detected after transfection for 48 h and a very low standard deviation.

Based on these results, the factors DDX5, YTHDC1, PUF60 and XPO1 were considered as potential positive hits identified in the primary screening and included in the further validation. The targets DDX39B and RAN were excluded based on the highly reduced viability of the cancer cells after siRNA knockdown. Also, the target RBM14 was removed from further validation experiments based on the inefficient siRNA knockdown. Although SYMPK showed the same effect in these validation experiments as it did in the primary screening, it was replaced as control because of its molecular function as mRNA processing factor. As a new control target for showing no effect on T cell binding ZCCHC8 was picked which is also found to be involved in splicing events as most of the targets selected for further validation (Falk et al. 2016) (**Figure 4-21 B**). Results for the detailed validation of the picked targets are described in the next chapter.

4.6.3 Characterization of specific RNA-binding proteins as potential immune regulators

After the first validation experiments, most of the selected hits identified in the primary screening were confirmed to increase T cell binding upon siRNA knockdown and may function as potential immune regulators. The most promising candidates were the splicing factors DDX5 and PUF60, the m^6A reader protein YTHDC1 and the export factor XPO1. To analyse these targets and especially the induced effects in more detail, HCT 116 cells were transfected with overexpression constructs and siPOOLs for 48 h. Afterwards, supernatants were used for cell adhesion assays and

cells were harvested to check the knockdown and overexpression efficiency as well as the viability after transfection. All results were normalized to the siRNA control (siCtrl). In addition to the promising hits, the splicing factor ZCCHC8 was chosen as control target which – after the primary screening - was not expected to induce significant changes in T cell binding upon overexpression and siRNA knockdown.

First, the targets DDX5, YTHDC1 and as control ZCCHC8 were analysed (**Figure 4-24**). In the cell adhesion assay, for all targets the siCtrl was comparable to WT and therefore a valid reference for normalization (**Figure 4-24 A**, **grey**). Around 50 % less T cells bound after the siCtrl transfection compared to the growth medium. This proved again the fact that the supernatant of HCT 116 cells induced significant downregulation of T cell adhesion. Looking closer at the other tested targets, neither the overexpression nor the siRNA knockdown induced significant effects after normalization to siCtrl. Nevertheless, for DDX5 and YTHDC1 an increase of almost 40 % in T cell binding was observed comparing overexpression with siRNA knockdown (**Figure 4-24 A**, **red**). As expected, the effects after overexpression and siRNA knockdown of the negative control ZCCHC8 were similar to each other and had no obvious influence on T cell binding (**Figure 4-24 A**, **black**). Also, the standard deviations were much higher compared to the other tested targets. Therefore, effects induced by knockdown and overexpression of ZCCHC8 seemed be more variable compared to other factors. Viability of HCT 116 cells was tested to ensure equal cell numbers for the different, tested conditions (**Figure 4-24 B**). For all targets, neither overexpression nor siRNA knockdown seemed to have effects on cell viability. After normalization to siCtrl, there were no considerable changes detected between WT, overexpression or knockdown. This suggested that the cell adhesion effects were reliable and not caused by affecting HCT 116 cell viability and number.

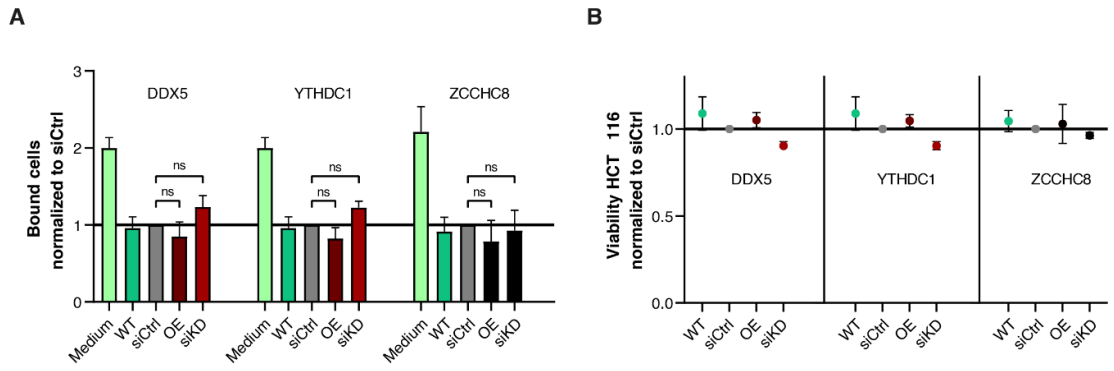

Figure 4-24: Analysis of potential immune regulators identified in primary screening. *Impact of potential hits of the primary screening on T cell binding was tested by overexpression and siRNA knockdown in HCT 116 cells followed by cell adhesion assay. (**A**) **Impact of identified targets on T cell binding.** In cell adhesion assay, DDX5 and YTHDC1 show slight downregulation of T cell adhesion after overexpression and mild upregulation after siRNA knockdown (**red**). As control, ZCCHC8 was tested, which has no effect on T cell binding, neither after overexpression nor siRNA knockdown (**black**). (**B**) **HCT 116 viability after transfections.** Induced effects are not influenced by reduced cell viability of HCT 116 cells after treatment. Analyses were performed as biological replicates (n ≥ 3). The mean was calculated and error bars represent the standard deviation.*

Furthermore, the efficiency of the transfection of the HCT 116 cells was validated (**Figure 4-25**). For the siRNA knockdown, RNA was extracted and used for qPCR measurements, which were normalized to the siCtrl (**Figure 4-25 A**). The successful transfection of the different overexpression constructs was checked via Western Blot using an α-HA antibody detecting the F/HA tag of the proteins (**Figure 4-25 B**).

The qPCR proved high efficiency of the siRNA knockdown. For DDX5 and YTHDC1, only 15-20 % remaining mRNA was detected. Also, the siRNA knockdown of the control target ZCCHC8 was very efficient with approximately 30 % remaining mRNA (**Figure 4-25 A**). Also, the overexpression resulted in high expression of the proteins. The Western Blot using antibodies against the F/HA tag showed clear signals at the expected molecular weights. For YTHDC1 and ZCCHC8, additional bands were visible, which might be caused by different splice variants. To ensure and prove equal loading of the lanes, an antibody against beta-Tubulin was used. The HCT 116 WT sample (lane 1) showed no signal using the α-HA antibody, which again confirmed the specificity and efficiency of the transfection (**Figure 4-25 B**).

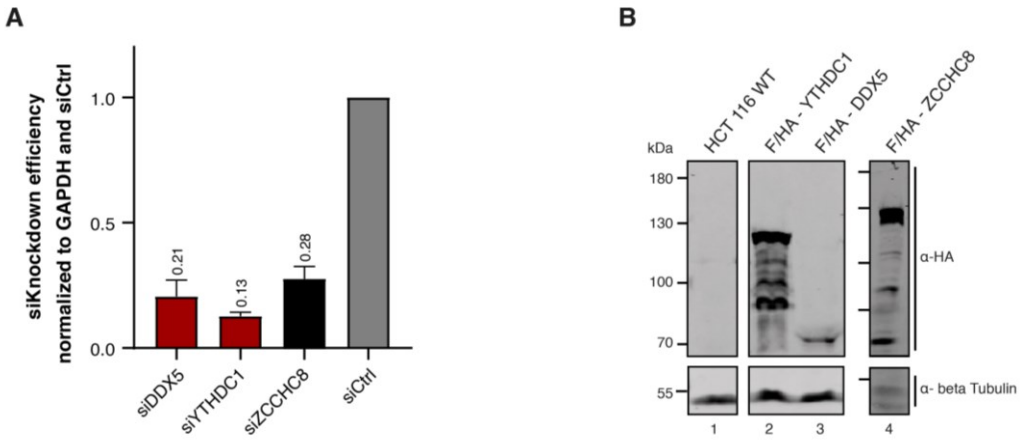

Figure 4-25: Validation of siKnockdown and overexpression efficiency. *(A)* ***siKnockdown efficiency.*** *siRNA knockdown of tested targets was validated via qPCR and analysed with the $\Delta\Delta C_T$ method and normalized to the siRNA control (siCtrl). siRNA knockdown is very efficient with only 10 -30 % remaining mRNA. Analyses were performed as biological replicates (n ≥ 3). The mean was calculated and error bars represent the standard deviation. (**B**)* ***Overexpression efficiency.*** *Overexpression was checked via Western Blot using an α-HA antibody and beta-Tubulin as loading control. All targets are expressed highly after transfection. (YTHDC1 = 85 kDa; DDX5 = 70 kDa; ZCCHC8 = 82 kDa; Tubulin = 50 kDa).*

Secondly, also the splicing factor PUF60 and the export factor XPO1 were investigated in more detail (**Figure 4-26**). For both targets the expected effect of WT compared to the growth medium was detected. As seen before, the siCtrl transfection showed no effect on T cell binding compared to WT and was used for normalization (**Figure 4-26 A, grey**). For PUF60, the overexpression construct significantly decreased T cell binding (**Figure 4-26 A**, **red**). The standard deviation was low indicating a stable and reliable effect. In contrast, the siRNA knockdown seemed to have no influence on the binding ability of T cells. Only a slight increase of approximately 10 % could be detected although the effect in the primary screening was much higher (**Figure 4-22**). For XPO1, overexpression had almost no impact compared to the siRNA control and resulted in a small decrease of the detected signal. But on the other hand, the siRNA knockdown increased the number of bound cells significantly by 40 % (**Figure 4-26 A**, **blue**). The standard deviations were higher as seen for PUF60, but still the effect induced by the siRNA knockdown was significant. Additionally, for both targets, the viability of HCT 116 cells after the transfection was tested (**Figure 4-26 B**). For PUF60 and XPO1, the WT and overexpression showed no change in viability after normalization to siCtrl. The siRNA knockdown for both

targets decreased the viability to 75-80 % compared to the control, which was considered insignificant.

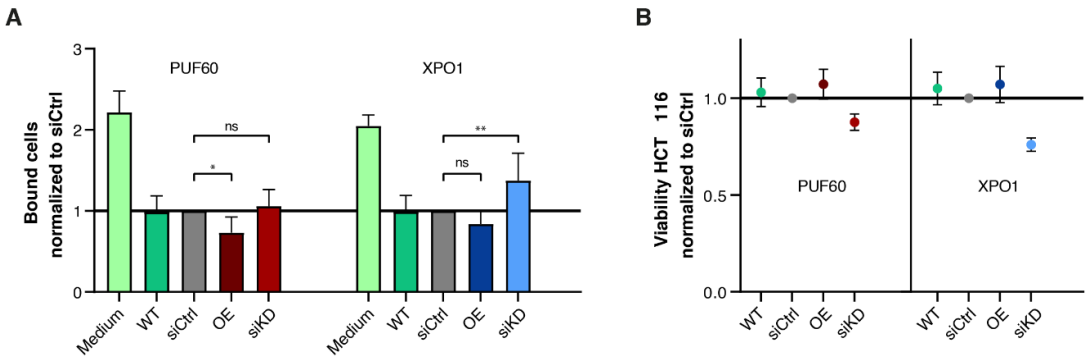

Figure 4-26: Identification and analysis of potential immune regulators identified in primary screening. *Impact of potential hits PUF60 and XPO1 on T cell binding was tested by overexpression and siRNA knockdown in HCT 116 cells followed by cell adhesion assay. (**A**)* ***Impact of PUF60 and XPO1 on T cell adhesion.*** *PUF60 shows significant downregulation of T cell binding after overexpression and only minor effects after siRNA knockdown (**red**). In contrast, XPO1 shows no effect after overexpression, but increases the number of bound cells significantly after siRNA knockdown (**blue**). (**B**)* ***HCT 116 viability after transfection.*** *Viability of HCT 116 cells is not significantly impaired after transfection of siPOOLs or overexpression constructs. Analyses were performed as biological replicates (n ≥ 4). The mean was calculated, and error bars represent the standard deviation.*

Moreover, knockdown and overexpression were tested to ensure that the induced effects were reliable and based on either siRNA knockdown or overexpression (**Figure 4-27**). To validate the siRNA knockdown, RNA was extracted, and qPCR was performed and results were normalized to siCtrl (**Figure 4-27 A**). The success of the overexpression was checked via Western Blot detecting the targets by an α-HA antibody (**Figure 4-27 B**).

The knockdown of both targets was highly efficient (**Figure 4-27 A**). For PUF60, only 7 % remaining mRNA was detected after normalization to the siCtrl. For XPO1, the knockdown was not as efficient as for PUF60, but with 17 % remaining mRNA it was still very effective. In Western Blots, clear signals for the validated targets were visible at the expected molecular weights (**Figure 4-27 B**). For PUF60, an additional dominant band at 180 kDa was present. As loading control an antibody detecting beta-Tubulin was used, which showed equal loading of the lanes.

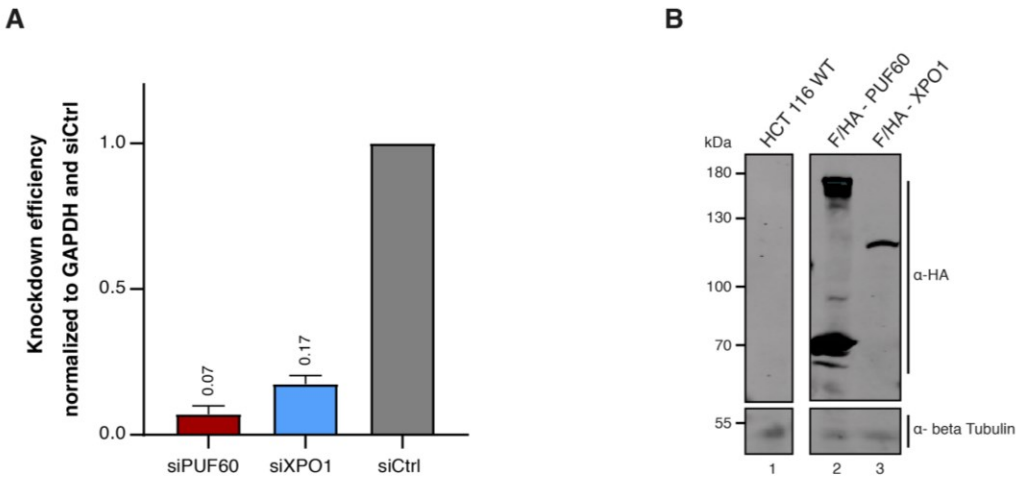

Figure 4-27: Validation of siRNA knockdown and overexpression efficiency. *(**A**)* ***siKnockdown efficiency.*** *siRNA knockdown of PUF60 and XPO1 was validated via qPCR and analysed with the $\Delta\Delta C_T$ method and normalized to the siRNA control (siCtrl). siRNA knockdown was very efficient with only 10 -20 % remaining RNA. Analyses were performed as biological replicates (n ≥ 4). The mean was calculated and error bars represent the standard deviation. (**B**)* ***Overexpression efficiency.*** *Overexpression was checked via Western Blot using an α-HA antibody and beta-Tubulin as loading control. Both targets are strongly expressed after transfection (PUF60 = 65 kDa; XPO1 = 125 kDa; Tubulin = 50 kDa).*

In summary, the detailed validation of the identified hits of the primary screening suggests an immune relevant function of these targets based on their effect on T cell binding to hICAM-1 in cell adhesion assays. Although for DDX5 and YTHDC1 no significant effects were detected after normalization to the siCtrl, a clear increase of the number of bound T cells was observed comparing the siRNA knockdown to the overexpression. Even greater effects were identified for PUF60 and XPO1. Overexpression of PUF60 was inducing significant decrease of T cell binding and siRNA knockdown of XPO1 was highly increasing adhesion of T cells. Therefore, these two targets were analysed further to identify a possible connection to important immune regulatory pathways. The detailed analysis is described in the next chapter.

4.7 Identification of alternative splicing factor PUF60 as regulator of CTNNB1 expression

After the primary screening and the detailed validation, the alternative splicing factor PUF60 and the nuclear export factor XPO1 were identified as promising targets with immune regulatory functions. The obtained results indicate that both targets could influence the binding of T cells to ICAM-1, which is the main specific ligand of the integrin LFA-1. The overexpression of PUF60 showed a negative effect on the binding ability of T cells whereas the siRNA knockdown of XPO1 increased the binding of T cells *in vitro*. CTNNB1 is a well-studied oncogene, which was identified to be involved in the exclusion of T cells from tumours (**3.1.3**). Moreover, CTNNB1 as well showed significant effects on T cell binding in *in vitro* cell adhesion assays (**4.5**). The overexpression of CTNNB1 downregulated and the siRNA knockdown upregulated T cell binding significantly. Additionally, several publications claimed that expression of CTNNB1 is post-transcriptionally regulated on RNA levels by alternative splicing events (Thiele et al. 2006; Chan et al. 2022). Therefore, we focused further studies on PUF60 and its potential effects on CTNNB1 by regulating alternative splicing.

4.7.1 Interaction of PUF60 with CTNNB1 on RNA Level

In order to identify a possible connection of the target effects observed in the cell adhesion assays with CTNNB1, both PUF60 and XPO1 were overexpressed in HEK 293T cells and immunoprecipitation followed by RNA extraction (RNA-IP; RIP) was performed. The IP was performed using α-FLAG beads binding to the F/HA tag of the overexpression constructs. The extracted RNA was reverse transcribed into cDNA followed by qPCR to validate a potential enrichment of CTNNB1 on RNA level. In addition to CTNNB1, ATF3 RNA level was analysed because this transcription repressor is the downstream factor of the β-catenin signalling pathway. As control target, the splicing factor ZCCHC8 was used, which had no effect in the primary screening and in the validation experiments. LIN28A was also included as additional control, which is known to specifically bind primary miRNAs (pri-miRNAs) (Parisi et al. 2021). The enrichment of the RNA level was determined by the ratio of IP over

input and normalized to an empty F/HA control plasmid. The success of the IP itself was validated via Western Blot (**Figure 4-28**).

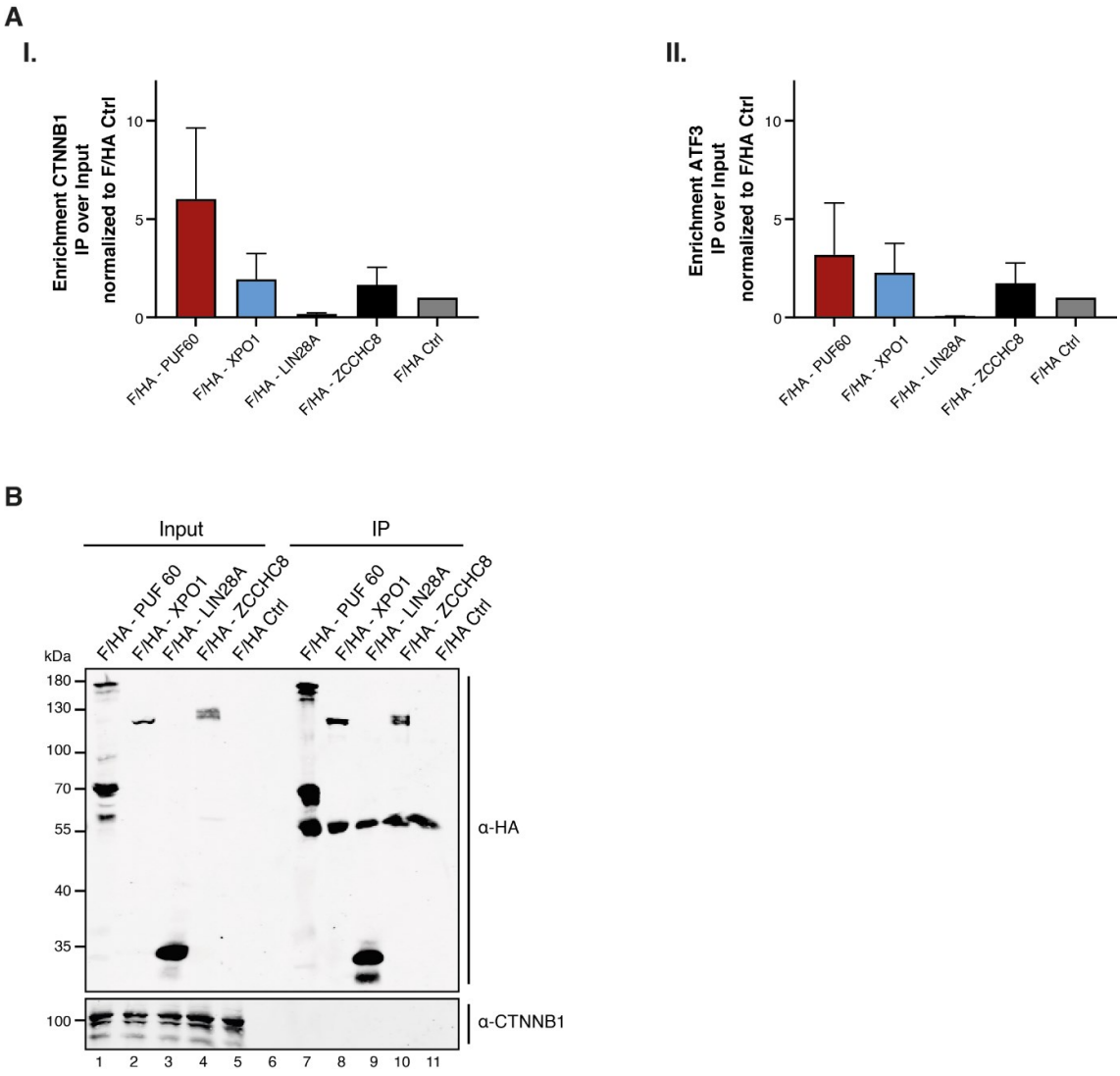

Figure 4-28: Validation of the interaction of PUF60 and XPO1 with CTNNB1 on RNA level and on protein level. *(**A I.**) **CTNNB1 Enrichment.** Validation of RNA enrichment of CTNNB1 after F/HA – IP of PUF60, XPO1, LIN28A, ZCCHC8 and F/HA control (F/HA Ctrl). (**A II.**) **ATF3 Enrichment.** Validation of RNA enrichment of ATF3 after F/HA – IP of PUF60, XPO1, LIN28A, ZCCHC8 and F/HA control (F/HA Ctrl). Enrichment was calculated IP over input and normalized to the F/HA Ctrl. PUF60 clearly enriches both CTNNB1 and ATF3 RNA (**red**), whereas the other targets enrich neither CTNNB1 nor ATF3 at all or only to small extent (**black**). Analyses were performed as biological replicates (n = 3). The mean was calculated, and error bars represent the standard deviation (**B**) **Western Blot after IP.** Success of the F/HA – IP is validated via Western Blot using an α-HA antibody. However, no increase of CTNNB1 on protein level is detected using a specific antibody detecting CTNNB1 (PUF60 = 65 kDa; XPO1 = 125 kDa; Lin28A = 25 kDa; ZCCHC8 = 82 kDa; CTNNB1 = 88 kDa).*

The RIP experiments clearly revealed an almost 6-fold enrichment of CTNNB1 mRNA association with overexpressed PUF60 (**Figure 4-28 A I.**, **red**). The standard

deviation was high. However, this showed a rate of high variability in our assays. The control targets showed no increase of CTNNB1 on the RNA level after IP compared to the F/HA control (F/HA Ctrl). LIN28A showed no binding of the target mRNA, which was expected. ZCCHC8 seemed to bind the CTNNB1 mRNA weakly and is thus considered as background binding (**Figure 4-28 A I.**, **black**). For XPO1, the enrichment could not be determined clearly. Although binding of the CTNNB1 RNA was detected, enrichment of approximately 2-fold was not significant and rather similar to background (**Figure 4-28 A I.**, **blue**).

A similar pattern was seen for the ATF3 RNA level (**Figure 4-28 A II.**). A mild enrichment could be seen for PUF60 overexpression (**red**), for XPO1 this effect was rather small (**blue**) and for the controls LIN28A and ZCCHC8 again no clear increase was detected (**black**). Because ATF3 mRNA may not be directly bound by the tested factors, an enrichment might only result from increased CTNNB1 levels. Thereby, the observed enrichment of ATF3 with overexpressed PUF60, served as another confirmation of the specificity for the CTNNB1 mRNA enrichment.

To test the success of the IP, a Western Blot was performed detecting the tested targets via an α-HA antibody (**Figure 4-28 B**). In the IP samples (lane 7 - 11) a clear enrichment of PUF60, XPO1, LIN28A and ZCCHC8 was detected with visible bands migrating with corresponding molecular weight. Because of the stringent elution of the antibody-protein complex from the beads, the additional antibody bands at 55 kDa were visible. As already seen before, a rather unspecific band running at 180 kDa could be seen for PUF60 (lane 7). Empty F/HA Ctrl did not show any unspecific signals, which ensured a clean and effective IP. Furthermore, using a specific antibody, endogenous protein levels of CTNNB1 were tested. Although there was a clear signal for CTNNB1 in the input samples (lane 1-5), there was no enrichment detected in the IP lanes (lane 7-11).

The results of the RIP indicated an interaction of PUF60 with CTNNB1 on mRNA level without affecting protein levels as seen in the Western Blot. For XPO1, an unclear interaction with CTNNB1 mRNA was identified. Consequently, the focus was set on finding a functional explanation for the interaction between PUF60 and the CTNNB1 mRNA. As a first step to investigate this interaction, rescue experiments were

performed to figure out if the downregulation of T cell binding in *in vitro* cell adhesion assays detected after the overexpression of PUF60 could be induced by increased CTNNB1 levels. The results are described below.

4.7.2 Rescue of reduced T cell binding induced by PUF60 via knockdown of CTNNB1

After the identification of an interaction between the alternative splicing factor PUF60 and the CTNNB1 mRNA, the next focus of interest was whether the effect of PUF60 overexpression in cell adhesion assays is indeed connected to CTNNB1. In order to address this question, rescue experiments were performed. Therefore, HCT 116 cells were transfection with a F/HA-PUF60 overexpression construct and an empty control vector (F/HA Ctrl). Reasoning that PUF60 overexpression leads to increased CTNNB1 mRNA levels, 24 h after transfection, siRNA knockdown of CTNNB1 and a siRNA control were performed using specific siPOOLs. 48 h after the knockdown, the supernatants were used for cell adhesion assays and cells were harvested to check knockdown and overexpression efficiency via qPCR and Western Blot. For each of the tested conditions, the PUF60 overexpression was normalized to the F/HA Ctrl transfections. Consequently, three different conditions were compared to each other: overexpression only ("only"), overexpression with siRNA knockdown of the siCtrl ("+ siCtrl") and overexpression in combination with the knockdown of CTNNB1 ("+ siCTNNB1") (**Figure 4-29**).

The first two conditions did not show any significant difference when compared to each other (**Figure 4-29 A**). The overexpression only and in combination with the siRNA knockdown control (+siCtrl) had similar influence on T cell adhesion in the assay. After normalization to the control plasmid F/HA Ctrl, the overexpression of PUF60 caused a reduction of T cell binding of 10 – 15 %. Although this effect was smaller than detected before (**Figure 4-26**), it was still robust because of low standard deviations in the biological replicates. When the overexpression was combined with the siRNA knockdown of CTNNB1, an increase in T cell binding was detected in the cell adhesion assay. By performing the knockdown, the number of binding T cells approximately doubled comparing PUF60 overexpression to the

empty F/HA Ctrl. The standard deviation in this condition was high, due to many steps which were performed.

To verify the results of the cell adhesion assay, one half of the harvested cells was used for RNA and cDNA synthesis followed by qPCR analysis. The other half of the harvested cells was lysed, and Western Blot was performed (**Figure 4-29 B**).

The qPCR proved high efficiency of the CTNNB1 knockdown, which resulted in only 15 % remaining mRNA. The overexpression showed an increase of PUF60 on mRNA level. The control plasmid F/HA Ctrl did not influence RNA levels of PUF60 (**Figure 4-29 B I.**). In the Western Blot, the success of the overexpression was clearly visible with a band detected at the expected molecular weight using an α-HA antibody directed against the tag (**Figure 4-29 B II.**). In the control transfection, no unspecific signal was detected with the antibody indicating high specificity. When detecting CTNNB1 protein levels using a specific antibody, the detected signal was reduced after the siRNA knockdown, although there was still a band visible (lane 4 and lane 8). In the other samples, no clear difference in expression of CTNNB1 was observed. The control antibody α-alpha-Tubulin showed equal loading of the samples.

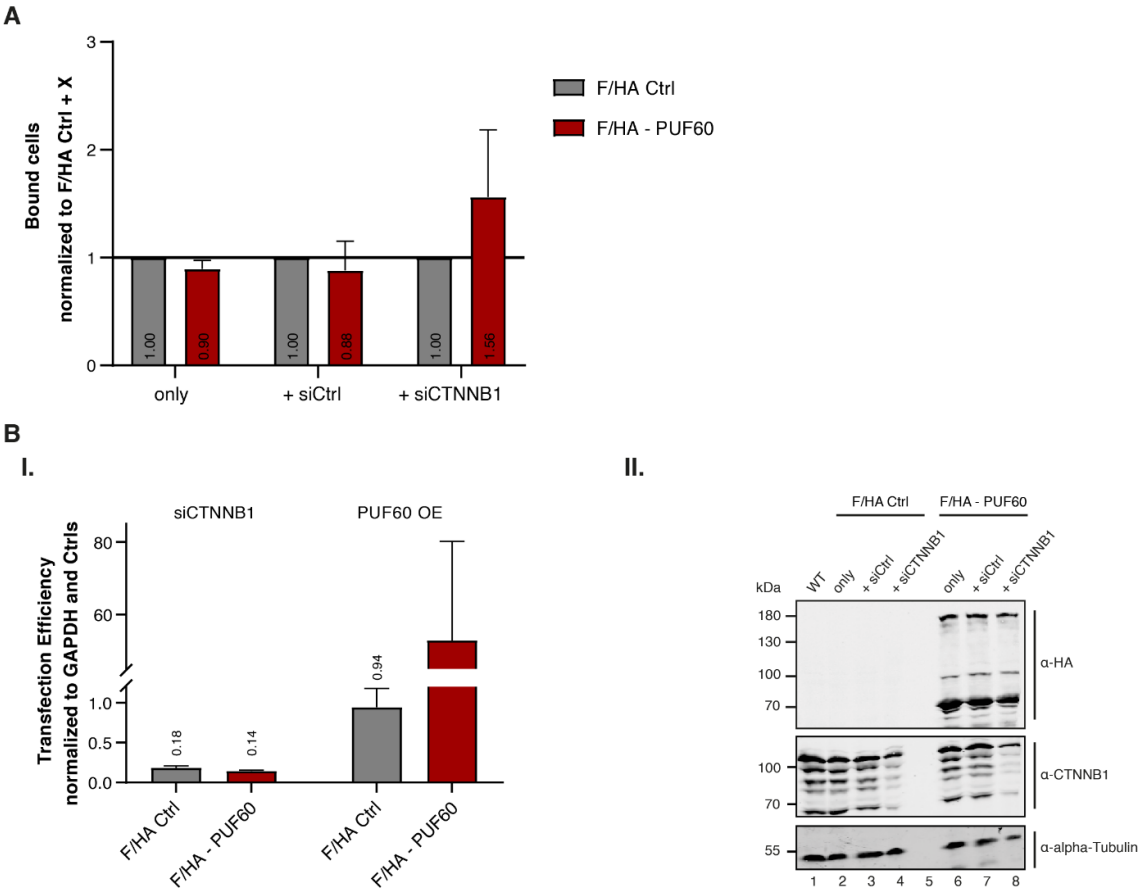

Figure 4-29: Rescue of PUF60 overexpression via CTNNB1 siRNA knockdown. *HCT 116 cells were transfected with overexpression constructs of PUF60 and an empty control. 24 h after, siRNA knockdown of CTNNB1 and a siRNA control was performed on top for 48 h. Supernatants were used in cell adhesion assay and cells were harvested.* ***(A) Rescue PUF60 Overexpression with CTNNB1 knockdown.*** *Cell adhesion assay was performed using the supernatant of transfected HCT 116 cells. With the siRNA knockdown of CTNNB1 after the overexpression of PUF60, the T cell binding is increased compared to the F/HA Ctrl in combination with siCTNNB1.* ***(B I.) siKnockdown and overexpression efficiency in qPCR.*** *The knockdown and overexpression efficiencies were determined by qPCR and analysed with the $\Delta\Delta C_T$ method. The siRNA knockdown and overexpression are highly efficient.* ***(B II.) siKnockdown and overexpression efficiency in Western Blot****. The overexpression and knockdown efficiency were also checked by Western Blot. The overexpression of PUF60 works well using an α-HA antibody detecting the tag of the protein. After the knockdown, there is still remaining CTNNB1 protein visible using a specific α-CTNNB1 antibody. The control antibody α-alpha-Tubulin indicates equal loading of the samples. Analyses were performed as biological replicates (n = 4). The mean was calculated, and error bars represent the standard deviation (PUF60 = 65 kDa; CTNNB1 = 88 kDa; Tubulin = 50 kDa).*

These results demonstrated that the effect of PUF60 overexpression in cell adhesion assays could be connected to the expression levels of CTNNB1. The reduction of T cell binding in the cell adhesion assays after overexpression of PUF60 was reversed when a knockdown of CTNNB1 was performed on top. The knockdown and overexpression were very efficient. Interestingly, after the siRNA knockdown, the CTNNB1 protein

was still detected in Western Blot, although the qPCR showed only small amount of remaining mRNA. Additionally, no clear increase of CTNNB1 protein levels could be determined in the Western Blot.

Because PUF60 is promoting alternative splicing, the obtained results might be connected to different splice variants of CTNNB1. Therefore, the alternative splicing of CTNNB1 was further investigated and results are described below.

4.7.3 Detection of alternative spliced 3' UTR isoforms of CTNNB1 based on PUF60 overexpression

With the results obtained so far, we can clearly show that PUF60 interacts with the CTNNB1 mRNA and that the siCTNNB1 knockdown is able to reverse and increase T cell binding in cell adhesion assays after PUF60 overexpression. Since PUF60 is involved in alternative splicing and binds the mRNA of CTNNB1, we checked for alternative spliced isoforms of CTNNB1. Screening the literature, already in 2006 Thiele et al. suggested three different 3' UTR splice variants of CTNNB1. They annotated the longest detected UTR as intron-containing and un-spliced, an intermediated one as the canonical UTR containing the full exon and a short variant missing parts of this exon (Thiele et al. 2006). The recent publication by Chan et al. also claims, that the 3' UTR of CTNNB1 is target of alternative splicing causing a long "full-length" (3' FL) and a "short" (3' SP) 3' UTR variant. Furthermore, they suggest that the 3' SP is the oncogenic isoform of CTNNB1 causing higher protein levels and being responsible for its tumorigenic functions (Chan et al. 2022).

To verify this possible connection in more detail, CTNNB1 mRNA levels and possible splice variants were compared after siRNA knockdown and overexpression of PUF60 by analysing the samples of the rescue experiments (**Figure 4-29**). cDNA of the samples from the rescue experiment were used as DNA template for RT-PCR to amplify potential isoforms of the CTNNB1 3' UTR. PCR products were analysed on agarose gels (**Figure 4-30**).

In order to identify these splice variants, the RT-PCR was performed with a specific primer pair (RT - primer) detecting different 3' UTR isoforms by binding late in the last exon of the coding sequence (exon 14) and shortly before the polyadenylation

signal (**Figure 4-30 A**, **indicated in green**). As internal control, the CDS primer pair was used. To ensure equal input levels, a primer pair against GAPDH was utilized. The RT – primers were expected to produce products of 1100 bp for the 3' FL, 800 bp for the canonical and 640 bp for the 3' SP splice isoform.

The analysis of the RT PCR on the agarose gel revealed the amplification of several different 3' UTR isoforms using the specific RT – primers (**Figure 4-30 B I.,** upper panel). Intense bands were visible at 1100 bp and 650 bp which corresponded to the sizes for the 3' FL and the 3' SP. An additional band was detected in between these two at approximately 800 bp corresponding to the size of the canonical 3' UTR. Interestingly, all potential splice variants could be detected in the HCT 116 WT with equal intensities. Although the control siRNA (siCtrl, lane 2) did not induce any change, the knockdown of CTNNB1 (siCTNNB1, lane 3) showed a clear band for the long isoform and a significant reduction of the two shorter variants simultaneously. A similar pattern was identified for the samples, in which overexpression and knockdown were combined. For overexpression only and in combination with siCtrl, the ratio between the short and long isoforms was clearly on the side of the canonical and 3' SP variant (lane 4 - 5 and lane 8 - 9). For the overexpression of PUF60 (lane 8 – 9), the short isoform appeared more intense compared to the F/HA Ctrl (lane 4 – 5). When the overexpression was combined with the knockdown of CTNNB1, again the 3' FL isoform was detected along with a reduced intensity of the middle and short band (lane 6 and lane 10). Moreover, when a knockdown of PUF60 was performed (lane 11), the most dominant band detected was the middle one and the 3' FL was highly reduced. The control lane (H_2O, lane 12) indicated no contamination and reliable results.

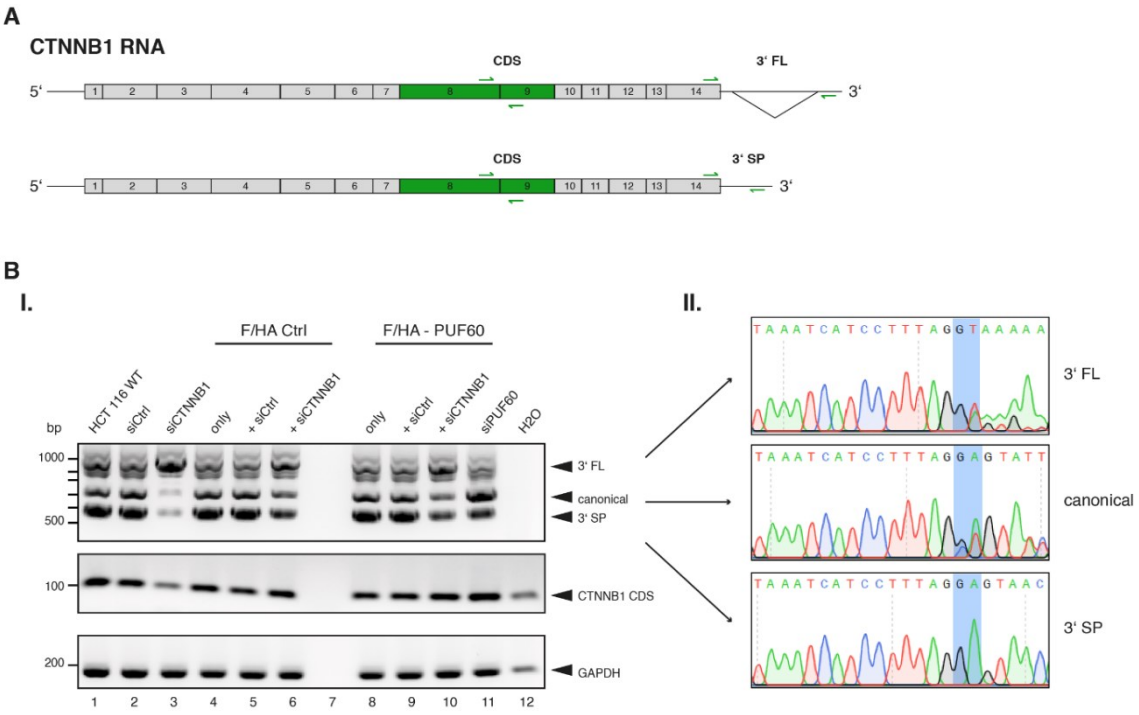

Figure 4-30: RT-PCR for the detection of different 3' UTR splice variants of CTNNB1. *(**A**) Schematic representation of CTNNB1 RNA with indicated primer pairs used for RT-PCR to detect alternative spliced 3' UTR variants (**green**). (**B I.**) PCR products were analysed on agarose gels. At least 3 distinct splice variants of the CTNNB1 3' UTR are detected using the specific RT – primer pair (upper panel). The largest and shortest correspond to the expected sizes for the 3' FL (1100 bp) and 3' SP (640 bp). The band at around 750 bp represents the canonical 3' UTR. Upon knockdown of PUF60 the isoform switches from the 3' SP to longer isoforms. The CDS primer pair indicates equal levels of CTNNB1, except in the siRNA knockdown samples (middle panel). Amplification of GAPDH proves equal DNA input amounts (lower panel). (**B II.**) Sanger sequencing results of different bands identify the 5' splice site only for the 3' FL (highlighted in blue). For the other two variants the 5' splice side cannot be detected anymore.*

For the CDS primers equal amounts of CTNNB1 were detected with a slight reduction in intensity for the lanes of the siCTNNB1 knockdown samples (**Figure 4-30 B I.,** middle panel). The control PCR amplifying GAPDH indicated equal DNA input amounts (**Figure 4-30 B I.,** lower panel).

In order to verify the results of the RT-PCR in more detail, sanger sequencing of the detected bands was performed (**Figure 4-30 B II.**). For sequencing, a primer was chosen detecting the 5' splice site of the 3' UTR, which was the same for every potential splice event. For the longest PCR product, the sequence for the 5' splice site was clearly detected (**Figure 4-30 B II.,** upper panel). Although the sequencing indicated a mixture of different sequences at this position, the G-T nucleotides were

the predominant ones. Therefore, the highest band matched the postulated un-spliced 3' FL isoform. For the other two potential splice variants, the 5' splice site was not detected anymore (**Figure 4-30 B II.**, middle and lower panel). Instead of a G-T sequence at this position, a G-A was detected for both. Nevertheless, the following sequences for the middle and the lowest band differed indicating different splice variants. Moreover, sequencing results for the middle band corresponded to the canonical 3' UTR and the sequence of lowest band matched the postulated 3' SP isoform.

In order to compare the different bands of the RT-PCR better, the intensities of the upper band (3' FL), the middle band (canonical) and the lower band (3' SP) were quantified and normalized to the siCtrl (**Figure 4-31 A**). Additionally, Western Blot was performed and signals detected with the α-CTNNB1 antibody were quantified to correlate splice variants of CTNNB1 with resulting protein levels. Protein levels were normalized to the loading control α-alpha-Tubulin and to siCtrl. The quantification represents the mean of performed biological replicates (**Figure 4-31 B**).

The quantification of the band intensities in the RT-PCR clearly highlighted the isoform switch from the shorter splice variants (lower band) to the longer isoforms (middle and upper band) after knockdown of PUF60 (**Figure 4-31 A**). Although in the WT, all three bands were visible and showed similar intensities (lane 1), the levels of the 3' FL reduced after overexpression of PUF60 and the F/HA Ctrl (lane 4 – 5 and lane 7 - 8). The siCTNNB1 knockdowns shifted the intensity levels to the upper band, while decreasing the intensity of the two shorter ones (lane 3, 6 and 9). The quantification also showed that the signal of the lower band representing the 3' SP was slightly higher than the signal of the middle band in all the tested conditions. The only exception was the knockdown of PUF60 (siPUF60, lane 10). There, the isoform switched from the short variant to longer 3' UTRs, especially the canonical one.

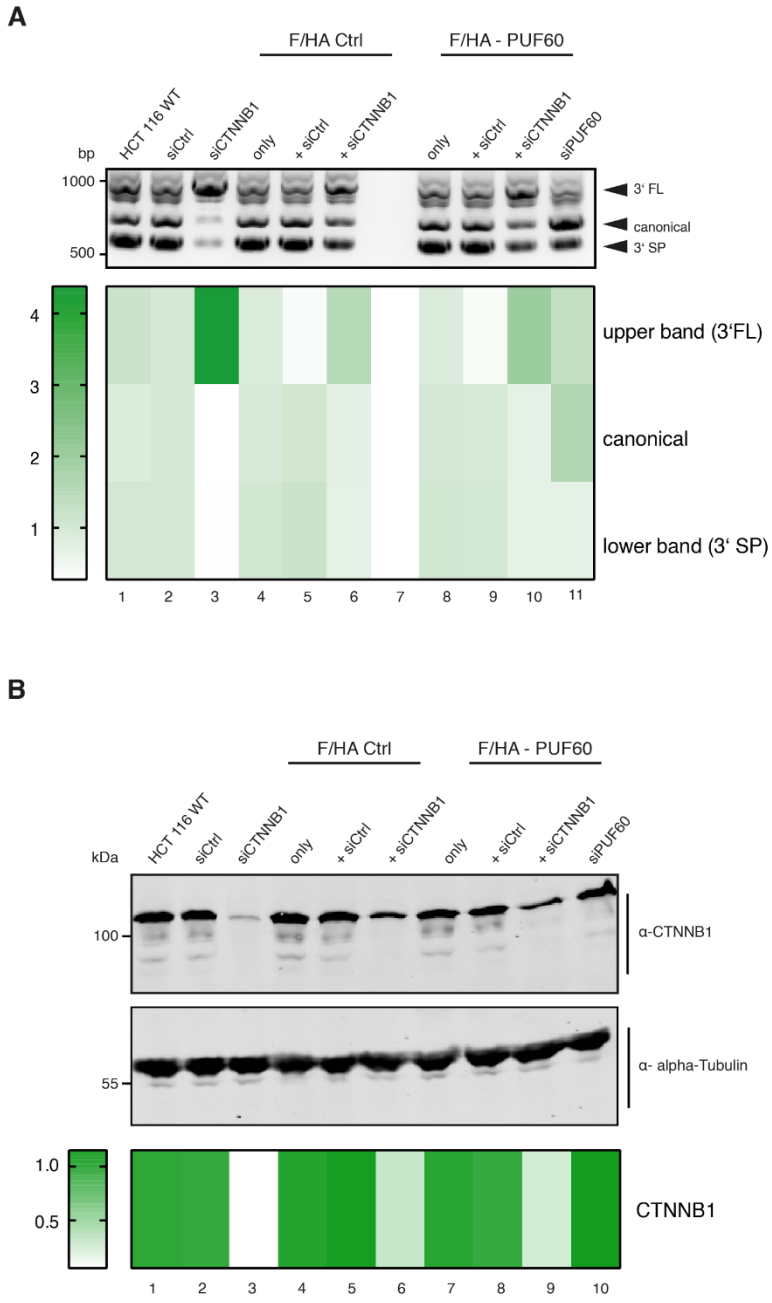

Figure 4-31: Quantification of changes in CTNNB1 levels after PUF60 overexpression and knockdown. *CTNNB1 protein levels and splice variants were detected by RT-PCR and Western Blot after rescue experiments performing siRNA knockdown of CTNNB1 after PUF60 overexpression.* ***(A) Quantification RT-PCR.*** *RT-PCR quantification shows a switch from the short splice variants to longer isoforms upon knockdown of PUF60 (Agarosegel from* ***Figure 4-30****).* ***(B) Quantification Western Blot.*** *Western Blot quantification shows the highest level of CTNNB1 protein after PUF60 overexpression, whereas the knockdown reduces protein levels significantly. Low levels of CTNNB1 protein might correlate with the long 3' UTR isoform. Knockdown of PUF60 does not show reduced protein levels. Quantification shows mean of biological replicates (n ≥ 3)*

Connecting the different 3' UTR isoforms to the protein expression levels, a correlation of the short isoform with higher protein levels was identified

(**Figure 4-31 B**). For the samples with the highest levels of the 3' SP variant, the highest levels of protein were detected. In the PUF60 overexpression only, where the 3' SP isoform was the prominent one, the highest level of CTNNB1 protein was confirmed, which was even higher than in the WT. In the siCTNNB1 knockdown samples, almost no protein was detected although the 3' FL splice variant was identified in the RT-PCR. In the siCtrl samples some variations on protein level could be seen. But the level was still lower than in the PUF60 overexpression. Unexpectedly, after the knockdown of PUF60 (siPUF60, lane 10), the protein levels of CTNNB1 were as high as in the overexpression and hence higher than in the WT.

Additionally, Northern Blot analyses were performed to verify a potential isoform switch in the 3' UTR of CTNNB1 mRNA in more detail. So far, no clear results could be obtained (data not shown). Moreover, qPCR was performed to detected different splice variants. But the obtained results were not conclusive although for the knockdown of PUF60 a reduction of the 3' FL and 3' SP variant levels could be assumed (data not shown). For both approaches further optimization is needed to identify distinct splice patterns.

By performing RT-PCR, different 3' UTR splice variants of CTNNB1 could be identified. The three distinct isoforms detected could correspond to the 3' FL, the canonical and the 3' SP variant, which were already published (Thiele et al. 2006; Chan et al. 2022). After quantification, a clear correlation was revealed between CTNNB1 protein levels and the predominant 3' UTR isoform expressed. With higher levels of the short splice variant, also the protein level was increased. These results indicate that PUF60 might be responsible for alternative splicing events in the 3' UTR of CTNNB1. By generating a shorter 3' UTR predominantly, CTNNB1 protein levels increase causing reduced binding of T cells to ICAM-1, which we observed in cell adhesion assays.

.

5 Discussion

The infiltration of T cells is an important step in the cancer immunity cycle, which is essential for an effective anti-cancer immune response. However, T cells are often prevented to efficiently invade tumours due to a repulsive tumour microenvironment (TME). The exclusion of T cells does not only preclude spontaneous killing of cancer cells but also interferes with therapeutic approaches like immune checkpoint blockade. Infiltration of T cells is mediated by the interaction of endothelial adhesion molecules such as ICAM-1 and integrins like LFA-1 expressed on T cells. So far, it is not fully understood whether or how RNA-based regulatory pathways might be involved in the generation of the immunosuppressive TME and T cell exclusion. Therefore, we have chosen to investigate these regulatory events originating from cancer cells and interfering in the interaction between ICAM-1 and LFA-1 by designing and performing a RNAi screening approach. Further on we focused on the validation and characterization of newly identified, potential therapeutic targets.

5.1 Affecting and monitoring T cell binding *in vitro* by stable and robust cell adhesion assay

Cell adhesion assays enable the investigation of the binding affinity and efficiency of T cells to an immobilized ligand *in vitro* under a variety of enhancing or suppressing conditions. These *in vitro* studies highly contribute to the detailed understanding of the process of T cell adhesion and to the future application of this knowledge for developing new therapy approaches.

In order to mimic T cell adhesion and infiltration *in vitro*, we established a stable and robust protocol for cell adhesion, taking advantage of the strong interaction between the endothelial adhesion molecule ICAM-1 and the integrin LFA-1 expressed on T cells. Therefore, the human ICAM-1 protein has been purified recombinantly and used as immobilized ligand on 96-well plates. After addition of primary T cells, their binding to the coated ligand has been detected using a plate reader. Several adhesion protocols have already been published, which we used as basis for our approach and which we optimized further to be suitable for our applications (Weitz-Schmidt and Chreng 2012; Strazza et al. 2014; Khalili and Ahmad 2015).

5.1.1 Purification of recombinant hICAM-1-Fc protein

For the purification of recombinant human ICAM-1 protein (hICAM-1), a two-step protocol has been established consisting of batch purification as first step using Protein A affinity purification beads followed by size exclusion chromatography as second step (**Figure 4-1**). Because of a N-terminal nuclear export signal (NES), the expressed protein was secreted to the supernatant of transfected HEK 293T cells. Nonetheless, some protein was still detected in the cell lysate because of incomplete secretion. Both, supernatant and cell lysate were used for purification (data not shown). Although either purified protein was functional, T cells showed higher affinity and increased binding to the secreted hICAM-1 protein, which was used for all performed experiments. When the protein is secreted, hICAM-1 is post-translationally modified, especially glycosylated, which corresponded more to the native state of the protein. Glycosylation at specific sites of the protein is known to enhance ligand binding and specificity *in vivo* (Jiménez et al. 2005). These modifications could explain why also in *in vitro* assays, T cells showed higher specificity to purified hICAM-1 from supernatants compared to not-secreted protein. Moreover, the post-translational modifications could explain the running behaviour of the protein in SDS-PAGE. Although the actual size of recombinant hICAM-1-Fc protein is around 80 kDa, in SDS-PAGE the corresponding band was observed at approximately 120 kDa (**Figure 4-2**). Because the protein is known to have eight glycosylation sites (Scott and Patel 2013), upon secretion the actual mass of the protein was increased by these modifications and hence caused the different running behaviour under denaturating conditions.

The yield of purified hICAM-1-Fc from adherent HEK 293T cells was sufficient for our applications, but for large scale purification the established protocol is quite limited. In order to optimize and increase the yield of the protein purification and still ensure the essential post-translational modifications (PTMs), insect cells or mammalian suspension cultures could be used for instance. The purification of biotherapeutics from mammalian systems is rapidly growing and is already used commercially (Dumont et al. 2016; Tan et al. 2021). Using these techniques, the purification of hICAM-1-Fc could be improved and upscaled to yield high protein amounts for our planned studies.

5.1.2 Monitoring T cell binding under different conditions by *in vitro* cell adhesion assays

The initially established *in vitro* cell adhesion assay was performed as it was already described (Weitz-Schmidt and Chreng 2012; Strazza et al. 2014). Primary T cells were fluorescently labelled using CellTracker™ Green CMFDA reagent beforehand (**Figure 4-7**). Although T cell binding under activating or inhibitory conditions could be observed clearly, the fluorescent readout showed high standard deviations and was highly dependent on the distribution of labelled T cells in the wells. The more cells had accumulated in the middle of the wells, the higher was the measured signal of the plate reader. Hence, very careful handling was essential to ensure no disturbance of the T cell – ligand interaction in the wells.

Several other already published protocols used different readouts, like for example crystal violet staining after fixation (Humphries 2001) or biotin labelling (Mould 2011), which suggested a more robust assay. To optimize our protocol and not include too many additional steps, we chose a luminescent readout using the CellTiter Glo® reagent (**Figure 4-8**). The reagent is lysing the cells bound in each well causing the release of ATP, which is further used in a reaction generating the luminescent signal (Alimov et al. 2019). The new readout had many advantages. For instance, the distribution of T cells in the wells had no influence on the measured signal intensity and no additional fixation or labelling steps were needed. But most importantly, the number of cells correlated with the induced luminescent signal, which allowed the quantification of bound cells in each well. The CellTiter Glo readout made the established protocol for *in vitro* cell adhesion assays more robust, stable and reproducible indicated by very low standard deviations.

Nevertheless, considering the assay was performed under static conditions instead of shear flow conditions, the range of observable effects was limited. Although strong activation and inhibition of T cells worked well and induced clearly distinguishable signals, the possibility remained that small effects might get lost or could not be detected under static conditions. In order to overcome such limitations, *in vitro* cell adhesion assays could be performed under flow conditions and shear stress (Strazza

et al. 2016). Because the activation of integrins is dependent on the remodelling of cytoskeletal components and binding to endothelial cells has to resist shear stress in the blood vessel (Harjunpää et al. 2019), the flow conditions *in vitro* would mimic the natural environment of T cell adhesion more accurately and could enhance the detection of possible effects. Moreover, T cell adhesion mediated by ICAM-1 – LFA-1 interaction is dependent on other arrest signals like E-selectins – PGSL-1 or CXCL8 – CXCR1 interactions, which are involved in the activation of integrins and hence firm adhesion of T cells to the endothelium (Wen et al. 2022). Therefore, combined coating of ICAM-1 with other factors under shear flow conditions might additionally increase potential effects in *in vitro* cell adhesion assays, which could be missed under static conditions and in our assays.

5.1.3 Affecting T cell binding in *in vitro* cell adhesion assay by tissue culture supernatants

In the established and optimized *in vitro* cell adhesion assay, T cell binding could be observed under activating or inhibitory conditions. When T cells were treated with specific activating ions like manganese or magnesium (Walling and Kim 2018), binding affinity was increased. Whereas the treatment with a specific LFA-1 inhibitor blocked binding to the coated ligand (Neri et al. 2018) (**Figure 4-8 B I.**). Moreover, we were able to show that the treatment of T cells with tissue culture supernatants exerted different effects on their binding ability. The colorectal cancer (CRC) cell lines HCT 116 and HT 29 were identified to generate an immunosuppressive tissue culture supernatant, which downregulated T cell binding significantly compared to normal growth media or a non-cancerous human dermal fibroblast cell line (hDF), that served as control cell line (**Figure 4-10**). Supernatants of melanoma cell lines did not induce these downregulating effects except A 375 cells. This cell lines showed reduced T cell binding as observed for HCT 116 and HT 29 cells (**Figure 4-11**). Supernatants of other tested cancer cell lines as well showed immunosuppressive activity but again not to the same extent as the CRC cell lines (**Figure 4-12**).

In most cases, colorectal cancer is only modestly or not responsive to immunotherapy treatments based on decreased T cell infiltration and low mutational burden

indicating genomic stability (**3.1.2**) (Grasso et al. 2018; Hegde and Chen 2020). In contrast to that, melanoma patients were already successfully treated by immunotherapy approaches especially using immune checkpoint inhibitors (Hodi et al. 2010). Our *in vitro* data is suggesting similar outcomes as detected in *in vivo* studies. In cell adhesion assays, T cell binding was impaired based on the treatment with supernatants of colorectal cancer cell lines while most of the tested melanoma cell lines did not induce an inhibitory effect on T cell adhesion. Therefore, our *in vitro* approach simulates features of the *in vivo* state of tumours with high and low T cell infiltration based on the generated microenvironment.

But T cell infiltration is not only regulated by the composition of the tumour microenvironment, as described above (**3.1.3**). It also highly depends on the endothelial barrier created by tumours. Tumour endothelial cells (TECs) are considered as "gatekeepers" for immune cell infiltration and play a central role in interfering with anti-cancer immune response. Additionally, they are suggested to be involved in tumour progression and metastasis (Maishi et al. 2019; Nagl et al. 2020). Moreover, the tumour endothelium builds a selective barrier, allowing immunosuppressive cell types to pass and in contrary effectively block immune supporting cells to enter (Duru et al. 2020). Identifying factors regulating this selectivity and understanding the mechanisms how this barrier excludes T cells could be a promising aspect for the improvement of current immunotherapy approaches.

5.1.4 Equal levels of LFA-1 activation and inhibition in tissue culture supernatants

LFA-1 activation involves conformational change from a bent to an extended open conformation. Essential for this rearrangement are cytoskeletal components like talin and kindlin and divalent cations like manganese and magnesium. Moreover, integrins can be kept in an inactive state by calcium ions (Dransfield et al. 1992; Arnaout 2016).

In order to validate whether detected effects caused by tissue culture supernatants in the *in vitro* cell adhesion assays are the result of impaired or restored activation of the integrin LFA-1, LC-AA assays were performed. In this approach, T cells with active or inactive LFA-1 can be distinguished from each other in FACS measurements. The

supernatants of HCT 116, MCF7 and SK-MEL-28 were compared to their growth medium (**Figure 4-13**; **Figure 4-14**). MCF7 and SK-MEL-28 were intended to be control cell lines because they were shown to not significantly downregulate T cell binding in previous experiments (**Figure 4-11**; **Figure 4-12**). Unfortunately, there was no clear difference in LFA-1 activation detected between growth media and cancer cell supernatants. Only a slight decrease of active LFA-1 was determined for supernatants of HCT 116 cells, which was insignificant.

In order to even be able to detect active LFA-1 in medium or supernatants, T cells had to be activated by high magnesium concentrations and a specific T cell activator beforehand. Moderate magnesium concentrations or only magnesium was not able to activate LFA-1, which is known to be sufficient under normal conditions (Gahmberg et al. 2009). This indicated high inhibitory effects of the growth media itself and made it difficult to detect inhibition of LFA-1 in cancer cell supernatants. The media contains calcium ions, which could lead to the LFA-1 inhibition. Calcium ions need to be replaced in order to activate LFA-1. Only high concentrations of magnesium are able to achieve this replacement (Dransfield et al. 1992), explaining some of the difficulties in the LC-AA assays. Moreover, also the remodelling of the cytoskeletal is essential for full activation of LFA-1 (Wen et al. 2022). The effect induced by the supernatants in the adhesion assay could also have an impact on this mechanism. But with the LC-AA approach, only soluble ICAM-1 is added for binding and hence essential forces needed for the cytoskeletal rearrangements are not given. Further optimizations like special media with low calcium concentrations or other assays involving forces inducing cytoskeletal rearrangements could help to validate a similar effect on LFA-1 activation caused by tissue culture supernatants like we have seen in cell adhesion assays (**4.3**).

5.2 Restoring reduced T cell binding induced by cancer cell lines via performing RNAi knockdowns

After demonstrating that supernatants of cancer cell lines induced a reduction of T cell binding in *in vitro* cell adhesion assays, we focused on the identification of regulatory events originating from cancer cells, which are involved in impairing the binding of T cells to ICAM-1. Therefore, siRNA knockdown experiments have been

performed in cancer cell lines HCT 116, HT 29 and A 375. We hypothesize that knockdowns could induce changes of the secretome of these cell lines to a less immunosuppressive state and hence restore T cell binding in adhesion assays.

5.2.1 Increase of T cell binding upon siRNA knockdown of CTNNB1 in HCT 116 cells

In order to prove that RNAi knockdowns are able to reverse the effect of impaired T cell binding in the first place, proteins involved in well-known oncogenic signalling pathways were targeted with specific siPOOLs. The main driver of the Wnt/β-catenin pathway CTNNB1 with its downstream factor ATF3 (Luke et al. 2019; Li et al. 2019b) and the transcription factor STAT3 (Yang et al. 2007; Yu et al. 2009) were chosen. These pathways are known to be involved in T cell exclusion from tumours (**3.1.3**) and appeared to be suitable controls in our experiments.

In the colorectal cancer cell line HCT 116, the siRNA knockdown of CTNNB1 effectively increased T cell binding compared to a control siRNA and wildtype. Targeting STAT3 and ATF3 showed only mild effects. Moreover, the overexpression of CTNNB1 and STAT3 even further decreased T cell binding in adhesion assays (**Figure 4-16**). These results demonstrate that by performing siRNA knockdowns with specific siPOOLs targeting oncogenic pathways, the supernatant of HCT 116 was less immunogenic and T cell binding was restored to some extent. Due to a very low transfection efficiency in HT 29 cells, the detected effects were very little and not significant, but indicated a slight increase in T cell binding induced by siRNA knockdown of CTNNB1 (**Figure 4-18**). For the melanoma cell line A 375, none of the tested targets induced significant effects. Only CTNNB1 induced a small increase upon knockdown and a mild decrease upon overexpression (**Figure 4-19**).

Overall, the detected effects after siRNA knockdowns are rather small but with only minor standard deviations. Little effects could be explained by the limitations of the *in vitro* cell adhesion assay. Due to the static conditions of the assay, induced effects might be lost and excluded from a detectable range, as already discussed above (**5.1**). Additionally, longer incubation times for 72 h instead of 48 h after the knockdowns seemed to have more severe effects on the state of health of transfected cells, which

might explain the higher standard deviations obtained for this timepoint. Nevertheless, at 48 h, the low standard deviations of biological replicates indicated stable and reproducible results.

The *in vitro* approach used in this work reflects to some extent the *in vivo* state, where high levels of CTNNB1 are involved in T cell exclusion from tumours. Of all tested cell lines, HCT 116 had the best transfection efficiency, which might be one reason why higher effects in the knockdown experiments were detected compared to other cell lines. T cell exclusion based on beta-catenin signalling was not only shown for colorectal cancer (Grasso et al. 2018), but also for melanoma (Spranger et al. 2015; Spranger and Gajewski 2018). Still, for the melanoma cell line A 375, the knockdown of CTNNB1 did not induce significant effects. The inhibition of T cell infiltration from tumours *in vivo* is a very dynamic process, which involves many different pathways, factors and also cell types (Spranger and Gajewski 2018; Yang et al. 2019). Considering this, the effects detected in the performed *in vitro* assay were just a snapshot of a larger picture and therefore detectable results concerning T cell binding could be small. Especially, in the performed cell adhesion assay, only factors having an influence on the interaction of ICAM-1 with LFA-1 were validated, which are just two of many mediators of T cell infiltration (Harjunpää et al. 2019). With this *in vitro* approach only very specific effects could be detected rather than getting a global picture of the binding efficiency of T cells.

The siRNA knockdown of both STAT3 and ATF3 did not show distinct effects and results were less reliable. Both targets are important transcription factors regulating expression of a variety of genes (Yu et al. 2009; Zhao et al. 2016). With the knockdown of these two factors, the expression landscape in cells could be change to great extent, which might affect other cellular pathways but does not impair T cell binding. Additionally, STAT3 and ATF3 are not as highly expressed in the tested cell lines as CTNNB1 (Uhlén et al. 2015) *Human Protein Atlas*; proteinatlas.org), which could also explain lower or no detectable effects.

For further validation of the results obtained by the siRNA knockdown of CTNNB1 and other targets, secretome analyses could be performed for example via SILAC metabolic labelling followed by mass spectrometry (Severino et al. 2013; Weng et al. 2016). By comparing the supernatant of WT cells with cells transfected with the

siRNA control and with the specific siRNA of tested targets, changes in the secretome environment and specific biomarkers could be verified. Identified differences in secretome composition or expressed factors secreted into the supernatants could generate a valid dataset of the microenvironment of cancer cells and could be relevant for identifying specific molecules regulating the interaction between ICAM-1 and LFA-1. Using secretome analysis or ELISA experiments, also changes in chemokine levels could be detected and validated. The levels of different chemokines are essential for migration and infiltration of immune cells and shape the tumour microenvironment to escape and downregulate the immune response (Kohli et al. 2021; Aleksandra J. Ozga et al. 2021). Downregulation of immunosuppressive chemokines and increased expression of chemoattractants could explain an increase in T cell binding detected in adhesion assays. Additionally, binding of chemokines to their respective chemokine receptor is involved in LFA-1 activation and clustering, which could also explain effects detected in the assays (Wen et al. 2022).

5.2.2 Identification of potential immune regulatory RBPs by RNAi screening approach

RNA-binding proteins (RBPs) are essential for post-transcriptional regulation of gene expression. They control the "mRNA life cycle", which includes, for example, mRNA processing steps, localization, turnover, storage and translation (Coppin et al. 2018; Masuda and Kuwano 2018). Cancer cells are able to dysregulate the expression and activity of RBPs and hence use these post-transcriptional regulatory machinery to adjust protein levels in a quick and stable manner dependent on specific signals (Pereira et al. 2017). Therefore, we wanted to investigate the role of this class of proteins in the generation of the immunosuppressive tumour microenvironment and in T cell exclusion.

In order to identify RNA-based regulatory events in cancer cells, which are interfering in the interaction between ICAM-1 and LFA-1, a RNAi screening approach was designed targeting around 700 different RBPs. By performing siRNA knockdowns of these targets followed by cell adhesion assays, essential proteins could be found enhancing the binding of T cells, although these were treated with cancer cell

supernatants. This was already shown for the knockdown of CTNNB1 (**Figure 4-16 A**), which served as a positive control for the screening approach and was discussed above (**5.2.1**). As a proof of principle, whether targets can be identified at all, only a part of the RBP siPOOL library was screened and a set of experiments was established to validate potential hits. The full screening is ongoing and will generate a valid dataset of promising RBP candidates, which are involved in T cell exclusion.

The primary screening revealed several RBPs clearly upregulating T cell binding after siRNA knockdown in HCT 116 cells (**Figure 4-21**). Although most targets scattered around the level of the siRNA control, several factors especially involved in splicing and nucleocytoplasmic transport induced an obvious effect in the adhesion assay. The screening was performed in biological replicates. The high standard deviations obtained were therefore expected. The screening approach included many different steps from transfection until measurement of bound T cells. Therefore, it is likewise that biological replicates differ and show high deviations Additionally, all steps were performed manually increasing variability in biological replicates as well. In order to exclude potential "false-positive" hits, a "cut-off" was set at a specific level. The threshold was determined by the SRRM4 protein, which was included in the library but is not expressed in the used cell line at detachable levels (Uhlén et al. 2015) *Human Protein Atlas*; proteinatlas.org). The ratio of increased T cell binding induced upon knockdown of this target could be caused for instance by off-target effects or similar.

For further validation of the primary screening and possible hits (**Figure 4-22**), a set of experiments was performed to narrow down the identified targets and make sure, the induced effects on T cell binding are valid and reliable (**Figure 4-23** - **Figure 4-27**). Besides performing cell adhesion assays, also cell viability of cancer cells after knockdown, knockdown efficiency and transfection efficiency were checked. Based on the obtained results, several of the initially assumed potential hits were considered "false-positive" and were excluded. DDX39B and RAN for instance showed upregulation of T cell binding, but the knockdown decreased viability of HCT 116 cells severely (**Figure 4-23 C**). Because cells were not growing anymore, they did not secrete enough factors to generate a conditioned supernatant, which

might affect the ICAM-1 – LFA-1 interaction in the adhesion assay. The supernatants equalled more normal growth media than supernatant of actively growing cancer cells, which could explain the increase in T cell binding (**Figure 4-23 A**). Besides DDX39B and RAN, also RBM14 was considered a potential hit, but was excluded from further validations because the siRNA knockdown of this target was not very efficient (**Figure 4-23 B**). Detected effects for the knockdown of this target could be caused by off-target effects or similar. Nonetheless, we were able to validate different RBPs as potential immune regulators affecting T cell binding *in vitro* (**Figure 4-24**; **Figure 4-26**).

Consequently, RNA binding proteins are interesting targets, which could have immune regulatory functions and hence have an impact on the generation of the immunosuppressive tumour microenvironment. However, in such a screening approach it is crucial to validate possible hits in detail and make sure "false-positive" are excluded. Especially, high standard deviations can make it difficult to identify real hits. But these need to be tolerated in biological replicates because of the many different steps performed in the protocol and a high variability in cell-based assays like this. To reduce standard deviations and ensure higher reproducibility, the screening workflow could be automated instead of performing it manually. By using automated systems for transfection or washing steps in the adhesion assay, the single wells of 96-well plates are expected to be treated more equally, which makes results less error-prone. In other already published screening approaches similar difficulties had to be approached. Of hundreds of identified hits in the primary screening, real targets were narrowed down to a small number which, were worth further validation (Tang et al. 2008).

In the end, we were able to identify the alternative splicing factor PUF60 and the export factor XPO1 as potential immune regulators significantly affecting T cell binding *in vitro*. These two factors were further validated in more detail, which will be discussed in the next chapter (**Figure 4-26**; **5.3; 5.4**). However, with the identification of the two factors as potential immune regulators out of almost 90 proteins tested, the initial screen was already successful. The ongoing full screening could identify even more RBPs, which can have essential functions and support T cell exclusion. In this regard, it is worth noting, that the established RNAi screening

approach is universally adaptable for testing many different protein classes. Not only RBPs, but also kinases and phosphatases for instance might be interesting targets to validate. Post-translational modifications can be crucial for protein function of RBPs and therefore could also be involved in impairing the interaction of ICAM-1 with LFA-1. Additionally, cancer cells are known to use PTMs to alter and dysregulate protein functions (Pereira et al. 2017; Theivendran et al. 2020). Therefore, RBPs itself or other proteins regulating RBP function could be targeted for modulating the cancer cell secretome.

Ultimately, we were able to establish a genome-wide screening approach, which is easily adaptable for different targets of interest basically by changing the siRNAs used. Moreover, besides RNAi screenings, also CRISPR screens are a powerful approach to identify gene functions in a wide range of applications and different species, which might differ from essential genes identified by RNAi (Morgens et al. 2016; Bock et al. 2022). Therefore, combination of both, CRISPR and RNAi screens could improve performance and shed light on even more potential factors involved in T cell infiltration.

5.3 Identification of splicing factor PUF60 as new targets involved in reducing T cell infiltration

In our RNAi screening approach, the alternative splicing factor PUF60 and the export factor XPO1 were identified as hits with potential immune regulatory function. In cell adhesion assays, the overexpression of PUF60 induced significant decrease in T cell binding, whereas the siRNA knockdown of XPO1 significantly increased the binding (**Figure 4-26**). We focused firstly on PUF60 and intended to validate this target in more detail to propose a potential model regarding its potential function as regulator of T cell infiltration.

The nucleic acid-binding protein Poly(U) binding splicing factor 60 (PUF60) plays an essential role in nuclear processes like pre-mRNA splicing and transcriptional regulation (Page-McCaw et al. 1999). PUF60 recognizes weak 3' splice sites and functions in similar capacity to its related factor $U2AF^{65}$ (Hastings et al. 2007). $U2AF^{65}$ together with $U2AF^{35}$ builds the U2AF heterodimer, which is the most important U2

small nuclear ribonucleoprotein particle (snRNP) auxiliary factor supporting the recognition of the 3' splice sites and promoting spliceosome assembly. The heterodimer together with splicing factor 1 (SF1) identifies the 3' splice site junction and the surrounding branch point sequence, subsequently recruits U2 snRNP and dissociates from the active spliceosome (Wu and Fu 2015; Agrawal et al. 2016). PUF60 and U2AF^{65} can work together and by regulating their expression levels, alternative splicing events can be affected within cells (Hastings et al. 2007). High levels of PUF60 were identified to be involved in the development and progression of multiple cancers including colon cancer (Kobayashi et al. 2016). Moreover, between all well-established RNA splicing factors, PUF60 was found to be one of the most differentially expressed genes and is thought to play a pro-tumorigenic role in bladder cancer (Long et al. 2020). Recently, PUF60 was postulated to be a major oncogenic splicing factor supporting the progression of lung cancer by regulating alternative splicing of genes involved in the cell cycle (Xu et al. 2023).

PUF60 was identified in the primary screening to upregulate T cell binding after siRNA knockdown. In further validation experiments, this upregulating effect was not as strong anymore. But we found that upon overexpression of PUF60, T cell binding was even more decreased in HCT 116 cells (**Figure 4-26**). Additionally, after overexpression, PUF60 was identified to interact strongly with CTNNB1 on mRNA level and also ATF3 mRNA levels were increased to some extent. Acting as the downstream factor of CTNNB1, this increase additionally confirms the specificity of PUF60 to CTNNB1 mRNA (**Figure 4-28**). In rescue experiments, the reduced T cell binding in cell adhesion assays upon PUF60 overexpression was reversed and strongly increased after performing a siRNA knockdown of CTNNB1 on top (**Figure 4-29**).

It was reported that CTNNB1 pre-mRNA can be alternatively spliced generating three distinct splice variants of the 3' UTR (Thiele et al. 2006). These variants are assumed to be a full-length (3' FL), a short (3' SP) or the canonical isoform. Moreover, the 3' SP was postulated to be the main isoform in cancer and to be responsible for higher protein expression and the oncogenic functions of CTNNB1 (Chan et al. 2022). The shortening of the 3' UTR is a global feature in cancer cells and results from alternative polyadenylation (APA) mainly. APA is suggested to cause an increase in mRNA

stability and protein levels of especially oncogenes, which subsequently show enhanced activity (Mayr and Bartel 2009). The deregulation of 3' UTRs processing is suggested to promote cancer pathogenesis and hence is a very interesting research topic to improve therapeutic developments (Chan et al. 2023).

Taking these facts into account, alternative splicing of the 3' UTR of CTNNB1 dependent on PUF60 overexpression and siRNA knockdown was validated. By performing RT-PCR, three distinct splice variants were detected (**Figure 4-30**). Sanger sequencing of the identified bands affirmed our theory that the three published 3' UTRs were detected (**Figure 4-30 B II.**). The longest PCR product corresponded to the full-length isoform (3'FL), which is not spliced indicated by the detection of the 5' splice site. The middle band could be assigned to the canonical isoform and the smallest band to the short 3' UTR variant. Moreover, upon siRNA knockdown of PUF60, an isoform shift was detected. The smallest and highest band decreased in intensity significantly, while the canonical isoform was identified as the predominant one (**Figure 4-31 A**). Regarding protein levels, we were not able to clearly correlate different splice variants and protein levels yet. Although the overexpression of PUF60 induced the highest CTNNB1 protein levels and showed predominately the 3' SP splice variant, the Western Blot did no show a decrease of CTNNB1 levels upon the siRNA knockdown of PUF60 (**Figure 4-31 B**).

Nevertheless, the obtained results indicate a potential model of PUF60 being responsible for alternative splicing of the CTNNB1 pre-mRNA, generating a short 3' UTR variant, which increases translation resulting in higher CTNNB1 protein levels and hence cause T cell exclusion (**Figure 5-1**).

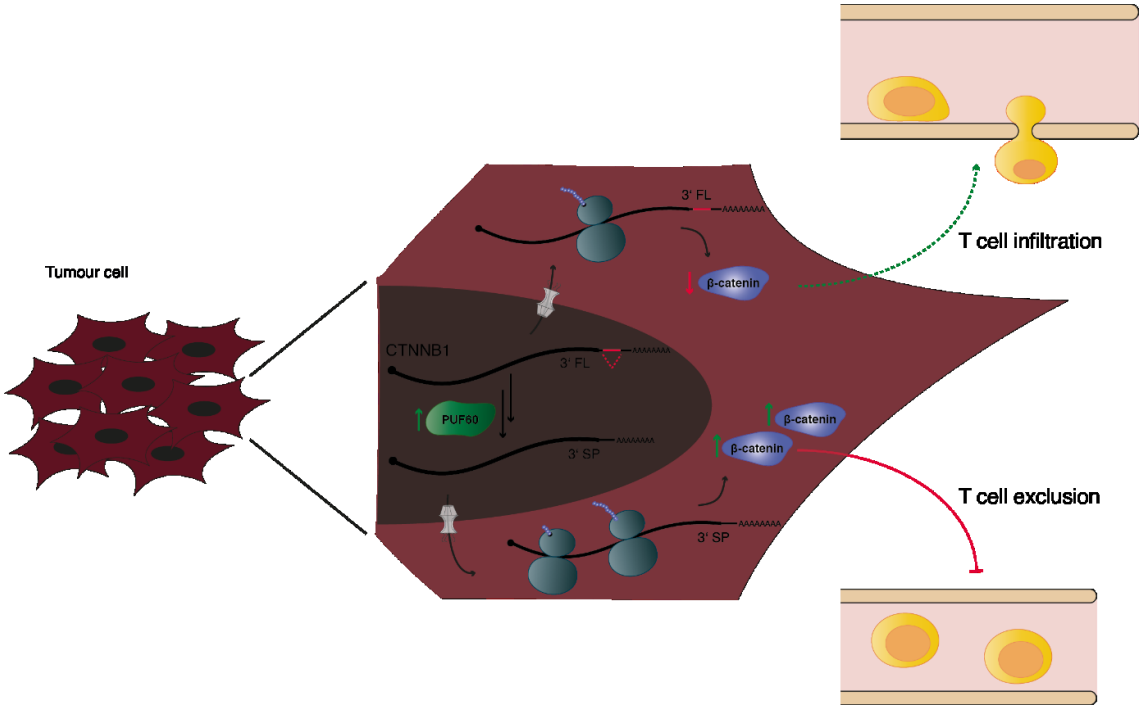

Figure 5-1: Potential model of the effect on T cell infiltration induced by PUF60. *High levels of PUF60 support alternative splicing of the 3' UTR of CTNNB1. The resulting short isoform (3' SP) is strongly translated and increases CTNNB1 protein levels. High levels of CTNNB1 lead to T cell exclusion. Lower levels of PUF60 favour different 3' UTR isoforms of CTNNB1. Moderate protein levels of CTNNB1 then are not excluding T cells as strongly allowing infiltration to some extent.*

The performed experiments suggest the postulated model but there are still many details missing to fully prove it. For once, after knockdown of CTNNB1, the long 3' UTR of CTNNB1 mRNA was detected by RT-PCR. Nevertheless, the knockdown reduced protein levels significantly, which indicates amplification of an unspecific band. Secondly, the knockdown of PUF60 indicates splicing of the 3' UTR of CTNNB1 generating mainly the canonical 3' UTR. Being only one of many splice factors, which are involved in 3' splice site recognition, upon knockdown other splicing factors like U2AF^{65} could substitute for the loss of the protein (Hastings et al. 2007). This might explain the generation of the canonical CTNNB1 3' UTR. Instead of using an alternative 3' splice site in the UTR, splicing factors like U2AF^{65} preferentially bind to stronger ones (Agrawal et al. 2016). Therefore, the detection of the canonical 3' UTR suggests the prevention of alternative splicing in the 3' UTR of CTNNB1 pre-mRNA and the support of canonical splicing events.

Lastly, we were not able to show a reduced CTNNB1 protein level upon knockdown of PUF60. But already in WT, high CTNNB1 levels were detected (**Figure 4-31 B**). Without knowing the half-life of the protein and degradation rates, it is difficult to clearly identify a decrease in protein levels in Western Blot.

All these results support our model, but there is still evidence missing to clearly prove the oncogenic function of PUF60. Another point to consider is that CTNNB1 is not the only target of PUF60 and probably many more splicing events of different genes are induced upon overexpression of the splicing factor. To get a clearer picture, deep sequencing in the conditions of PUF60 overexpression versus siRNA knockdown could help to identify specific targets and alternative splicing events. Additionally, secretome analysis of the same conditions could reveal changes of the microenvironment which could be connected with alternative splicing events.

5.4 Increased T cell binding by targeting RNA-based regulatory pathways

Besides the alternative splicing factor PUF60, we also identified the nuclear export factor XPO1 in our screening approach as potential immune regulator. Moreover, we were able to reproduce the effect of the primary screening and prove, that upon siRNA knockdown of XOP1, T cell binding was significantly increased (**Figure 4-26**). But for now, we were not able to identify a connection of XPO1 with known immune regulatory pathways yet. Different experiments are needed to gain reliable results, which will help to reveal the immune regulatory function and interaction partners of this factor. For example, it is suggested that there is an indirect interaction of XPO1 with CTNNB1, which is mediated by galectin-3 causing platinum resistance (Hu et al. 2015; Azmi et al. 2021). Therefore, further validation of this target and validation of a potential interaction with galectin-3 or other immune regulatory pathways are of great interest.

All in all, we were able to demonstrate that RNA-based regulatory pathways are involved in T cell - cancer communication and are promising targets for future immunotherapy approaches. The full RNAi screening is still ongoing and will provide a valid dataset of RBPs, RNA modifying enzymes, or components of the miRNA

pathway involved in the generation of the immunosuppressive microenvironment and T cell exclusion. By performing secretome analysis and deep sequencing in knockdown conditions versus WT or controls, altered expression of targets and affected pathways can be identified and validated in detail. Moreover, not only RBPs, but also other classes of proteins like kinases and phosphatases can be targeted in the established RNAi screening approach to even extent the list of promising candidates involved in T cell - cancer cell communication. With the established approach, we contribute to a better understanding of the regulation of T cell infiltration and provide a valuable dataset of potential targets for RNA-based immunotherapy in the future.

6 Material and Methods

6.1 Materials

6.1.1 Enzymes, Antibodies and Kits

Following enzymes, antibodies and kits were used for the performed experiments. For the used enzymes the appropriate buffers were purchased from the same company. Experiments were performed according to the manufacture's protocol.

Table 6-1: List of Enzymes

Enzymes	Supplying company
DNase I	Thermo Fisher Scientific (Waltham, USA)
Phusion Polymerase	Thermo Fisher Scientific (Waltham, USA)
T4 Polynucleotide Kinase (PNK)	Thermo Fisher Scientific (Waltham, USA)
T4 DNA Ligase	Thermo Fisher Scientific (Waltham, USA)
Taq Polymerase	Thermo Fisher Scientific (Waltham, USA)
Restriction enzymes	
AscI	New England Biolabs (Ipswich, USA)
BamHI	Thermo Fisher Scientific (Waltham, USA)
Bsu15I	Thermo Fisher Scientific (Waltham, USA)
DpnI	Thermo Fisher Scientific (Waltham, USA)
Eco52I	Thermo Fisher Scientific (Waltham, USA)
EcoRI	Thermo Fisher Scientific (Waltham, USA)
FseI	New England Biolabs (Ipswich, USA)
HindIII	Thermo Fisher Scientific (Waltham, USA)
KpnI	Thermo Fisher Scientific (Waltham, USA)
Not I	Thermo Fisher Scientific (Waltham, USA)

Table 6-2: List of Antibodies

Antibody	Origin	Purpose	Dilution	Sypplying Company
Primary antibodies				
α-HA	Mouse	Western Blot	1:1000	Covance (Munich, Germany)
α-GFP	Rabbit	Western Blot	1:5000	GeneTex (Irvine, USA)
α-αlpha-Tubulin	Mouse	Western Blot	1:10000	Sigma-Aldrich (Steinheim, Germany)
α-beta-Tubulin	Rabbit	Western Blot	1:1000	LI-COR (Lincoln, USA)
α-β Catenin	Rabbit	Western Blot	1:5000	Proteintech (Manchester, UK)
α-ICAM-1	Mouse	Western Blot	1:25000	Proteintech (Manchester, UK)
α-IgG-HRP	Goat	Western Blot & ELISA	1:40000	Sigma-Aldrich (Steinheim, Germany)
α-Fibronectin	Mouse	Western Blot	1:5000	Thermo Fisher Scientific (Waltham, USA)
Secondary antibodies				
α-mouse IgG (H+L) IRDye 800C	Goat	Western Blot	1:10000	LI-COR Biosciences (Lincoln, USA)
α-rabbit IgG (H+L) IRDye 800C	Goat	Western Blot	1:10000	LI-COR Biosciences (Lincoln, USA)
Additional antibodies				
α-CD18	Mouse	Cell Adhesion Assay	1:1000	Thermo Fisher Scientific (Waltham, USA)
α-human IgG Fc-Spec.	Rabbit	Cell Adhesion Assay	10 µg/mL	Jackson ImmunoResearch Laboratories (Baltimore, USA)

Fluorescent antibodies

CellTracker™ Green CMFDA dye		Cell Adhesion Assay	5 µM	Thermo Fisher Scientific (Waltham, USA)
KIRVAVIA Blue anti-human CD3	Mouse clone UCHT2	LC-AA Assay	1:300	BioLegend (San Diego, USA)
APC anti-human CD4	Mouse clone OKT4	LC-AA Assay	1:300	BioLegend (San Diego, USA)
Brilliant Violet 510™ anti-human CD8(a)	Mouse clone HIT8a or SK1	LC-AA Assay	1:300	BioLegend (San Diego, USA)
PE anti-human-Fc Fab2	Mouse	LC-AA Assay	1:125	Jackson ImmunoResearch Laboratories (Baltimore, USA)
ICAM-1-Fc	Human	LC-AA Assay	1:40	Laboratory Jörg Wischhusen (Würzburg, Germany)

Table 6-3: List of Kits and Reagents

Kit and Reagent	Supplying Company
α-FLAG-M2 beads	Sigma-Aldrich (Steinheim, Germany)
CellTiter-Glo® Luminescent Cell Viability Assay	Promega (Madison, USA)
Clarity Western ECL substrate	Biorad (Herkules, USA)
DiaEasy Dialyzer (800µL) MWCO 3.5 kDa	Abcam (Cambridge, UK)
LFA-1 antagonist BI-1950	opnMe – Boerhringer Ingelheim (Ingelheim, Germany)
Lipofectamine® 2000	Thermo Fisher Scientific (Waltham, USA)
Lipofectamine® 3000	Thermo Fisher Scientific (Waltham. USA)
Lipofectamine® RNAiMax	Thermo Fisher Scientific (Waltham, USA)

Illustra™ MicroSpin™ G-25 Columns	Cytiva (Marlborough, USA)
ImmunoCult™ Human CD3/CD28/CD2 T Cell Activator (TCR)	Stemcell Technologies (Vancouver, Canada)
NucleoSpin® Gel and PCR Cleanup	Macherey-Nagel (Düren, Germany)
NucleoSpin® Plasmid	Macherey-Nagel (Düren, Germany)
NucleoSpin® RNA	Macherey-Nagel (Düren, Germany)
NucleoSpin® RNA XS	Macherey-Nagel (Düren, Germany)
NucleoSpin® Xtra Midi	Macherey-Nagel (Düren, Germany)
pGEM-T Easy Vector systems	Promega (Madison, USA)
RevertAid First Strand cDNA synthesis Kit	Thermo Fisher Scientific (Waltham, USA)
Roti®Sep 1077 human CELLPURE®	Carl Roth GmbH & Co.KG (Karlsruhe, Germany)
Takyon™ No ROX SYBR	Eurogentec (Seraing, Belgium)
TMB Ready to Use ELISA substrate	Serva Electrophoresis (Heidelberg, Germany)

6.1.2 Additional Reagents and Consumables

If not stated otherwise, all chemicals and reagents were obtained from the following suppliers: AppliChem (Darmstadt, Germany), Biorad (Herkules, USA), Boerhringer Ingelheim (Ingelheim, Germany), Carl Roth GmbH & Co.KG (Karlsruhe, Germany), Cytiva (Marlborough, USA), Merck (Darmstadt, Germany), New England Biolabs (Ipswich, USA), Roche Diagnostics (Penzberg, Germany), Serva Electrophoresis (Heidelberg, Germany), Sigma-Aldrich (Steinheim, Germany) and Thermo Fisher Scientific (Waltham, USA).

Radiochemicals were purchased from Hartmann Analytics GmbH (Braunschweig, Germany). DNA oligonucleotides were ordered from Metabion GmbH (Planegg, Germany) or from TWIST Bioscience (San Francisco, USA). RNA oligonucleotides were purchased from siTOOLs Biotech GmbH (Planegg, Germany).

Other consumables were purchased from Biorad (Herkules, USA), CAWO (Schrobenhausen, Germany), Cytiva (Marlborough, USA), Eppendorf (Hamburg,

Germany), Invitrogen (Carlsbad, USA), OMNI Life Science (Bremen, Germany), Sarstedt (Nümbrecht, Germany) and Sartorius (Göttingen, Germany).

6.1.3 Technical Equipment

Table 6-4: List of technical equipment

Name	Supplying Company
Attune NxT Acoustic Focusing Cytometer	Life Technologies (Carlsbad, USA)
Avanti™ J-20 Centrifuge	Beckman Coulter (Brea, USA)
Äkta purification System	GE Healthcare/ Cytiva (Marlborough, USA)
CASY Cell Counter & Analyzer	OMNI Life Science (Bremen, Germany)
Centrifuge 5427R	Eppendorf (Hamburg, Germany)
CFX96 Dx Real-Time PCR Detection System	Biorad (Hercules, USA)
ChemiDoc Touch Imaging System	Biorad (Hercules, USA)
Geiger Counter LB123 EG&G	Berthold (Bad Wildbach, Germany)
HeraCell 240i CO2 Incubator	Thermo Fisher Scientific (Waltham, USA)
Megafuge 40R Centrifuge	Thermo Fisher Scientific (Waltham, USA)
Milli-Q plus	Merck Millipore (Burlington, USA)
Mithras LB 940	Berthold (Bad Wildbach, Germany)
Molecular Imager FX Imaging Screen-K	Kodak (Rochester, USA)
Nanodrop 1000 Spectrophotometer	Thermo Fisher Scientific (Waltham, USA)
Odyssey Infrared Imaging System	LI-COR Biosciences (Lincoln, USA)
peqSTAR Thermocycler	PeqLab (Erlangen, Germany)
Personal Molecular Imager™ (PMI™) System	Biorad (Hercules, USA)
Quantum ST4	PeqLab (Erlangen, Germany)
Screen Eraser-K	Biorad (Hercules, USA)
Thermomixer Comfort	Eppendorf (Hamburg, Germany)
Trans-Blot SD	Biorad (Hercules, USA)
Ultrospec 3300 pro	Amersham Bioscience (Little Chalfont, UK)
UV Stratalinker 2400	Stratagene (Santa Clara, USA)

6.1.4 Buffers and Solutions

Phosphate buffered saline (PBS)

130 mM	NaCl
774 mM	Na_2HPO_4
226 mM	NaH_2PO_4

Tris/Borate/EDTA buffer (TBE)

89 mM	Tris-HCl pH 8,3
89 mM	Boric acid
2,5 mM	EDTA

Tris buffered saline (TBS)

10 mM	Tris-HCl pH 7,5
150 mM	NaCl

TBS-T

10 mM	Tris-HCl pH 7,5
150 mM	NaCl
0,1 %	Tween-20 (pH 8)

Tris/Actetate/EDTA buffer (TAE)

40 mM	Tris-HCl pH 8,5
20 mM	Acetic acetate
1 mM	EDTA

LB medium

5 g	Yeast extract
10 g	Tryptone
10 g/l	NaCl
Ad 1 L	H_2O

LB Agar

1 L	LB Medium
16,4 g	Agar

Easy-Prep Buffer

51 mM	Tris-HCl pH 8
1 mM	EDTA pH 8
15 %	Sucrose
2 mg/mL	Lysozyme
0,2 mg/mL	RNaseA
0,1 mg/mL	BSA

RIPA buffer

50 mM	Tris-HCl pH 8
150 mM	NaCl
1 %	NP-40
0,1 %	SDS
0,1 %	Sodium deoxycholate (DOC)
1 mM	AEBSF
1 mM	DTT

IP Wash Buffer

50 mM	Tris-HCl pH 8
500 mM	NaCl
2 mM	DTT

IP lysis buffer

20 mM	Tris-HCl pH 7,5
150 mM	KCl
2 mM	EDTA
1 mM	NaF
0,5 %	NP-40

RNA-IP Wash Buffer

20 mM	Tris-HCl pH 7,5
300 mM	KCl
1 mM	$MgCl_2$
0,5 %	NP-40

5x SDS sample buffer

300 mM	Tris-HCl pH 6,8
10 %	SDS
62,5 %	Glycerol
0,05 %	Bromphenol blue

SDS-Running buffer

25 mM	Tris-HCl pH 7,5
200 mM	Glycine
25 mM	SDS

10 % SDS-PAGE separation gel

10 %	30 % Acrylamide-Bis 37,5:1 (Serva, Heidelberg, Germany)
400 mM	Tris-HCl pH 8,8
0,1 %	SDS
0,1 %	APS
0,05 %	TEMED

5 % SDS-PAGE stacking gel

5 %	30 % Acrylamide-Bis 37,5:1 (Serva, Heidelberg, Germany)
75 mM	Tris-HCl pH 6,8
0,1 %	SDS
0,1 %	APS
0,05 %	TEMED

Towbin blotting buffer

38,6 mM	Glycine
48 mM	Tris
0,0037 % (w/v)	SDS
20 %	Methanol (MeOH)

Western Blot blocking buffer

5 %	Milk powder
0,025%	Sodium azide (NaN_3)
Add	TBS-T

Coomassie Staining solution

10 %	Acetic Acid
30 %	Ethanol (EtOH)
0,25 %	Coomassie R250

Coomassie Destaining solution

10 %	Acetiv Acid
20 %	EtOH

2x RNA loading dye

99,9 %	Formamide
0,05 %	Xylene cyanol
0,05 %	Bromphenol blue

2x RNA loading buffer

45 %	Formamide
1x	MOPS
6 %	37 % Formaldehyde
20 %	Blue juice

Blue juice

30 %	Glycerol
0,07 %	Bromphenol blue

10x MOPS

200 mM	MOPS
20 mM	NaAc
10 mM	EDTA

Adjust to pH 7

RNA Running Buffer

1x	MOPS
1/50	37 % Formaldehyde

20x SSC

3 M	NaCl
0,3 M	TriNa-Citrate

Adjust to pH 7

50x Denhardt's solution

1 %	Albumin Fraction V (BSA)
1 %	Polyvinylpyrrolidon K30
1 %	Ficoll 400

Hybridization solution

5x	SSC
20 mM	Sodium Phosphate pH 7,2
7 %	SDS
1x	Denhardt's solution

Northern Blot Wash I

5x	SSC
1 %	SDS

Northern Blot Wash II

1x	SSC
1 %	SDS

Northern Blot Wash III

2x	SSC
0,1 %	SDS

Northern Blot Wash IV

0,5x	SSC
0,1 %	SDS

Northern Blot Wash V

0,1x	SSC
0,1 %	SDS

Coating buffer for ELISA and Cell Adhesion Assay

0,1 M	Na_2CO_3
0,1 M	$NaHCO_3$

Adjust pH to 9,5

Adhesion assay blocking solution

1x	PBS pH 7,5
2 %	BSA

Adhesion assay wash buffer I

1x	PBS pH 7,5
0,05 %	Tween-20

Adhesion assay wash buffer II

50 mM	Tris-HCl pH 7,0
150 mM	NaCl
1,5 %	BSA

Adhesion buffer for cell adhesion assay

50 mM	Tris-HCl pH 7,5
150 mM	NaCl
1,5 %	BSA
2 mM	$MgCl_2$
2 mM	$MnCl_2$
5 mM	D-Glucose Monohydrat

LC-AA basic buffer

1x	PBS pH 7,5
2 mM	EGTA
1 %	BSA

LC-AA activation buffer

1x	PBS pH 7,5
2 mM	EGTA
1 %	BSA
10 mM	$MgCl_2$

2x HEPES buffered saline

274 mM	NaCl
1,5 mM	Na_2HPO_4
54,6 mM	HEPES pH 7,1

6.1.5 DNA and RNA Oligonucleotides

6.1.5.1 DNA Oligonucleotides

DNA oligonucleotides used in this work were ordered from Metabion GmbH (Planegg, Germany) and are listed below (**Table 6-5**). For molecular cloning, the restriction enzyme substrate sequences are shown in bold.

Table 6-5: DNA Oligonucleotides. Restriction enzyme substrates are shown in bold.

Name	Sequence (5' to 3')
Molecular Cloning	
hICAM_BamHI_FW	ATA **GGATCC** ATGAATTTTGGACTG
hICAM_NotI_R	AAA **GCGGCCGC** TCATTTCCC
hICAM_FLAG/HA_R	AAA CATCGTCGTCCTTGTAGTC CATCTCATACCG
IgG_FLAG/HA_FW	ATA GACTACAAGGACGACGATG ACAAGTACCCTTATGACGTGCCCGATTACGCT ATGGACCCCAAATCCTGTG
IgG_NotI_R	AAA **GCGGCCGC** TCATTTCCCGGGAGACA
ATF3_FW_FseI	ATA **GGCCGGCC** ATGATGCTTCAACACCCAGG
ATF3_R_AscI	AAA **GGCGCGCC** TTAGCTCTGCAATGTTCCTTC
CTNNB1_FW_FseI	ATA **GGCCGGCC** ATGGCTACTCAAGCTGATTTG
CTNNB1_R_AscI	AAA **GGCGCGCC** TTACAGGTCAGTATCAAACCAG
STAT3_FW_FseI	ATA **GGCCGGCC** ATGGCCCAATGGAATCAGC
STAT3_R_AscI	AAA **GGCGCGCC** TCACATGGGGGAGGTAGC
PUF60_FW_FseI	ATA **GGCCGGCC** ATGGCGACGGCGACCATAG
PUF60_R_AscI2	AAA **GGCGCGCC** TCACGCAGAGAGGTCACTG
XPO1_FW_FseI	ATA **GGCCGGCC** ATGCCAGCAATTATGACAATGTTAG
XPO1_R2_AscI	AAA **GGCGCGCC** ATCACACATTTCTTCTGGAATCTC
DDX5_FW_FseI	ATA **GGCCGGCC** ATGTCGGGTTATTCGAGTGAC
DDX5_R_AscI	AAA **GGCGCGCC** TTATTGGGAATATCCTGTTGGC
YTHDC1_FW_FseI	ATA **GGCCGGCC** ATGGCGGCTGACAGTCGGG
YTHDC1_R_AscI	AAA **GGCGCGCC** TTATCTTCTATATCGACCTCTCTCC

qPCR and RT-PCR primer

qPCR_GAPDH_Fw	TGGTATCGTGGAAGGACTCATGAC
qPCR_GAPDH_R	ATGCCAGTGAGCTTCCCGTTCAGC
qPCR_ATF3_F3	CGCTGGAATCAGTCACTGTCAG
qPCR_ATF3_R3	CTTGTTTCGGCACTTTGCAGCTG
qPCR_CTNNB1_F2	TGCAGTTCGCCTTCACTATG
qPCR_CTNNB1_R2	AGGGCAAGATTTCGAATCAA
qPCR_STAT3_F2	CAGTTTCTGGCCCCTTGGAT
qPCR_STAT3_R2	AAGCGGCTATACTGCTGGTC
qPCR_SYMPK_F2	CGACGCCAGGAGCATGATAT
qPCR_SYMPK_R2	CTGCCTTGCCCTCTTCCCATAG
qPCR_DDX5_F2	GGAAAAGCTCCTATTCTGATTGC
qPCR_DDX5_R2	GTGCCTGTTTTGGTACTGCG
qPCR_DDX39B_F2	TGGTGATGTGTCACACTCGG
qPCR_DDX39B_R2	ATGCGGGCAGTTCTTCTTCA
qPCR_PUF60_F1	CTTGGAGCAGATGAACTCGGTG
qPCR_PUF60_R1	CTCCTCAGCCAACTGGTCTATG
qPCR_RBM14_F2	CGACGATCCCTACAAAAAGGC
qPCR_RBM14_R2	GTAATCCAGCGAGGACTTTGTC
qPCR_YTHDC1_F2	TCCCCCTGAGTTTCACCAGA
qPCR_YTHDC1_R2	TCCTGAAAATCGTCTGTCCACT
qPCR_RAN_F1	CAGGTCATCATCCTCATCCGG
qPCR_RAN_R1	GAGCCCCAGGTCCAGTTCAAA
qPCR_XPO1_F1	CTACATCTGCCTCTCCGTTGCT
qPCR_XPO1_R1	CCAATACTTCCTCTGGTTTAGCC
qPCR_ZCCHC8_FW2	TGAACATTCTGACTCGACCGA
qPCR_ZCCHC8_R2	TGGGGCAAAAGATTAAAGGAAGT
RT hsLin28 1 fwd	GAAGCGCAGATCAAAAGGAG
RT hsLin28-1 rev	CGAAAGTAGGTTGGCTTTCC
qPCR_CTNNB1_3'FL_F	GCCACAGCTTTTGCAACTTA
qPCR_CTNNB1_3'FL_R	CTCGACCAAAAAGGACCAGA
qPCR_CTNNB1_3'SP_F	ATCATCCTTTAGGAGTAACAATAC
qPCR_CTNNB1_3'SP_R	AGCAAGCAAAGTCAGTACCA

RT_CTNNB1_FW	AGTTGATGGGCTGCCAGATCTG
RT_CTNNB1_R	CTGGTAAACTGTCCAAAACAAGGTTC

Northern Blot probes

NB_18S_R	CATGCATGGCTTAATCTTTGAGACAAGC

6.1.5.2 1.5.2 RNA Oligonucleotides

For RNAi screening experiments, a siPOOL library against 666 RNA binding proteins (RBPs) were designed by and ordered at siTOOLs Biotech GmbH (Planegg, Germany). Additionally, following siPOOLs were used during this work: siP NegC, siP CTNNB1, siP STAT3, siP ATF3, siP GDF15.

6.1.6 Plasmids and Constructs

For molecular cloning following plasmids were used.

Table 6-6: Plasmids available in advance of this work

Name	Description
VP5-Flag/HA-FA	Expression of protein with N-terminally fused FLAG-HA tag
VP5-FLAG/HA-eGFP	Expression of eGFP with N-terminally fused FLAG-HA tag
VP5-FLAG/HA- modified	Expression of protein with C-terminally fused FLAG-HA tag
pEF1α	Expression of protein with N-terminally fused FC-tag
pEF1α- modified	Expression of protein with N-terminally fused FC-tag; additional ClaI/Bsu15I restriction site inserted
pcDNA5-FRT/TO	Inducible expression vector designed for the use with the Flp-In™ T-REx™ System
pOG44	Flp recombinase expression vector used for the Flp-In™ T-REx™ System

6.1.7 Bacterial Strains and Cell Lines

Table 6-7: Bacterial Strains and Cell lines

Name	Specification
Bacteria strain	
E. coli XL1 blue	F- recA1 enA1 gyrA96 thi-1 hsdR17 supE44 relA1 lac F'[proAB lacIqZΔM15 Tn10 (TetR)]
Cell line	
HEK 293T	Human embryonic kidney cells
Flp-In™ T-REx™ 293	Human embryonic kidney cells containing pFRT/lacZeo and pcDNA™6/TR (from the T-REx™ System) stably integrated
hDF	Human dermal fibroblasts
HCT 116	Colorectal carcinoma cells
HT 29	Colorectal adenocarcinoma cells
A 375	Malignant melanoma cells
Mel-HO	Melanoma cells
SK-MEL-28	Melanoma cells
HeLa	Human cervical cancer cell line
Hep G2	Epithelial-like liver carcinoma cells
PANC-1	Epithelial pancreas carcinoma cells
A 549	Epithelial lung carcinoma cells
MCF7	Epithelial breast adenocarcinoma cells
HSB2	Acute lymphoblastic leukemia cells

6.2 Methods

6.2.1 Molecular Biological Methods

6.2.1.1 DNA cloning

6.2.1.1.1 General DNA cloning

For amplification of a gene of interest, Polymerase Chain Reaction (PCR) was performed using Phusion High-Fidelity DNA Polymerase (Thermo Fisher Scientific, Waltham, USA) according to the manufacturer's instructions. Annealing temperature of primers were individually determined and selected. Elongation time was set according to the size of the gene of interest, considering the approximate amplification rate of 1 kb/ 30sec at 72 °C. As DNA template for the reaction, cDNA from different cell lines or gDNA was used. PCR fragments were analysed and purified from agarose gels using NucleoSpin Gel and PCR Clean-Up Kit (Macherey-Nagel, Düren, Germany) following the manufacture's protocol. Obtained fragments and vector backbones were afterwards digested with restriction enzymes for 1 h at 37 °C. Vector backbones were analysed and purified from agarose gels using NucleoSpin Gel and PCR Clean-Up Kit. Digested PCR fragments were directly purified using the same kit. Digested vectors and PCR fragments were used for ligation using T4 DNA Ligase (Thermo Fisher Scientific, Waltham, USA) according to the manufacturer's instructions. Ligations were performed at room temperature (RT) for several hours or at 16 °C overnight (o/n).

Ligation reactions were transformed into chemical competent *Escherichia coli* (*E. coli*) cells by performing a heat shock at 42 °C for 1 min. After plating the cell suspension on LB_{Amp}-plates and incubation at 37 °C o/n, several colonies were picked and checked for positivity. Therefore, DNA was isolated using EasyPrep buffer and test digest was performed. Positive clones were re-purified with NucleoSpin Plasmid Kit (Macherey-Nagel, Düren, Germany) according to the manufacturer's protocol and send for sequencing to Eurofins Genomics (Ebersberg, Germany). DNA concentration and quality were validated using NanoDrop 1000 Spectrophotometer (Thermo Fisher Scientific, Waltham, USA).

For large-scale DNA preparations, Midis were inoculated and DNA was purified via NucleoSpin Xtra Midi Kit (Macherey-Nagel, Düren, Germany) following the manufacturer's instructions.

6.2.1.1.2 Site-directed mutagenesis

For site-directed mutagenesis ("Quikchange"), PCR reactions were performed using Phusion High-Fidelity DNA Polymerase as described above and mutagenic primers, which were used at 0,2 µM end concentration. The PCR was performed with 1 min/kb extension time at 68 °C for 30 cycles. After purification of the PCR reaction using NucleoSpin Gel and PCR Clean-Up Kit, DNA was digested with DpnI restriction enzyme for several hours at 37 °C. After again purifying DNA with the NucleoSpin Gel and PCR Clean-Up Kit, chemical competent *E. coli* cells were transformed, plated on LB_{Amp}-plates and incubated at 37 °C o/n. Afterwards, colonies were picked, DNA was isolated and successful mutagenesis was analysed by sequencing at Eurofins Genomics (Ebersberg, Germany).

6.2.1.1.3 Cloning strategies for plasmids produced in this work

Following plasmids were cloned and used in this work. Primers used for cloning are listed in **Table 6-5**.

pEF1alpha-hICAM1-EC-Fc The extracellular part (Q28 – E480) of the human ICAM-1 protein with the Fc- Fragment (P100 – K330) at its C-terminus was cloned into pEF1alpha vector. A signal sequence for protein secretion was added at the N-terminus. The construct was generated and kindly provided by the group of Jörg Wischhusen (Universitätsklinikum, Würzburg).

pcDNA5-hICAM1-EC-Fc hICAM-1-Fc was amplified from pEF1alpha-hICAM1-EC-Fc plasmid using specific primers and cloned via BamHI and NotI into pcDNA5-FRT/TO plasmid.

VP5-Flag/HA-CTNNB1 CTNNB1 cDNA was amplified via PCR using cDNA from HEK 293T cells. Cloning into VP5-FLAG/HA-FA was performed using FseI and AscI restriction sites for expression of N-terminally tagged CTNNB1.

VP5-Flag/HA-STAT3 STAT3 cDNA was amplified via PCR using cDNA from HEK 293T cells. Cloning into VP5-FLAG/HA-FA was performed using FseI and AscI restriction sites for expression of N-terminally tagged STAT3.

VP5-Flag/HA-AFT3 ATF3 cDNA was amplified via PCR using cDNA from HEK 293T cells. Cloning into VP5-FLAG/HA-FA was performed using FseI and AscI restriction sites for expression of N-terminally tagged ATF3.

VP5-Flag/HA-YTHDC1 YTHDC1 cDNA was amplified via PCR using cDNA from HCT 116 cells. Cloning into VP5-FLAG/HA-FA was performed using FseI and AscI restriction sites for expression of N-terminally tagged YTHDC1.

VP5-Flag/HA-DDX5 DDX5 cDNA was amplified via PCR using cDNA from HCT 116 cells. Cloning into VP5-FLAG/HA-FA was performed using FseI and AscI restriction sites for expression of N-terminally tagged DDX5.

VP5 -PUF60-Flag/HA PUF60 cDNA was amplified via PCR using cDNA from HCT 116 cells. Cloning into VP5-FLAG/HA-FA was performed using FseI and AscI restriction sites for expression of C-terminally tagged PUF60.

VP5-XPO1-Flag/HA XPO1 cDNA was amplified via PCR using cDNA from A459 cells. Cloning into VP5-FLAG/HA-FA was performed using FseI and AscI restriction sites for expression of C-terminally tagged XPO1.

VP5-Flag/HA-LIN28A LIN28A cDNA was amplified via PCR using cDNA from NTera cells. Cloning into VP5-FLAG/HA-FA was performed using FseI and AscI restriction sites for expression of N-terminally tagged LIN28A.

VP5- Flag/HA-ZCCHC8 ZCCHC8 cDNA was amplified via PCR using cDNA from HEK 293T cells. Cloning into VP5-FLAG/HA-FA was performed using FseI and AscI restriction sites for expression of N-terminally tagged ZCCHC8.

6.2.1.2 Working with RNA

6.2.1.2.1 RNA extraction

Dependent on the cell number, RNA extraction from cells for cDNA synthesis followed by quantitative real-time PCR (qPCR) was performed with NucleoSpin RNA Kit or

NucleoSpin RNA XS Kit (Macherey-Nagel, Düren, Germany) according to the manufacturer's instructions. RNA was eluted with H_2O.

RNA extraction from cells for Northern Blot analysis or cDNA synthesis was performed with TRIzol reagent (Life Technologies, Carlsbad, USA) as described in the manufacturer's protocol. For qPCR, the aqueous phase was extracted a second time with 1:1 volume of Chloroform. RNA was precipitated with 1 volume of Isopropanol and 0,5 µL RNA grade glycogen (Life Technologies, Carlsbad, USA) at -20 °C o/n. RNA pellet was collected by centrifugation for 30 min at 4 °C at full speed and washed twice with 75 % Ethanol (EtOH). After drying the pellet at RT for several minutes, it was resuspended in specific volumes of H_2O based on its size. RNA, which was used for cDNA synthesis, was digested with 1U/ µL DNaseI (Thermo Fisher Scientific, Waltham, USA) for 30 min at 37 °C. Reaction was stopped by adding 1 µL of 50 mM EDTA and incubation for 10 min at 65 °C.

Concentration of RNA was determined with the NanoDrop 1000 Spectrophotometer (Thermo Fisher Scientific, Waltham, USA) and RNA was stored at -20 °C or -80 °C until further use.

6.2.1.2.2 Agarose gel electrophoresis of RNA

For detection of RNA, an 2 % agarose gel was prepared with the appropriate amount of water, 1x MOPS buffer and 2 % Formaldehyse (37 %). Therefore, the agarose was first dissolved in H_2O and then cooled down to around 65 °C before the other components were added. After polymerization for approximately 1 h at RT, the gel was equilibrated in RNA running buffer for 15 min. 1- 20 µg RNA was mixed with 1x RNA loading buffer, incubated at 65 °C for 10 min and then chilled on ice. To the samples 2,3 µL of Ethidiumbromide (EtBr) (400 µg/mL) was added and loaded on the gel. Small gels were run at 70 V, big gels were run at 90 V up to several hours until the dye was approximately 1 cm above the end of the gel.

6.2.1.2.3 Capillary Northern Blot

After finishing the run, the agarose gel (**6.2.1.2.2**) was checked under UV light and washed with 50 mM NaOH, 50 mM Tris-HCl pH 7,5 and 20x SSC each for 30 min at RT while shaking. The transfer was set up by first placing a glass plate on top of 2 reservoirs filled with 20x SSC. Two stripes of Whatman paper were soaked in 2x SSC and arranged on the glass plate in a way that both ends were placed in the reservoirs. After removing bubbles, the gel was put face down on top and the ends were sealed with plastic foil or parafilm to avoid "short-circuiting". Then, the nitrocellulose membrane with the same size as the gel was soaked in Milli-Q water and 2x SSC and placed on the gel. Again, air bubbles were removed and 2 Whatman papers, which were soaked in 2x SSC, were placed on the membrane. The set up was finished with a stack of paper towels, followed by a second glass plate and on top an additional weight of approximately 500 g. The transfer was done at RT for 18 h. After crosslinking the RNA to the membrane using the UV stratalinker (Stratagene, Santa Clara, USA) at 254 nm, the success of the transfer was validated by UV light. Membranes were stored at -20 °C until further use or directly pre-hybridized in a hybridization oven at 50 – 60 °C in 20- 30 mL hybridization solution while rotating.

6.2.1.2.4 Probe labelling and RNA detection

Labelling of short probes up to 50 nt was performed by using 20 pmol of DNA oligonucleotide with 20 µCi of γ^{32}P-ATP (Hartmann Analytics, Braunschweig, Germany) in a 20 µL T4 PNK reaction (Life Technologies, Carlsbad, USA) according to the manufacturer's protocol. Reaction was incubated for 1 h at 37 °C and stopped afterwards with 30 µL of 30 mM EDTA.

Labelling of cDNA probes of 150 nt length or longer was done by performing a so-called "hot-PCR" using Phusion High-Fidelity DNA Polymerase, a template specific reverse primer and a dNTP mix, containing 10 mM of dTTP and dGTP and 1 mM of dATP and dCTP (Life Technologies, Carlsbad, USA). To the reaction 50 µCi of each α^{32}P-dATP and α^{32}P-dCTP were added. PCR was performed for 99 cycles with 30 sec/ kb extension time.

Afterwards, short or long probes were purified using MicroSpin G-25 columns (Cytiva, Marlborough, USA) and radioactivity of the probe was checked with Geiger Counter LB123 EG&G (Berthold, Bad Wildbach, Germany). The radioactively labelled probe was added to the pre-hybridized membrane and incubated o/n at 50 °C for short probes and at 60 °C for cDNA probes while rotating with about 30 mL of hybridization solution.

Membranes labeled with short oligonucleotide probes were washed twice with Northern Blot Wash I and once with Northern Blot Wash II, each for 10 min at 50 °C while rotating. Membranes labeled with cDNA probes were washed with Northern Blot Wash III, Northern Blot Wash IV and Northern Blot Wash V, each for 30 min at 60 °C while rotating. The liquid was discarded and the membrane was wrapped in saran foil for exposure. Signals were detected by exposing the membrane to a Molecular Imager FX Imaging Screen-K (Kodak, Rochester, USA) and detecting with the Personal Molecular Imager™ (PMI™) (Biorad, Hercules, USA).

For repeated hybridization of the same membrane with different probes, the current probe was stripped off. Therefore, the membrane was added twice to boiling water with 0,1 % SDS, twice to only boiling water and once to water at RT. Each washing step was performed for approximately 10 min at RT on a rocker. Afterwards, membrane was wrapped in saran foil and exposed to check for effective stripping.

6.2.1.3 cDNA synthesis and quantitative real-time PCR (qPCR)

6.2.1.3.1 cDNA synthesis

RNA extraction for cDNA synthesis followed by qPCR was performed with TRIzol reagent (Thermo Fisher Scientific, Waltham, USA), NucleoSpin RNA Kit or NucleoSpin RNA XS Kit (Macherey-Nagel, Düren, Germany) as described previously (**6.2.1.2.1**). cDNA was synthesized using First Strand cDNA synthesis Kit (Thermo Fisher Scientific, Waltham, USA) according to the manufacturer's protocol. In short, 100 ng – 1 µg RNA was mixed with 1 µl random hexamer or oligo-$(dT)_{18}$ primer, filled up to a final volume of 11 µL with nuclease-free H_2O and incubated for 5 min at 65 °C. Samples were cooled down on ice and mixed with 4 µL 5x reaction buffer, 2 µL 1 mM dNTP Mix, 1 µL of 2 U/µL RiboLock RNase Inhibitor and 1 µL 20 U/µL M-MuLV reverse

transcriptase. After mixing, reaction was incubated 5 min at 25 °C, 60 min at 37 °C and 5 min at 70 °C for reaction termination. For cDNA using oligo-$(dT)_{18}$ primer, the initial incubation at 25 °C for 5 min is not necessary. cDNA was filled up to 100 µL or 200 µL with nuclease-free H_2O and stored at -20 °C until further use.

6.2.1.3.2 qPCR for quantification of RNA levels

qPCR was performed using Takyon™ No ROX SYBR (Eurogentec, Seraing, Belgium) according to the manufacturer's instructions. In short, 10 µL of Takyon reagent were mixed with 1 µM of a 1:1 primer mix of forward and reverse primer, 4 µL of diluted cDNA and filled up with H_2O to 20 µL. qPCR primers are listed above (**Table 6-5**). qPCRs were run using CFX96 Dx Real-Time PCR Detection System (Biorad, Hercules, USA) using the standard program stated in the manufacturer's protocol. Additionally, a melting curve from 65- 95 °C was generated.

For siRNA knockdown efficiency, the data was analysed using the $\Delta\Delta C_T$ method with GAPDH as housekeeping gene and the siKnockdown Control (siCtrl) as control sample for normalization. Error bars were calculated from different numbers of biological replicates.

For RNA enrichment quantification after RNA-IP (**6.2.2.3**), the $\Delta\Delta C_T$ method was used by calculating enrichment in IP over input and normalization to an empty vector control.

6.2.1.3.3 RT-PCR for detection of splice variants

For the identification of different splice variants, Real-Time PCR (RT-PCR) was performed. For the RT-PCR, Phusion High-Fidelity DNA Polymerase (Thermo Fisher Scientific, Waltham, USA) was used according to the manufacturer's instructions. As DNA template, oligo-(dT) cDNA (**6.2.1.3.1**) was used. RT-PCR and qPCR primers are listed in **Table 6-5**. Annealing temperature of the primers were individually determined and selected. Elongation time was set according to the size of the gene of interest, considering the approximate amplification rate of 1 kb/ 30sec at 72 °C.

Amplification cycles were repeated 40 times. Reactions were analysed on 1 – 2 % agarose gels dependent on the product size.

6.2.1.4 Immunological assays

6.2.1.4.1 Enzyme-linked immunosorbent Assay (ELISA)

For ELISA experiments, recombinant purified protein, which was tagged with the Fc-fragment of antibodies, was diluted to different concentrations using a sodium-carbonate buffer at pH 9,5. 100 µL of the prepared stock solutions were added to different wells of 96-well plates which were then incubated at 4 °C o/n while shaking on an orbital shaker. After plates were warmed up to RT again the next day, wells were washed three times with 100 µL adhesion assay wash buffer I and blocked with 200 µL Blocking solution for 2,5 h at RT while shaking on an orbital shaker. After three washing steps with each 100 µL adhesion assay wash buffer I, α-human IgG-HRP antibody (Sigma-Aldrich, Steinheim, Germany) diluted 1:40000 in Blocking solution was added and again incubated for at least 1 h at RT while shaking on an orbital shaker. Wells were again washed three times with 100 µL of adhesion assay wash buffer I. For signal development, 100 µL of TMB Ready to Use ELISA substrate (Serva Electrophoresis, Heidelberg, Germany) was added to each well and incubated for 10 min at RT. Reaction was stopped by adding 50 µL of 0,1 M H_2SO_4. Absorbance was measured at 450 nm using the Mithras LB 940 plate reader (Berthold, Bad Wildbach, Germany).

6.2.1.4.2 Cell adhesion assay with human ICAM-1-Fc protein (hICAM-1-Fc)

Cell adhesion assays are performed with recombinant purified hICAM-1-Fc protein using HighBinding white ELISA 96 well plates (Sarstedt, Nümbrecht, Germany). Therefore, the hICAM-1-Fc protein was diluted to a concentration of 5 µg/mL in Coating Buffer and 100 µL of stock solution were added to each well. Uncoated control wells kept by adding 100 µL coating buffer containing no protein. The plate was incubated at 4 °C o/n shaking on an orbital shaker. After plate was brought back to RT the following day, wells were washed with 100 µL adhesion assay wash buffer I and blocked with 200 µL adhesion assay blocking solution for 3,5 h at RT while shaking

on an orbital shaker. Afterwards, the coated plate was washed two times with 100 µL adhesion assay wash buffer I and two times with 100 µL adhesion assay wash buffer II before prepared T cells were added.

While blocking the coated plate, T cells were counted using the CASY Cell Counter & Analyzer (OMNI Life Science, Bremen, Germany) and diluted to 1 x 10^6 cells/ mL in serum-free RPMI medium (Sigma-Aldrich, Steinheim, Germany). Cells were incubated for 30 min at 37 °C. T cells were then divided in different cups, spun down at 200 xg for 5 min and resuspended appropriate volumes of adhesion buffer, media or cancer cell supernatants to obtain 1 x 10^6 cells/ mL. Cancer cell supernatants were also spun down for 5 min at 200 xg before use. After a short incubation time of 5 – 10 min at RT, 100 µL cell suspension was added to each well of prepared hICAM-1-Fc coated plate. The plate was then incubated at 37 °C for 20 min.

After incubation, wells were washed three times with 100 µL adhesion buffer. Afterwards, 100 µL adhesion buffer and 100 µL CellTiter-Glo® Luminescent Cell Viability Assay reagent (Promega, Madison, USA) were added to each well and protocol was proceeded as described in the manufacturer's instructions. In short, after incubation for 2 min at RT on an orbital shaker and another 10 min without shaking, the induced luminescent signal was measured using the Mithras LB 940 plate reader (Berthold, Bad Wildbach, Germany). As reference for normalization, wells were kept without washing after T cell adhesion. As background, untreated wells without T cells containing 100 µL adhesion buffer were used.

6.2.1.4.3 LC-AA Assay

As first step, soluble ICAM-1 was incubated with anti-human IgG antibody PE for 30 min at RT in the dark for labelling and generating ICAM-1c. Isolated PBMCs (**6.2.3.6**) were spun down at 400 xg for 7 min and resuspended in appropriate volumes of cell culture medium DMEM, RPMI or McCoy or cancer cell supernatants to a final density of 2,5*10^6 cells/ mL. Cells were incubated at 37 °C for 10 min. Different master mixes were prepared in LC-AA basic buffer for labelling CD3, CD4, CD8 cells. Used labelling antibodies are listed in **Table 6-2** (FACS labelling antibodies). Master mixes contained either 0 mM $MgCl_2$, 2 mM $MgCl_2$, 4mM $MgCl_2$, 4 mM $MgCl_2$ together

with TCR Activator or 4 mM $MgCl_2$ together with LFA-1 Inhibitor BI-1950. To all master mixes ICAM-1c was added at a final dilution of 1:40. Labelling mixes were added to the pre-treated PBMCs and incubated another 10 min at 37 °C. Afterwards, PBMCs were diluted 1:1 with fresh 4 % PFA for fixation and incubated at 37 °C for 10 min. Fixed PBMCs were transferred to a 96-well plate with V-bottom and mixed with 1x PBS at a ratio of 1:1. Optional, one washing step was performed. Therefore, the 96-well plate was spun down at 400 xg for 5 min. The supernatant was discarded and 200 µL 1x PBS was added to each well. Plates were measured using the Attune NxT Acoustic Focusing Cytometer (Life Technologies, Carlsbad, USA).

6.2.2 Protein Biochemical Methods

6.2.2.1 Preparation of whole cell extracts

To prepare whole cell extracts for analysis of expression of different target proteins on endogenous or overexpressed level, cells were lysed in RIPA lysis buffer containing 1 mM DTT and 1 mM AEBSF. About 1 x 10^6 cells were resuspended in 250 µL RIPA lysis buffer by pipetting up and down and incubated for 20 min on ice. To clear lysates, centrifugation at full speed for 20 min at 4 °C was performed and supernatants were transferred to a new cup. Lysates were supplemented with SDS sample buffer or used for Immunoprecipitation (IP) or RNA-IP (**6.2.2.2**, **6.2.2.3**).

Concentration of lysates was determined by Bradford using Roti®Quant 5x Concentrate (Carl Roth GmbH, Karlsruhe, Germany). In short, 1 µL of lysate was mixed with 1 mL of 1x Roti®Quant solution and absorbance was measured at 595 nm. Samples were then diluted in equal concentrations, mixed with 1x SDS sample buffer and loaded on SDS-PAGE followed by Western Blot analysis (**6.2.2.6**).

6.2.2.2 Immunoprecipitation (IP)

HEK 293T cells were transfected with plasmids for 2 days on 15 cm plates (**6.2.3.2**). Based on the further use, cells or cell culture supernatants were harvested. Cell lysates were prepared as described above (**6.2.2.1**) and supernatants were centrifuged at 500 xg for approximately 30 min at 4 °C. 50 µL of FLAG-M2 beads (Sigma-Aldrich,

Steinheim, Germany), Protein-G or nProtein A - Sepharose 4 Fast Flow Beads (Cytiva, Marlborough, USA) were washed 3x with 1x PBS before incubation with supernatants and 2x with 1x PBS and 1x with RIPA lysis Buffer prior to incubation with cell lysates. After the second washing step, beads were transferred to new cups. Subsequently, beads were incubated with cell lysates or cell culture supernatants for 2-3 h at 4 °C on a turning wheel. After three washings steps with IP wash buffer, beads were transferred to a new cup and washed once with PBS. All centrifugation steps with beads were performed at 1000 xg for 1:30 min at 4 °C. Elution was performed with 50 µL 2,5x SDS loading buffer or in case of further use of the enriched protein with elution buffer as described below (**6.2.2.4**).

6.2.2.3 RNA-Immunoprecipitation (RNA-IP)

Transfected HEK 293T cells were harvested 2 days after transfection with calcium phosphate (**6.2.3.2**). Cells were lysed in 1 mL IP lysis buffer per 15 cm plate, incubated for 20 min on ice and then spun down at full speed for 20 min at 4 °C. Two aliquots of 50 µL of the lysate were collected. One aliquot was mixed with 5x SDS sample buffer for Western Blot analysis and the other aliquot was used for RNA extraction. For each IP sample, 50 µL of the α-FLAG-M2 beads (Sigma-Aldrich, Steinheim, Germany) were used per 15 cm plate and prepared by washing 3x with IP lysis buffer using centrifugation at 1000 xg for 2 min at 4 °C. Beads were transferred to a new cup after the second washing step. The cell lysate was added to the beads and incubation was performed for 2-3 h at 4 °C rotating. Afterwards, beads were washed three times with RNA-IP Wash Buffer. With the last washing step, beads were split in two cups. 100 µL IP-beads were mixed with 2,5x SDS sample buffer for Western Blot (**6.2.2.6**) and 900 µL IP-beads were used for RNA extraction. RNA extraction was performed with TRIzol reagent (Life Technologies, Carlsbad, USA) as described previously (**6.2.1.2.1**). 150 µL TRIzol reagent were used for 50 µL input sample and 500 µL was added to 900 µL IP-beads. RNA pellets were dissolved and 8 µL water. 1 µg of the input sample and the whole volume of the IP sample were first DNaseI digested and then used for cDNA synthesis (**6.2.1.3.1**) followed by qPCR (**6.2.1.3.2**).

6.2.2.4 Batch purification of proteins

For batch purification of adhesion molecule hICAM-1-Fc, the supernatant of transiently transfected HEK 293T cells 48 h after transfection (**6.2.3.2**) or the supernatant of stable T-REx-hICAM-1-Fc cell line induced for 72 h with 1 µg/mL Tetracycline was collected. To 50 mL supernatant, 2 mM DTT and 50 µL of prepared nProtein A - Sepharose 4 Fast Flow Beads (Cytiva, Marlborough, USA) were added and samples were incubated for 2-3 h at 4 °C rotating. Beads were prepared by washing 3x with 1x PBS before adding to the supernatant. After incubation, beads were washed 3x with IP wash buffer containing 2 mM DTT, transferred to a new cup and again washed once with 1x PBS. Elution was performed acidic with 0,1 M Glycine pH 3,0 for 5 min at RT shaking at 750 rpm. The elution fractions were neutralized with 5 µL 1 M Tris-HCl pH 9,5 per 100 µL eluate. All centrifugation steps with beads were performed at 1000 xg, 4 °C for 1:30 min. After validating the success of the batch purification on a SDS-PAGE (**6.2.2.6**), fractions containing the protein were pooled and concentrated to a final volume of 400 – 500 µL with a Filter-PES Vivaspin Concentrator MWCO 50 kDa (Sartorius, Göttingen, Germany). Concentrated sample was centrifuged for at full speed at 4 °C for 2 min and further purified via Size Exclusion Chromatography (SEC) as described below (**6.2.2.5**).

6.2.2.5 Size exclusion chromatography (SEC)

As final purification step after batch purification, a gel filtration column packed with Superdex 200 resin (Cytiva, Marlborough, USA) was loaded with the concentrated protein. The column was equilibrated with 1x PBS prior to loading of the sample. The run was performed according to the manufacturer's instructions, setting the flowrate at 0,5 mL/ min with a high pressure of 1,5 MPa. Fractions of 600 µL volume were collected. After checking on a SDS-PAGE, fractions containing the recombinant protein were pooled and concentrated with Filter-PES Vivaspin Concentrator MWCO 10 kDa (Sartorius, Göttingen, Germany). Purified protein was stored in 50 % glycerol at – 80 °C.

6.2.2.6 SDS-PAGE and Western Blot

SDS-PAGE gels were prepared with a 5 % stacking gel and a 10 % separation gel and stored at 4 °C until use. Prior to loading, samples were mixed with 5x SDS loading buffer and heated for 5 min at 95 °C. The run was performed in SDS running buffer at 180 V for until running front reached the end of the gel. Gels were either stained in Coomassie staining solution for 1h at RT or blotted onto a Hybond-ECL membrane (GE Healthcare, Little Chalfont, UK) using Towbin blotting buffer for approximately 1 min per kDa, 2 mA per cm^2 membrane size and maximum 25 V.

Coomassie stained gels were destained with Coomassie destaining solution for several hours at RT or o/n at 4 °C.

After Western blotting, the membranes were blocked with Western Blot blocking buffer at RT shaking for 1 h and incubated with primary antibodies diluted in Western Blot blocking buffer o/n at 4 °C shaking. After three washing steps for around 10 min with TBS-T, membranes were incubated with secondary antibodies diluted in Western Blot blocking buffer for 1h at RT shaking. Three washing steps for 10 min with TBS-T were performed and membranes were detected at the Odyssey Infrared Imaging System (LI-COR Biosciences, Lincoln, USA).

6.2.3 Cell Biological Methods

6.2.3.1 Cultivation of mammalian cells

All cells were cultivated at 37 °C in a humified chamber with ait atmosphere and addition of 5 % CO_2. Melanoma cell lines A 375, Mel-HO and SK-MEL-28 were grown in special Dulbecco's modified eagle media (DMEM) without pyruvate (Thermo Fisher Scientific, Waltham, USA) supplemented with 10 % Fetal bovine serum (FBS) (Sigma-Aldrich, Steinheim, Germany) and 1 % Penicillin/Streptavidin (Sigma-Aldrich, Steinheim, Germany). The HSB-2 suspension cell line was grown in RPMI complete media (Sigma-Aldrich, Steinheim, Germany) supplemented with 10 % FBS. All other cell lines listed in **Table 6-7** were cultivated in normal DMEM with 10 % FBS and 1 % Penicillin/ Streptavidin.

Every two to three days, cells were passaged and splitted. For adherent cell lines, cells were washed once with 1x PBS and treated with 1- 2- mL Trypsin (Sigma-Aldrich, Steinheim, Germany) to detach the cells. Trypsination was stopped by adding new media. The cell suspension was partially transferred to a new sterile plate. Suspension cells were counted using CASY Cell Counter & Analyzer and diluted to the desired densities with fresh RPMI media in new T75 flasks.

6.2.3.2 Cell transfection with Calcium phosphate

For overexpression of plasmids in HEK 293T cells on a 15 cm plate, 10 µg plasmid DNA were mixed with 123 µL 2 M $CaCl_2$ and filled up to 1 mL with H_2O. To the mix, 2x HEPES was added dropwise in a ratio of 1:1 while vortexing. After approximately 10 min incubation at RT, 2 mL of transfection mix were added dropwise to the plate. Cells were incubated at 37 °C and 5 % CO_2 for 2 days.

6.2.3.3 Cell transfection with Lipofectamine2000 / 3000

For transfection of cancer cells with plasmids, the Lipofectamine 2000 or Lipofectamine 3000 reagents (Life Technologies, Carlsbad, USA) were used according to the manufacturer's instructions. Cells were seeded 24 h prior transfection to reach approximately 80 % confluency on day of transfection in media without antibiotics. Success of transfection was checked via Western Blot (**6.2.2.6**) or qPCR (**6.2.1.3.2**).

Using Lipofectamine 2000 for transfection of a 6 well, tow mixes were prepared. Mix A was containing 125 µL Opti-MEM™ media mixed with 2,5 µg DNA and Mix B was consisting of 125 µL Opti-MEM™ and 5 µL Lipofectamine 2000 reagent. Both mixes were shortly mixed by vortexing and incubated 5 min at RT. Afterwards, Mix A and Mix B were combined in a 1:1 ratio, shortly vortexed and incubated additional 20 min at RT. 250 µL transfection mix was added dropwise to the seeded cells which were then incubated for 2 to 4 days at 37 °C and 5 % CO_2.

Transfection using Lipofectamine 3000 reagent was performed similar to the transfection just described. Two mixes were prepared with mix A containing 2,5 µg DNA, 5 µL P3000 and 125 µL Opti-MEM™ and mix B containing 125 µL Opti-MEM™

and 7,5 µL Lipofectamine 3000. After mixing and incubation of 5 min at RT separately, mix A and B were combined in a 1:1 ration, mixed by vortexing and incubated for 20 min at RT. 250 µL transfection mix was added to the seeded cells, which were harvested 2 to 4 days at 37 °C and 5 % CO_2 after.

6.2.3.4 siRNA Knockdown with Lipofectamine RNAiMAX

For transfection of siPOOLs, Lipofectamine RNAiMAX (Life Technologies, Carlsbad, USA) was used according to the protocol provided by siTOOLs Biotech GmbH (Planegg, Germany). For a 6 well, tow mixes were prepared with mix A containing 210 µL Opti-MEM™ and 40 µL of siPOOL with a concentration of 150 nM and mix B consisting of 246 µL Opti-MEM™ and 4 µL RNAiMAX reagent. After vortexing, mix A and B were combined, mixed by vortexing and incubated for 5 min at RT. 500 µL of the transfection mix were transferred to the bottom of the 6 well and 1,5 mL of cell suspension was added. Cells were incubated 1 to 4 days at 37 °C and 5 % CO_2 until harvesting. Knockdown efficiency was determined with qPCR (**6.2.1.3.2**).

6.2.3.5 Generation of stable cell lines

For generation of stable Flp-In™ T-REx™ 293 cell lines, cells were seeded 24 h prior transfection in a 24 well in media without Zeocin and Blasticidin (Life Technologies, Carlsbad, USA) to reach a density of approximately 70 % on day of transfection. Cells were cotransfected with pOG44 and pcDNA5-FRT/TO in a 9:1 ratio using Lipofectamine 2000 reagent. 24 h after transfection media was changed and after 48 h cells were splitted to a 10 cm dish for selection using media containing 15 µg/mL Blasticidin and 100 µg/mL Hygromycin (Life Technologies, Carlsbad, USA). Clones were picked two weeks later and tested zeocin sensitivity, inducibility and expression levels. Expression was induced using 1 µg/ mL Tetracycline or Doxycycline (Sigma-Aldrich, Steinheim, Germany) for 24 h up to 72 h. Stable clones were cultivated in selection medium at 37 °C and 5 % CO_2.

6.2.3.6 PBMCs isolation from whole blood

For the extraction of peripheral blood mononuclear cells (PBMCs), whole blood samples were mixes 1:1 with 1x PBS and mixed by resuspending. 11 mL of the diluted blood were loaded carefully on 4 mL of Roti®Sep 1077 human CELLPURE® (Carl Roth GmbH & Co.KG, Karlsruhe, Germany) without disturbing the density gradient. Centrifugation was performed at 1200 xg for at least 20 min with slow acceleration and without deceleration. Of the four appearing phases, the third, cloudy one was transferred to a new cup. PBMCs were washed twice with 1x PBS via centrifugation firstly at 300 xg for 7 min and secondly 200 xg for 10 min. Cells were resuspended in RPMI medium (Thermo Fisher Scientific, Waltham, USA) supplemented with 10 % FBS (Sigma-Aldrich, Steinheim, Germany) and 1 % Penicillin/Streptavidin (Sigma-Aldrich, Steinheim, Germany) at a density of $1*10^6$/ mL and cultured at 37 °C in a humified chamber with ait atmosphere and addition of 5 % CO_2. Cultivation was not extended over 2 days.

7 Supplements

7.1 List of Figures

7.2 List of Tables

7.3 List of Abbreviations

3'FL	CTNNB1 full length 3'UTR
3'SP	CTNNB1 short 3'UTR splice variant
ADMIDAS	adjacent to metal ion – dependent adhesion site
Ago2	Argonaute 2
APA	Alternative polyadenylation
APCs	Antigen presenting cells
ASO	Antisense oligonucleotide
BSA	Albumin Fraction V
CAMs	Cell adhesion molecules
CAR-T	Chimeric antigen receptor T cell
CCL4	CC-chemokine ligand 4
CCL5	CC-chemokine ligand 5
CCL9	CC-chemokine ligand 9
CCL21	CC-chemokine ligand 21
CTLA-4	cytotoxic T lymphocyte-associated protein 4
CRC	Colorectal cancer
CXCL10	CXC-chemokine ligand 10
CXCL11	CXC-chemokine ligand 11
CXCL12	CXC-chemokine ligand 12
CXCL13	CXC-chemokine ligand 13
CXCR1	CXC-chemokine receptor 1
CXCR2	CXC-chemokine receptor 2
DAMPs	Damage-associated molecular patterns
DCs	Dendritic cells
DGCR8	DiGeorge critical region 8
DMEM	Dulbecco's modified eagle media
DOC	Sodium deoxycholate
dsRNAs	double-stranded RNAs
eIF4E	eukaryotic translation initiation factor 4E
ELISA	Enzyme-linked immunoborbent Assay
ESL1	E-selectin ligand 1
EtBr	Ethidiumbromide
EtOH	Ethanol
F/HA	Flag/HA tag
FACS	fluorescence activated cell sorting
FBS	Fetal bovine serum
FDA	US Food and Drug Administration
FIR	FUSE-binding protein-interacting repressor
GAG	glycosaminoglycan
GBE1	glycogen branching enzyme
h	Hour
hDF	Human dermal fibroblasts
hICAM-1-Fc	Human ICAM-1-Fc protein
ICAM-1	Intracellular adhesion molecule 1
ICI	Immune checkpoint inhibitors
ICP	immune checkpoint
IDO	indoleamine-2,3-dioxygenase

IFN-γ	interferon-γ
Ig	Immunoglobulin
IL-6	Interleukin-6
IL-8	Interleukin-8
IL-10	Interleukin-10
IL-1β	interleukin 1 β
I-EGF	integrin epidermal growth-factor-like
IP	Immunoprecipitation
IVT	*In vitro* transcription
kDa	Kilo Dalton
LFA-1	Lymphocyte function-associated antigen 1
LIMBS	ligand-induced metal-binding site
LNPs	lipid nanoparticles
MAC-1	macrophage-1 antigen
MDSCs	Myleoid-derived suppressor cells
MeOH	Methanol
MFI	Mean fluorescence intensity
MHC	Major histocompatibility complex
MIDAS	metal ion – dependent adhesion site
Min	Minute
miRNA	miRNA
mRNA	messenger RNA
MWCO	Molecular weight cut off
NaN_3	Sodium azide
ncRNA	noncoding RNA
NES	Nuclear export signal
NF-κB	κ-light chain of enhancer-activated B cells
NK	Natural killer
NMD	non-sense mediated mRNA decay
nt	Nucleotides
o/n	Overnight
OE	overexpression
ORF	Open reading frame
PAF	platelet activating factor
PAMPs	Pathogen-associated molecular patterns
PBMCs	peripheral blood mononuclear cells
PBS	Phosphate buffered saline
PCR	Polymerase Chain Reaction
PD-1	Programmed cell death 1
PECAM1	platelet endothelial cell adhesion molecule 1
PI3K	Phosphatidylinositol 3-kinase
PMA	Phorbol myristate actetate
PSI	plexin/semaphorin/integrin
PNK	T4 Polynucleotide Kinase
pre-miRNAs	precursor miRNAs
pri-miRNAs	primary miRNAs
PSGL1	P-selectin glycoprotein ligand 1
PTM	post-translational modifications
PUF60	Poly(U) binding splicing factor 60

qPCR	quantitative real-time PCR
RBDs	RNA-binding domains
RIAM	Rap1-interacting adaptor molecule
RISC	RNA-induced silencing complex
RNA-IP	RNA-Immunoprecipitation
RNase	Ribonuclease
RNP	ribonucleoprotein
RT	Room temperature
Sec	Second
SEC	S*ize exclusion chromatography*
si	RNAi knockdown
siCtrl	scrambled siRNA control
siRNA	Silencing RNA
snRNP	small nuclear ribonucleoprotein particle
ss	single-stranded
STAT3	Signal transducer and activator of transcription 3
TAE	Tris/Actetate/EDTA buffer
TBE	Tris/Borate/EDTA buffer
TBS	Tris buffered saline
TCR	T cell receptor
TCR	Human CD3/CD28/CD2 T cell Activator
TECs	Tumour endothelial cells
TGFβ	transforming growth factor β
TMB	Tumour mutational burden
TME	Tumour microenvironment
TNF	tumour necrosis factor
UTR	Untranslated region
VCAM-1	vascular cell adhesion molecule 1
VLA-4	very late activation antigen-4
WT	Wildtype

7.4 References

Agrawal, Anant A.; Salsi, Enea; Chatrikhi, Rakesh; Henderson, Steven; Jenkins, Jermaine L.; Green, Michael R. et al. (2016): An extended U2AF(65)-RNA-binding domain recognizes the 3' splice site signal. In *Nature communications* 7, p. 10950. DOI: 10.1038/ncomms10950.

Ai, Wenchao; Li, Haishan; Song, Naining; Li, Lei; Chen, Huiming (2013): Optimal method to stimulate cytokine production and its use in immunotoxicity assessment. In *International journal of environmental research and public health* 10 (9), pp. 3834–3842. DOI: 10.3390/ijerph10093834.

Aleksandra J. Ozga; Melvyn T. Chow; Andrew D. Luster (2021): Chemokines and the immune response to cancer. In *Immunity* 54 (5), pp. 859–874. DOI: 10.1016/j.immuni.2021.01.012.

Alimov, Irina; Menon, Suchithra; Cochran, Nadire; Maher, Rob; Wang, Qiong; Alford, John et al. (2019): Bile acid analogues are activators of pyrin inflammasome. In *The Journal of biological chemistry* 294 (10), pp. 3359–3366. DOI: 10.1074/jbc.RA118.005103.

Arnaout, M. Amin (2016): Biology and structure of leukocyte β (2) integrins and their role in inflammation. In *F1000Research* 5. DOI: 10.12688/f1000research.9415.1.

Azmi, Asfar S.; Uddin, Mohammed H.; Mohammad, Ramzi M. (2021): The nuclear export protein XPO1 — from biology to targeted therapy. In *Nature Reviews Clinical Oncology* 18 (3), pp. 152–169. DOI: 10.1038/s41571-020-00442-4.

Bader, Andreas G.; Brown, David; Winkler, Matthew (2010): The promise of microRNA replacement therapy. In *Cancer research* 70 (18), pp. 7027–7030. DOI: 10.1158/0008-5472.CAN-10-2010.

Baltz, Alexander G.; Munschauer, Mathias; Schwanhäusser, Björn; Vasile, Alexandra; Murakawa, Yasuhiro; Schueler, Markus et al. (2012): The mRNA-Bound Proteome and Its Global Occupancy Profile on Protein-Coding Transcripts. In *Molecular cell* 46 (5), pp. 674–690. DOI: 10.1016/j.molcel.2012.05.021.

Behlke, Mark A. (2006): Progress towards in vivo use of siRNAs. In *Molecular Therapy* 13 (4), pp. 644–670. DOI: 10.1016/j.ymthe.2006.01.001.

Bell, Jessica L.; Wächter, Kristin; Mühleck, Britta; Pazaitis, Nikolaos; Köhn, Marcel; Lederer, Marcell; Hüttelmaier, Stefan (2013): Insulin-like growth factor 2 mRNA-binding proteins (IGF2BPs): post-transcriptional drivers of cancer progression? In *Cellular and Molecular Life Sciences* 70 (15), pp. 2657–2675. DOI: 10.1007/s00018-012-1186-z.

Bennett, C. Frank; Baker, Brenda F.; Pham, Nguyen; Swayze, Eric; Geary, Richard S. (2017): Pharmacology of Antisense Drugs. In *Annual Review of Pharmacology and Toxicology* 57 (1), pp. 81–105. DOI: 10.1146/annurev-pharmtox-010716-104846.

Bertoldo, J. B.; Müller, S.; Hüttelmaier, S. (2023): RNA-binding proteins in cancer drug discovery. In *Drug discovery today* 28 (6). DOI: 10.1016/j.drudis.2023.103580.

Beste, Michael T.; Hammer, Daniel A. (2008): Selectin catch-slip kinetics encode shear threshold adhesive behavior of rolling leukocytes. In *Proceedings of the National Academy of Sciences of the United States of America* 105 (52), pp. 20716–20721. DOI: 10.1073/pnas.0808213105.

Bock, Christoph; Datlinger, Paul; Chardon, Florence; Coelho, Matthew A.; Dong, Matthew B.; Lawson, Keith A. et al. (2022): High-content CRISPR screening. In *Nat Rev Methods Primers* 2 (1). DOI: 10.1038/s43586-021-00093-4.

Bohnsack, Markus T.; Czaplinski, Kevin; Gorlich, Dirk (2004): Exportin 5 is a RanGTP-dependent dsRNA-binding protein that mediates nuclear export of pre-miRNAs. In *RNA (New York, N.Y.)* 10 (2), pp. 185–191. DOI: 10.1261/rna.5167604.

Bonaventura, Paola; Shekarian, Tala; Alcazer, Vincent; Valladeau-Guilemond, Jenny; Valsesia-Wittmann, Sandrine; Amigorena, Sebastian et al. (2019): Cold Tumors: A Therapeutic Challenge for Immunotherapy. In *Front. Immunol.* 10, p. 168. DOI: 10.3389/fimmu.2019.00168.

Briskin, M. J.; McEvoy, L. M.; Butcher, E. C. (1993): MAdCAM-1 has homology to immunoglobulin and mucin-like adhesion receptors and to IgA1. In *Nature* 363 (6428), pp. 461–464. DOI: 10.1038/363461a0.

Burdelya, Lyudmila; Kujawski, Maciej; Niu, Guilian; Zhong, Bin; Wang, Tianhong; Zhang, Shumin et al. (2005): Stat3 activity in melanoma cells affects migration of immune effector cells and nitric oxide-mediated antitumor effects. In *Journal of immunology (Baltimore, Md. : 1950)* 174 (7), pp. 3925–3931. DOI: 10.4049/jimmunol.174.7.3925.

Camus, Matthieu; Tosolini, Marie; Mlecnik, Bernhard; Pagès, Franck; Kirilovsky, Amos; Berger, Anne et al. (2009): Coordination of intratumoral immune reaction and human colorectal cancer recurrence. In *Cancer research* 69 (6), pp. 2685–2693. DOI: 10.1158/0008-5472.CAN-08-2654.

Chan, Jia Jia; Tabatabaeian, Hossein; Tay, Yvonne (2023): 3′UTR heterogeneity and cancer progression. In *Trends in Cell Biology* 33 (7), pp. 568–582. DOI: 10.1016/j.tcb.2022.10.001.

Chan, Jia Jia; Zhang, Bin; Chew, Xiao Hong; Salhi, Adil; Kwok, Zhi Hao; Lim, Chun You et al. (2022): Pan-cancer pervasive upregulation of 3′ UTR splicing drives tumourigenesis. In *Nature Cell Biology* 24 (6), pp. 928–939. DOI: 10.1038/s41556-022-00913-z.

Chen, Daniel S.; Mellman, Ira (2013): Oncology meets immunology: the cancer-immunity cycle. In *Immunity* 39 (1), pp. 1–10. DOI: 10.1016/j.immuni.2013.07.012.

Church, Sarah E.; Galon, Jérôme (2017): Regulation of CTL Infiltration Within the Tumor Microenvironment. In Pawel Kalinski (Ed.): Tumor Immune Microenvironment in Cancer Progression and Cancer Therapy. Cham: Springer International Publishing, pp. 33–49. Available online at https://doi.org/10.1007/978-3-319-67577-0_3.

Coppin, Lucie; Leclerc, Julie; Vincent, Audrey; Porchet, Nicole; Pigny, Pascal (2018): Messenger RNA Life-Cycle in Cancer Cells: Emerging Role of Conventional and Non-Conventional RNA-Binding Proteins? In *International journal of molecular sciences* 19 (3). DOI: 10.3390/ijms19030650.

Corley, Meredith; Burns, Margaret C.; Yeo, Gene W. (2020): How RNA-Binding Proteins Interact with RNA: Molecules and Mechanisms. In *Molecular cell* 78 (1), pp. 9–29. DOI: 10.1016/j.molcel.2020.03.011.

Crooke, Stanley T.; Baker, Brenda F.; Crooke, Rosanne M.; Liang, Xue-Hai (2021): Antisense technology: an overview and prospectus. In *Nature reviews. Drug discovery* 20 (6), pp. 427–453. DOI: 10.1038/s41573-021-00162-z.

Crooke, Stanley T.; Witztum, Joseph L.; Bennett, C. Frank; Baker, Brenda F. (2018): RNA-Targeted Therapeutics. In *Cell Metabolism* 27 (4), pp. 714–739. DOI: 10.1016/j.cmet.2018.03.004.

Damase, Tulsi Ram; Sukhovershin, Roman; Boada, Christian; Taraballi, Francesca; Pettigrew, Roderic I.; Cooke, John P. (2021): The Limitless Future of RNA Therapeutics. In *Frontiers in bioengineering and biotechnology* 9, p. 628137. DOI: 10.3389/fbioe.2021.628137.

Dando, J.; Wilkinson, K. W.; Ortlepp, S.; King, D. J.; Brady, R. L. (2002): A reassessment of the MAdCAM-1 structure and its role in integrin recognition. In *Acta Crystallogr D Biol Crystallogr* 58 (2), pp. 233–241. DOI: 10.1107/S0907444901020522.

Deal, Cailin E.; Carfi, Andrea; Plante, Obadiah J. (2021): Advancements in mRNA Encoded Antibodies for Passive Immunotherapy. In *Vaccines* 9 (2). DOI: 10.3390/vaccines9020108.

Dransfield, I.; Cabañas, C.; Craig, A.; Hogg, N. (1992): Divalent cation regulation of the function of the leukocyte integrin LFA-1. In *The Journal of Cell Biology* 116 (1), pp. 219–226. DOI: 10.1083/jcb.116.1.219.

Duan, Qianqian; Zhang, Hualing; Zheng, Junnian; Zhang, Lianjun (2020): Turning Cold into Hot: Firing up the Tumor Microenvironment. In *Trends in cancer* 6 (7), pp. 605–618. DOI: 10.1016/j.trecan.2020.02.022.

Dumont, Jennifer; Euwart, Don; Mei, Baisong; Estes, Scott; Kshirsagar, Rashmi (2016): Human cell lines for biopharmaceutical manufacturing: history, status, and future perspectives. In *Critical reviews in biotechnology* 36 (6), pp. 1110–1122. DOI: 10.3109/07388551.2015.1084266.

Dunn, Gavin P.; Bruce, Allen T.; Ikeda, Hiroaki; Old, Lloyd J.; Schreiber, Robert D. (2002): Cancer immunoediting: from immunosurveillance to tumor escape. In *Nature immunology* 3 (11), pp. 991–998. DOI: 10.1038/ni1102-991.

Duru, Gizem; van Egmond, Marjolein; Heemskerk, Niels (2020): A Window of Opportunity: Targeting Cancer Endothelium to Enhance Immunotherapy. In *Frontiers in immunology* 11, p. 584723. DOI: 10.3389/fimmu.2020.584723.

Dustin, M. L.; Rothlein, R.; Bhan, A. K.; Dinarello, C. A.; Springer, T. A. (1986): Induction by IL 1 and interferon-gamma: tissue distribution, biochemistry, and function of a natural adherence molecule (ICAM-1). In *Journal of immunology (Baltimore, Md. : 1950)* 137 (1), pp. 245–254.

Dyrbuś, Krzysztof; Gąsior, Mariusz; Penson, Peter; Ray, Kausik K.; Banach, Maciej (2020): Inclisiran-New hope in the management of lipid disorders? In *Journal of clinical lipidology* 14 (1), pp. 16–27. DOI: 10.1016/j.jacl.2019.11.001.

Elbashir, S. M.; Harborth, J.; Lendeckel, W.; Yalcin, A.; Weber, K.; Tuschl, T. (2001): Duplexes of 21-nucleotide RNAs mediate RNA interference in cultured mammalian cells. In *Nature* 411 (6836), pp. 494–498. DOI: 10.1038/35078107.

Falk, Sebastian; Finogenova, Ksenia; Melko, Mireille; Benda, Christian; Lykke-Andersen, Søren; Jensen, Torben Heick; Conti, Elena (2016): Structure of the RBM7-ZCCHC8 core of the NEXT complex reveals connections to splicing factors. In *Nature communications* 7, p. 13573. DOI: 10.1038/ncomms13573.

Farkona, Sofia; Diamandis, Eleftherios P.; Blasutig, Ivan M. (2016): Cancer immunotherapy: the beginning of the end of cancer? In *BMC Medicine* 14 (1), p. 73. DOI: 10.1186/s12916-016-0623-5.

Fire, A.; Xu, S.; Montgomery, M. K.; Kostas, S. A.; Driver, S. E.; Mello, C. C. (1998): Potent and specific genetic interference by double-stranded RNA in Caenorhabditis elegans. In *Nature* 391 (6669), pp. 806–811. DOI: 10.1038/35888.

Fukao, Akira; Mishima, Yuichiro; Takizawa, Naoki; Oka, Shigenori; Imataka, Hiroaki; Pelletier, Jerry et al. (2014): MicroRNAs Trigger Dissociation of eIF4AI and eIF4AII from Target mRNAs in Humans. In *Molecular cell* 56 (1), pp. 79–89. DOI: 10.1016/j.molcel.2014.09.005.

Gahmberg, Carl G.; Fagerholm, Susanna C.; Nurmi, Susanna M.; Chavakis, Triantafyllos; Marchesan, Silvia; Grönholm, Mikaela (2009): Regulation of integrin activity and signalling. In *Biochimica et biophysica acta* 1790 (6), pp. 431–444. DOI: 10.1016/j.bbagen.2009.03.007.

Galon, Jérôme; Bruni, Daniela (2019): Approaches to treat immune hot, altered and cold tumours with combination immunotherapies. In *Nature Reviews Drug Discovery* 18 (3), pp. 197–218. DOI: 10.1038/s41573-018-0007-y.

Galon, Jérôme; Bruni, Daniela (2020): Tumor Immunology and Tumor Evolution: Intertwined Histories. In *Immunity* 52 (1), pp. 55–81. DOI: 10.1016/j.immuni.2019.12.018.

Ganesh, Shanthi; Shui, Xue; Craig, Kevin P.; Park, Jihye; Wang, Weimin; Brown, Bob D.; Abrams, Marc T. (2018): RNAi-Mediated β-Catenin Inhibition Promotes T Cell Infiltration and Antitumor Activity in Combination with Immune Checkpoint Blockade. In *Molecular Therapy* 26 (11), pp. 2567–2579. DOI: 10.1016/j.ymthe.2018.09.005.

Garrelfs, Sander F.; Frishberg, Yaacov; Hulton, Sally A.; Koren, Michael J.; O'Riordan, William D.; Cochat, Pierre et al. (2021): Lumasiran, an RNAi Therapeutic for Primary Hyperoxaluria Type 1. In *The New England journal of medicine* 384 (13), pp. 1216–1226. DOI: 10.1056/NEJMoa2021712.

Gattinger, Pia; Izadi, Shiva; Grünwald-Gruber, Clemens; Kallolimath, Somanath; Castilho, Alexandra (2021): The Instability of Dimeric Fc-Fusions Expressed in Plants Can Be Solved by Monomeric Fc Technology. In *Frontiers in plant science* 12, p. 671728. DOI: 10.3389/fpls.2021.671728.

Gebert, Luca F. R.; MacRae, Ian J. (2019): Regulation of microRNA function in animals. In *Nature Reviews Molecular Cell Biology* 20 (1), pp. 21–37. DOI: 10.1038/s41580-018-0045-7.

Gerstberger, Stefanie; Hafner, Markus; Tuschl, Thomas (2014): A census of human RNA-binding proteins. In *Nature Reviews Genetics* 15, 829 EP -. DOI: 10.1038/nrg3813.

Golan-Gerstl, Regina; Cohen, Michal; Shilo, Asaf; Suh, Sung-Suk; Bakàcs, Arianna; Coppola, Luigi; Karni, Rotem (2011): Splicing factor hnRNP A2/B1 regulates tumor suppressor gene splicing and is an oncogenic driver in glioblastoma. In *Cancer research* 71 (13), pp. 4464–4472. DOI: 10.1158/0008-5472.CAN-10-4410.

Grasso, Catherine S.; Giannakis, Marios; Wells, Daniel K.; Hamada, Tsuyoshi; Mu, Xinmeng Jasmine; Quist, Michael et al. (2018): Genetic Mechanisms of Immune Evasion in Colorectal Cancer. In *Cancer discovery* 8 (6), pp. 730–749. DOI: 10.1158/2159-8290.CD-17-1327.

Gregory, Richard I.; Yan, Kai-Ping; Amuthan, Govindasamy; Chendrimada, Thimmaiah; Doratotaj, Behzad; Cooch, Neil; Shiekhattar, Ramin (2004): The Microprocessor complex mediates the genesis of microRNAs. In *Nature* 432 (7014), pp. 235–240. DOI: 10.1038/nature03120.

Ha, Minju; Kim, V. Narry (2014): Regulation of microRNA biogenesis. In *Nature reviews. Molecular cell biology* 15 (8), pp. 509–524. DOI: 10.1038/nrm3838.

Habtemariam, Bahru A.; Karsten, Verena; Attarwala, Husain; Goel, Varun; Melch, Megan; Clausen, Valerie A. et al. (2021): Single-Dose Pharmacokinetics and Pharmacodynamics of Transthyretin Targeting N-acetylgalactosamine-Small Interfering Ribonucleic Acid Conjugate, Vutrisiran, in Healthy Subjects. In *Clinical pharmacology and therapeutics* 109 (2), pp. 372–382. DOI: 10.1002/cpt.1974.

Harjunpää, Heidi; Llort Asens, Marc; Guenther, Carla; Fagerholm, Susanna C. (2019): Cell Adhesion Molecules and Their Roles and Regulation in the Immune and Tumor Microenvironment. In *Frontiers in immunology* 10, p. 1078. DOI: 10.3389/fimmu.2019.01078.

Hastings, Michelle L.; Allemand, Eric; Duelli, Dominik M.; Myers, Michael P.; Krainer, Adrian R. (2007): Control of pre-mRNA splicing by the general splicing factors PUF60 and U2AF(65). In *PloS one* 2 (6), e538. DOI: 10.1371/journal.pone.0000538.

Haydinger, Cameron D.; Ashander, Liam M.; Tan, Alwin Chun Rong; Smith, Justine R. (2023): Intercellular Adhesion Molecule 1: More than a Leukocyte Adhesion Molecule. In *Biology* 12 (5). DOI: 10.3390/biology12050743.

Hegde, Priti S.; Chen, Daniel S. (2020): Top 10 Challenges in Cancer Immunotherapy. In *Immunity* 52 (1), pp. 17–35. DOI: 10.1016/j.immuni.2019.12.011.

Hegde, Priti S.; Karanikas, Vaios; Evers, Stefan (2016): The Where, the When, and the How of Immune Monitoring for Cancer Immunotherapies in the Era of Checkpoint Inhibition. In *Clinical cancer research : an official journal of the American Association for Cancer Research* 22 (8), pp. 1865–1874. DOI: 10.1158/1078-0432.CCR-15-1507.

Hentze, Matthias W.; Castello, Alfredo; Schwarzl, Thomas; Preiss, Thomas (2018): A brave new world of RNA-binding proteins. In *Nature Reviews Molecular Cell Biology* 19 (5), pp. 327–341. DOI: 10.1038/nrm.2017.130.

Herbst, Roy S.; Soria, Jean-Charles; Kowanetz, Marcin; Fine, Gregg D.; Hamid, Omid; Gordon, Michael S. et al. (2014): Predictive correlates of response to the anti-PD-L1 antibody MPDL3280A in cancer patients. In *Nature* 515 (7528), pp. 563–567. DOI: 10.1038/nature14011.

Hiam-Galvez, Kamir J.; Allen, Breanna M.; Spitzer, Matthew H. (2021): Systemic immunity in cancer. In *Nature Reviews Cancer* 21 (6), pp. 345–359. DOI: 10.1038/s41568-021-00347-z.

Hodi, F. Stephen; O'Day, Steven J.; McDermott, David F.; Weber, Robert W.; Sosman, Jeffrey A.; Haanen, John B. et al. (2010): Improved survival with ipilimumab in patients with metastatic melanoma. In *The New England journal of medicine* 363 (8), pp. 711–723. DOI: 10.1056/NEJMoa1003466.

Hopkins, Andrew L.; Groom, Colin R. (2002): The druggable genome. In *Nature reviews. Drug discovery* 1 (9), pp. 727–730. DOI: 10.1038/nrd892.

Hou, J.; Baichwal, V.; Cao, Z. (1994): Regulatory elements and transcription factors controlling basal and cytokine-induced expression of the gene encoding intercellular adhesion molecule 1. In *Proceedings of the National Academy of Sciences of the United States of America* 91 (24), pp. 11641–11645. DOI: 10.1073/pnas.91.24.11641.

Hu, Kaimin; Gu, Yanjun; Lou, Lixia; Liu, Lizhen; Hu, Yongxian; Wang, Binsheng et al. (2015): Galectin-3 mediates bone marrow microenvironment-induced drug resistance in acute leukemia cells via Wnt/β-catenin signaling pathway. In *Journal of Hematology & Oncology* 8, p. 1. DOI: 10.1186/s13045-014-0099-8.

Hubbard, A. K.; Rothlein, R. (2000): Intercellular adhesion molecule-1 (ICAM-1) expression and cell signaling cascades. In *Free radical biology & medicine* 28 (9), pp. 1379–1386. DOI: 10.1016/s0891-5849(00)00223-9.

Humphries, Martin J. (2001): Cell Adhesion Assays. In *MB* 18 (1), pp. 57–62. DOI: 10.1385/MB:18:1:57.

Ihara, Shoichi; Kida, Hiroshi; Arase, Hisashi; Tripathi, Lokesh P.; Chen, Yi-An; Kimura, Tetsuya et al. (2012): Inhibitory roles of signal transducer and activator of transcription 3 in antitumor immunity during carcinogen-induced lung tumorigenesis. In *Cancer research* 72 (12), pp. 2990–2999. DOI: 10.1158/0008-5472.CAN-11-4062.

Ishida, Y.; Agata, Y.; Shibahara, K.; Honjo, T. (1992): Induced expression of PD-1, a novel member of the immunoglobulin gene superfamily, upon programmed cell death. In *The EMBO Journal* 11 (11), pp. 3887–3895. DOI: 10.1002/j.1460-2075.1992.tb05481.x.

Jiménez, David; Roda-Navarro, Pedro; Springer, Timothy A.; Casasnovas, José M. (2005): Contribution of N-linked glycans to the conformation and function of intercellular adhesion molecules (ICAMs). In *The Journal of biological chemistry* 280 (7), pp. 5854–5861. DOI: 10.1074/jbc.M412104200.

Karikó, Katalin; Buckstein, Michael; Ni, Houping; Weissman, Drew (2005): Suppression of RNA Recognition by Toll-like Receptors: The Impact of Nucleoside Modification and the Evolutionary Origin of RNA. In *Immunity* 23 (2), pp. 165–175. DOI: 10.1016/j.immuni.2005.06.008.

Kelly, Terence A.; Jeanfavre, Deborah D.; McNeil, Daniel W.; Woska, Joseph R.; Reilly, Patricia L.; Mainolfi, Elizabeth A. et al. (1999): Cutting Edge: A Small Molecule Antagonist of LFA-1-Mediated Cell Adhesion. In *Journal of immunology (Baltimore, Md. : 1950)* 163 (10), pp. 5173–5177. DOI: 10.4049/jimmunol.163.10.5173.

Khalili, Amelia Ahmad; Ahmad, Mohd Ridzuan (2015): A Review of Cell Adhesion Studies for Biomedical and Biological Applications. In *International journal of molecular sciences* 16 (8), pp. 18149–18184. DOI: 10.3390/ijms160818149.

Khvorova, Anastasia; Watts, Jonathan K. (2017): The chemical evolution of oligonucleotide therapies of clinical utility. In *Nature biotechnology* 35 (3), pp. 238–248. DOI: 10.1038/nbt.3765.

Kinashi, Tatsuo (2005): Intracellular signalling controlling integrin activation in lymphocytes. In *Nature Reviews Immunology* 5, 546 EP -. DOI: 10.1038/nri1646.

Kobayashi, Sohei; Hoshino, Tyuji; Hiwasa, Takaki; Satoh, Mamoru; Rahmutulla, Bahityar; Tsuchida, Sachio et al. (2016): Anti-FIRs (PUF60) auto-antibodies are detected in the sera of

early-stage colon cancer patients. In *Oncotarget* 7 (50), pp. 82493–82503. DOI: 10.18632/oncotarget.12696.

Kohli, Karan; Pillarisetty, Venu G.; Kim, Teresa S. (2021): Key chemokines direct migration of immune cells in solid tumors. In *Cancer gene therapy*. DOI: 10.1038/s41417-021-00303-x.

Kolev, Nikolay G.; Steitz, Joan A. (2005): Symplekin and multiple other polyadenylation factors participate in 3'-end maturation of histone mRNAs. In *Genes & development* 19 (21), pp. 2583–2592. DOI: 10.1101/gad.1371105.

Kortlever, Roderik M.; Sodir, Nicole M.; Wilson, Catherine H.; Burkhart, Deborah L.; Pellegrinet, Luca; Brown Swigart, Lamorna et al. (2017): Myc Cooperates with Ras by Programming Inflammation and Immune Suppression. In *Cell* 171 (6), 1301-1315.e14. DOI: 10.1016/j.cell.2017.11.013.

Kristen, Arnt V.; Ajroud-Driss, Senda; Conceição, Isabel; Gorevic, Peter; Kyriakides, Theodoros; Obici, Laura (2019): Patisiran, an RNAi therapeutic for the treatment of hereditary transthyretin-mediated amyloidosis. In *Neurodegenerative disease management* 9 (1), pp. 5–23. DOI: 10.2217/nmt-2018-0033.

Krummel, M. F.; Allison, J. P. (1995): CD28 and CTLA-4 have opposing effects on the response of T cells to stimulation. In *The Journal of experimental medicine* 182 (2), pp. 459–465. DOI: 10.1084/jem.182.2.459.

Kumar, Sandeep Rp; Markusic, David M.; Biswas, Moanaro; High, Katherine A.; Herzog, Roland W. (2016): Clinical development of gene therapy: results and lessons from recent successes. In *Molecular therapy. Methods & clinical development* 3, p. 16034. DOI: 10.1038/mtm.2016.34.

Kumar, Sunny; Basu, Malini; Ghosh, Pratyasha; Ansari, Aafreen; Ghosh, Mrinal K. (2023): COVID-19: Clinical status of vaccine development to date. In *British journal of clinical pharmacology* 89 (1), pp. 114–149. DOI: 10.1111/bcp.15552.

Kumari, Neeraj; Dwarakanath, B. S.; Das, Asmita; Bhatt, Anant Narayan (2016): Role of interleukin-6 in cancer progression and therapeutic resistance. In *Tumour biology : the journal of the International Society for Oncodevelopmental Biology and Medicine* 37 (9), pp. 11553–11572. DOI: 10.1007/s13277-016-5098-7.

Lam, Jenny K. W.; Chow, Michael Y. T.; Zhang, Yu; Leung, Susan W. S. (2015): siRNA Versus miRNA as Therapeutics for Gene Silencing. In *Molecular Therapy - Nucleic Acids* 4 (9), e252. DOI: 10.1038/mtna.2015.23.

Lee, R. C.; Feinbaum, R. L.; Ambros, V. (1993): The C. elegans heterochronic gene lin-4 encodes small RNAs with antisense complementarity to lin-14. In *Cell* 75 (5), pp. 843–854. DOI: 10.1016/0092-8674(93)90529-y.

Lee, Stanley Chun-Wei; Abdel-Wahab, Omar (2016): Therapeutic targeting of splicing in cancer. In *Nature Medicine* 22 (9), pp. 976–986. DOI: 10.1038/nm.4165.

Lee, Yoontae; Ahn, Chiyoung; Han, Jinju; Choi, Hyounjeong; Kim, Jaekwang; Yim, Jeongbin et al. (2003): The nuclear RNase III Drosha initiates microRNA processing. In *Nature* 425 (6956), pp. 415–419. DOI: 10.1038/nature01957.

Lee, Yoontae; Kim, Minju; Han, Jinju; Yeom, Kyu-Hyun; Lee, Sanghyuk; Baek, Sung Hee; Kim, V. Narry (2004): MicroRNA genes are transcribed by RNA polymerase II. In *The EMBO Journal* 23 (20), pp. 4051–4060. DOI: 10.1038/sj.emboj.7600385.

Ley, Klaus (2014): Arrest chemokines. In *Frontiers in immunology* 5, p. 150. DOI: 10.3389/fimmu.2014.00150.

Ley, Klaus; Laudanna, Carlo; Cybulsky, Myron I.; Nourshargh, Sussan (2007): Getting to the site of inflammation: the leukocyte adhesion cascade updated. In *Nature Reviews Immunology* 7, 678 EP -. DOI: 10.1038/nri2156.

Li, Lifeng; Yang, Li; Cheng, Shiqi; Fan, Zhirui; Shen, Zhibo; Xue, Wenhua et al. (2019a): Lung adenocarcinoma-intrinsic GBE1 signaling inhibits anti-tumor immunity. In *Molecular cancer* 18 (1), p. 108. DOI: 10.1186/s12943-019-1027-x.

Li, Xin; Xiang, Yanwei; Li, Fulun; Yin, Chengqian; Li, Bin; Ke, Xisong (2019b): WNT/β-Catenin Signaling Pathway Regulating T Cell-Inflammation in the Tumor Microenvironment. In *Frontiers in immunology* 10. DOI: 10.3389/fimmu.2019.02293.

Liang, Xue-Hai; Sun, Hong; Nichols, Joshua G.; Crooke, Stanley T. (2017): RNase H1-Dependent Antisense Oligonucleotides Are Robustly Active in Directing RNA Cleavage in Both the Cytoplasm and the Nucleus. In *Molecular Therapy* 25 (9), pp. 2075–2092. DOI: 10.1016/j.ymthe.2017.06.002.

Lim, Kenji Rowel Q.; Maruyama, Rika; Yokota, Toshifumi (2017): Eteplirsen in the treatment of Duchenne muscular dystrophy. In *Drug design, development and therapy* 11, pp. 533–545. DOI: 10.2147/DDDT.S97635.

Linares-Fernández, Sergio; Moreno, Julien; Lambert, Elise; Mercier-Gouy, Perrine; Vachez, Laetitia; Verrier, Bernard; Exposito, Jean-Yves (2021): Combining an optimized mRNA template with a double purification process allows strong expression of in vitro transcribed mRNA. In *Molecular Therapy - Nucleic Acids* 26, pp. 945–956. DOI: 10.1016/j.omtn.2021.10.007.

Liu, Yuan-Tong; Sun, Zhi-Jun (2021): Turning cold tumors into hot tumors by improving T-cell infiltration. In *Theranostics* 11 (11), pp. 5365–5386. DOI: 10.7150/thno.58390.

Lokugamage, Melissa P.; Vanover, Daryll; Beyersdorf, Jared; Hatit, Marine Z. C.; Rotolo, Laura; Echeverri, Elisa Schrader et al. (2021): Optimization of lipid nanoparticles for the delivery of nebulized therapeutic mRNA to the lungs. In *Nature biomedical engineering* 5 (9), pp. 1059–1068. DOI: 10.1038/s41551-021-00786-x.

Long, Qian; An, Xin; Chen, Miao; Wang, Nan; Sui, Silei; Li, Yixin et al. (2020): PUF60/AURKA Axis Contributes to Tumor Progression and Malignant Phenotypes in Bladder Cancer. In *Frontiers in Oncology* 10. Available online at https://www.frontiersin.org/articles/10.3389/fonc.2020.568015.

Luke, Jason J.; Bao, Riyue; Sweis, Randy F.; Spranger, Stefani; Gajewski, Thomas F. (2019): WNT/β-catenin Pathway Activation Correlates with Immune Exclusion across Human Cancers. In *Clinical cancer research : an official journal of the American Association for Cancer Research* 25 (10), pp. 3074–3083. DOI: 10.1158/1078-0432.CCR-18-1942.

Lunde, Bradley M.; Moore, Claire; Varani, Gabriele (2007): RNA-binding proteins: modular design for efficient function. In *Nature Reviews Molecular Cell Biology* 8 (6), pp. 479–490. DOI: 10.1038/nrm2178.

Luo, Bing-Hao; Carman, Christopher V.; Springer, Timothy A. (2007): Structural Basis of Integrin Regulation and Signaling. In *Annual Review of Immunology* 25 (1), pp. 619–647. DOI: 10.1146/annurev.immunol.25.022106.141618.

Lv, Yang; Kim, Kyungho; Sheng, Yue; Cho, Jaehyung; Qian, Zhijian; Zhao, You-Yang et al. (2018): YAP Controls Endothelial Activation and Vascular Inflammation Through TRAF6. In *Circulation Research* 123 (1), pp. 43–56. DOI: 10.1161/CIRCRESAHA.118.313143.

Maishi, Nako; Annan, Dorcas A.; Kikuchi, Hiroshi; Hida, Yasuhiro; Hida, Kyoko (2019): Tumor Endothelial Heterogeneity in Cancer Progression. In *Cancers* 11 (10). DOI: 10.3390/cancers11101511.

Malone, Daniel C.; Dean, Rebecca; Arjunji, Ramesh; Jensen, Ivar; Cyr, Phil; Miller, Beckley et al. (2019): Cost-effectiveness analysis of using onasemnogene abeparvocec (AVXS-101) in spinal muscular atrophy type 1 patients. In *Journal of market access & health policy* 7 (1), p. 1601484. DOI: 10.1080/20016689.2019.1601484.

Mao, Debin; Lü, Shouqin; Zhang, Xiao; Long, Mian (2020): Mechanically Regulated Outside-In Activation of an I-Domain-Containing Integrin. In *Biophysical Journal* 119 (5), pp. 966–977. DOI: 10.1016/j.bpj.2020.07.022.

Mariathasan, Sanjeev; Turley, Shannon J.; Nickles, Dorothee; Castiglioni, Alessandra; Yuen, Kobe; Wang, Yulei et al. (2018): TGFβ attenuates tumour response to PD-L1 blockade by contributing to exclusion of T cells. In *Nature* 554 (7693), pp. 544–548. DOI: 10.1038/nature25501.

Marshall, Bryan T.; Long, Mian; Piper, James W.; Yago, Tadayuki; McEver, Rodger P.; Zhu, Cheng (2003): Direct observation of catch bonds involving cell-adhesion molecules. In *Nature* 423 (6936), pp. 190–193. DOI: 10.1038/nature01605.

Martin, Georges; Gruber, Andreas R.; Keller, Walter; Zavolan, Mihaela (2012): Genome-wide analysis of pre-mRNA 3' end processing reveals a decisive role of human cleavage factor I in the regulation of 3' UTR length. In *Cell reports* 1 (6), pp. 753–763. DOI: 10.1016/j.celrep.2012.05.003.

Martinez, Javier; Patkaniowska, Agnieszka; Urlaub, Henning; Lührmann, Reinhard; Tuschl, Thomas (2002): Single-Stranded Antisense siRNAs Guide Target RNA Cleavage in RNAi. In *Cell* 110 (5), pp. 563–574. DOI: 10.1016/S0092-8674(02)00908-X.

Martins, Filipe; Sofiya, Latifyan; Sykiotis, Gerasimos P.; Lamine, Faiza; Maillard, Michel; Fraga, Montserrat et al. (2019): Adverse effects of immune-checkpoint inhibitors: epidemiology, management and surveillance. In *Nature reviews. Clinical oncology* 16 (9), pp. 563–580. DOI: 10.1038/s41571-019-0218-0.

Masuda, Kiyoshi; Kuwano, Yuki (2018): Diverse roles of RNA-binding proteins in cancer traits and their implications in gastrointestinal cancers. In *Wiley interdisciplinary reviews. RNA*, e1520. DOI: 10.1002/wrna.1520.

Mathew, Veena; Wang, Annabel K. (2019): Inotersen: new promise for the treatment of hereditary transthyretin amyloidosis. In *Drug design, development and therapy* 13, pp. 1515–1525. DOI: 10.2147/DDDT.S162913.

Matia-González, Ana M.; Laing, Emma E.; Gerber, André P. (2015): Conserved mRNA-binding proteomes in eukaryotic organisms. In *Nature Structural & Molecular Biology* 22 (12), pp. 1027–1033. DOI: 10.1038/nsmb.3128.

Mayr, Christine; Bartel, David P. (2009): Widespread shortening of 3'UTRs by alternative cleavage and polyadenylation activates oncogenes in cancer cells. In *Cell* 138 (4), pp. 673–684. DOI: 10.1016/j.cell.2009.06.016.

Medzhitov, Ruslan (2008): Origin and physiological roles of inflammation. In *Nature* 454 (7203), pp. 428–435. DOI: 10.1038/nature07201.

Meister, Gunter; Landthaler, Markus; Patkaniowska, Agnieszka; Dorsett, Yair; Teng, Grace; Tuschl, Thomas (2004): Human Argonaute2 mediates RNA cleavage targeted by miRNAs and siRNAs. In *Molecular cell* 15 (2), pp. 185–197. DOI: 10.1016/j.molcel.2004.07.007.

Meister, Gunter; Landthaler, Markus; Peters, Lasse; Chen, Po Yu; Urlaub, Henning; Lührmann, Reinhard; Tuschl, Thomas (2005): Identification of novel argonaute-associated proteins. In *Current biology : CB* 15 (23), pp. 2149–2155. DOI: 10.1016/j.cub.2005.10.048.

Meister, Gunter; Tuschl, Thomas (2004): Mechanisms of gene silencing by double-stranded RNA. In *Nature* 431 (7006), pp. 343–349. DOI: 10.1038/nature02873.

Mellman, Ira; Coukos, George; Dranoff, Glenn (2011): Cancer immunotherapy comes of age. In *Nature* 480 (7378), pp. 480–489. DOI: 10.1038/nature10673.

Mittendorf, Elizabeth A.; Philips, Anne V.; Meric-Bernstam, Funda; Qiao, Na; Wu, Yun; Harrington, Susan et al. (2014): PD-L1 expression in triple-negative breast cancer. In *Cancer immunology research* 2 (4), pp. 361–370. DOI: 10.1158/2326-6066.CIR-13-0127.

Mohibi, Shakur; Chen, Xinbin; Zhang, Jin (2019): Cancer the'RBP'eutics–RNA-binding proteins as therapeutic targets for cancer. In *Pharmacology & Therapeutics* 203, p. 107390. DOI: 10.1016/j.pharmthera.2019.07.001.

Morgens, David W.; Deans, Richard M.; Li, Amy; Bassik, Michael C. (2016): Systematic comparison of CRISPR/Cas9 and RNAi screens for essential genes. In *Nature biotechnology* 34 (6), pp. 634–636. DOI: 10.1038/nbt.3567.

Morigi, M.; Zoja, C.; Figliuzzi, M.; Foppolo, M.; Micheletti, G.; Bontempelli, M. et al. (1995): Fluid shear stress modulates surface expression of adhesion molecules by endothelial cells. In *Blood* 85 (7), pp. 1696–1703.

Motz, Greg T.; Coukos, George (2013): Deciphering and reversing tumor immune suppression. In *Immunity* 39 (1), pp. 61–73. DOI: 10.1016/j.immuni.2013.07.005.

Mould, A. Paul (2011): Analyzing integrin-dependent adhesion. In *Current protocols in cell biology* Chapter 9, Unit 9.4. DOI: 10.1002/0471143030.cb0904s53.

Mulhbacher, Jérôme; St-Pierre, Patrick; Lafontaine, Daniel A. (2010): Therapeutic applications of ribozymes and riboswitches. In *Current opinion in pharmacology* 10 (5), pp. 551–556. DOI: 10.1016/j.coph.2010.07.002.

Mullard, Asher (2020): 2019 FDA drug approvals. In *Nature Reviews Drug Discovery* 19 (2), pp. 79–84. DOI: 10.1038/d41573-020-00001-7.

Müller-McNicoll, Michaela; Neugebauer, Karla M. (2013): How cells get the message: dynamic assembly and function of mRNA–protein complexes. In *Nature Reviews Genetics* 14 (4), pp. 275–287. DOI: 10.1038/nrg3434.

Nagl, Laurenz; Horvath, Lena; Pircher, Andreas; Wolf, Dominik (2020): Tumor Endothelial Cells (TECs) as Potential Immune Directors of the Tumor Microenvironment - New Findings and Future Perspectives. In *Frontiers in cell and developmental biology* 8, p. 766. DOI: 10.3389/fcell.2020.00766.

Neelamraju, Yaseswini; Gonzalez-Perez, Abel; Bhat-Nakshatri, Poornima; Nakshatri, Harikrishna; Janga, Sarath Chandra (2018): Mutational landscape of RNA-binding proteins in human cancers. In *RNA biology* 15 (1), pp. 115–129. DOI: 10.1080/15476286.2017.1391436.

Neil, Erin E.; Bisaccia, Elizabeth K. (2019): Nusinersen: A Novel Antisense Oligonucleotide for the Treatment of Spinal Muscular Atrophy. In *The journal of pediatric pharmacology and therapeutics : JPPT : the official journal of PPAG* 24 (3), pp. 194–203. DOI: 10.5863/1551-6776-24.3.194.

Neri, Tommaso; Scalise, Valentina; Passalacqua, Ilaria; Giusti, Ilaria; Lombardi, Stefania; Balia, Cristina et al. (2018): CD18-mediated adhesion is required for the induction of a proinflammatory phenotype in lung epithelial cells by mononuclear cell-derived extracellular vesicles. In *Experimental cell research* 365 (1), pp. 78–84. DOI: 10.1016/j.yexcr.2018.02.023.

Nishida, Noritaka; Xie, Can; Shimaoka, Motomu; Cheng, Yifan; Walz, Thomas; Springer, Timothy A. (2006): Activation of Leukocyte β2 Integrins by Conversion from Bent to Extended Conformations. In *Immunity* 25 (4), pp. 583–594. DOI: 10.1016/j.immuni.2006.07.016.

Nourshargh, Sussan; ALON, RONEN (2014): Leukocyte migration into inflamed tissues. In *Immunity* 41 (5), pp. 694–707. DOI: 10.1016/j.immuni.2014.10.008.

Ogawa, Hitoshi; Binion, David G.; Heidemann, Jan; Theriot, Monica; Fisher, Pamela J.; Johnson, Nathan A. et al. (2005): Mechanisms of MAdCAM-1 gene expression in human intestinal microvascular endothelial cells. In *American journal of physiology. Cell physiology* 288 (2), C272-81. DOI: 10.1152/ajpcell.00406.2003.

Oiseth, Stanley J.; Aziz, Mohamed S. (2017): Cancer immunotherapy: a brief review of the history, possibilities, and challenges ahead. In *JCMT* 3 (10), p. 250. DOI: 10.20517/2394-4722.2017.41.

Osborn, L.; Vassallo, C.; Benjamin, C. D. (1992): Activated endothelium binds lymphocytes through a novel binding site in the alternately spliced domain of vascular cell adhesion molecule-1. In *The Journal of experimental medicine* 176 (1), pp. 99–107. DOI: 10.1084/jem.176.1.99.

Page-McCaw, P. S.; Amonlirdviman, K.; Sharp, P. A. (1999): PUF60: a novel U2AF65-related splicing activity. In *RNA (New York, N.Y.)* 5 (12), pp. 1548–1560. DOI: 10.1017/s1355838299991938.

Paik, Julia; Duggan, Sean (2019): Volanesorsen: First Global Approval. In *Drugs* 79 (12), pp. 1349–1354. DOI: 10.1007/s40265-019-01168-z.

Parisi, Silvia; Castaldo, Daniela; Piscitelli, Silvia; D'Ambrosio, Chiara; Divisato, Giuseppina; Passaro, Fabiana et al. (2021): Identification of RNA-binding proteins that partner with Lin28a to regulate Dnmt3a expression. In *Scientific reports* 11 (1), p. 2345. DOI: 10.1038/s41598-021-81429-8.

Paunovska, Kalina; Sago, Cory D.; Monaco, Christopher M.; Hudson, William H.; Castro, Marielena Gamboa; Rudoltz, Tobi G. et al. (2018): A Direct Comparison of in Vitro and in Vivo Nucleic Acid Delivery Mediated by Hundreds of Nanoparticles Reveals a Weak Correlation. In *Nano letters* 18 (3), pp. 2148–2157. DOI: 10.1021/acs.nanolett.8b00432.

Pereira, Bruno; Billaud, Marc; Almeida, Raquel (2017): RNA-Binding Proteins in Cancer: Old Players and New Actors. In *Trends in cancer* 3 (7), pp. 506–528. DOI: 10.1016/j.trecan.2017.05.003.

Pettinato, Mark C. (2021): Introduction to Antibody-Drug Conjugates. In *Antibodies (Basel, Switzerland)* 10 (4). DOI: 10.3390/antib10040042.

Pio, Ruben; Ajona, Daniel; Ortiz-Espinosa, Sergio; Mantovani, Alberto; Lambris, John D. (2019): Complementing the Cancer-Immunity Cycle. In *Frontiers in immunology* 10, p. 774. DOI: 10.3389/fimmu.2019.00774.

Pober, Jordan S.; Sessa, William C. (2007): Evolving functions of endothelial cells in inflammation. In *Nature reviews. Immunology* 7 (10), pp. 803–815. DOI: 10.1038/nri2171.

Qin, Shuang; Xu, Linping; Yi, Ming; Yu, Shengnan; Wu, Kongming; Luo, Suxia (2019): Novel immune checkpoint targets: moving beyond PD-1 and CTLA-4. In *Molecular cancer* 18 (1), p. 155. DOI: 10.1186/s12943-019-1091-2.

Qin, Shugang; Tang, Xiaoshan; Chen, Yuting; Chen, Kepan; Fan, Na; Xiao, Wen et al. (2022): mRNA-based therapeutics: powerful and versatile tools to combat diseases. In *Signal transduction and targeted therapy* 7 (1), p. 166. DOI: 10.1038/s41392-022-01007-w.

Ray, Debashish; Kazan, Hilal; Cook, Kate B.; Weirauch, Matthew T.; Najafabadi, Hamed S.; Li, Xiao et al. (2013): A compendium of RNA-binding motifs for decoding gene regulation. In *Nature* 499 (7457), pp. 172–177. DOI: 10.1038/nature12311.

Rehwinkel, Jan; Behm-Ansmant, Isabelle; Gatfield, David; Izaurralde, Elisa (2005): A crucial role for GW182 and the DCP1:DCP2 decapping complex in miRNA-mediated gene silencing. In *RNA (New York, N.Y.)* 11 (11), pp. 1640–1647. DOI: 10.1261/rna.2191905.

Ribas, Antoni; Wolchok, Jedd D. (2018): Cancer immunotherapy using checkpoint blockade. In *Science (New York, N.Y.)* 359 (6382), pp. 1350–1355. DOI: 10.1126/science.aar4060.

Rose, David M.; Liu, Shouchun; Woodside, Darren G.; Han, Jaewon; Schlaepfer, David D.; Ginsberg, Mark H. (2003): Paxillin binding to the alpha 4 integrin subunit stimulates LFA-1 (integrin alpha L beta 2)-dependent T cell migration by augmenting the activation of focal adhesion kinase/proline-rich tyrosine kinase-2. In *Journal of immunology (Baltimore, Md. : 1950)* 170 (12), pp. 5912–5918. DOI: 10.4049/jimmunol.170.12.5912.

Sahin, Ugur; Karikó, Katalin; Türeci, Özlem (2014): mRNA-based therapeutics — developing a new class of drugs. In *Nature Reviews Drug Discovery* 13 (10), pp. 759–780. DOI: 10.1038/nrd4278.

Schenkel, Alan R.; Mamdouh, Zahra; Chen, Xia; Liebman, Ronald M.; Muller, William A. (2002): CD99 plays a major role in the migration of monocytes through endothelial junctions. In *Nature immunology* 3 (2), pp. 143–150. DOI: 10.1038/ni749.

Schlesinger, Martin; Bendas, Gerd (2015): Vascular cell adhesion molecule-1 (VCAM-1)--an increasing insight into its role in tumorigenicity and metastasis. In *International journal of cancer* 136 (11), pp. 2504–2514. DOI: 10.1002/ijc.28927.

Scott, David W.; Patel, Rakesh P. (2013): Endothelial heterogeneity and adhesion molecules N-glycosylation: implications in leukocyte trafficking in inflammation. In *Glycobiology* 23 (6), pp. 622–633. DOI: 10.1093/glycob/cwt014.

Severino, Valeria; Farina, Annarita; Chambery, Angela (2013): Analysis of secreted proteins. In *Methods in molecular biology (Clifton, N.J.)* 1002, pp. 37–60. DOI: 10.1007/978-1-62703-360-2_4.

Shi, Tao; Ma, Yanyu; Yu, Lingfeng; Jiang, Jiaxuan; Shen, Sunan; Hou, Yayi; Wang, Tingting (2018): Cancer Immunotherapy: A Focus on the Regulation of Immune Checkpoints. In *International journal of molecular sciences* 19 (5). DOI: 10.3390/ijms19051389.

Shimaoka, Motomu; Xiao, Tsan; Liu, Jin-Huan; Yang, Yuting; Dong, Yicheng; Jun, Chang-Duk et al. (2003): Structures of the alpha L I domain and its complex with ICAM-1 reveal a shape-shifting pathway for integrin regulation. In *Cell* 112 (1), pp. 99–111.

Shimonaka, Mika; Katagiri, Koko; Nakayama, Toshinori; Fujita, Naoya; Tsuruo, Takashi; Yoshie, Osamu; Kinashi, Tatsuo (2003): Rap1 translates chemokine signals to integrin activation, cell polarization, and motility across vascular endothelium under flow. In *The Journal of Cell Biology* 161 (2), pp. 417–427. DOI: 10.1083/jcb.200301133.

Shin, Hojeong; Park, Se-Jin; Yim, Yeajee; Kim, Jungho; Choi, Chulwon; Won, Cheolhee; Min, Dal-Hee (2018): Recent Advances in RNA Therapeutics and RNA Delivery Systems Based on Nanoparticles. In *Adv. Therap.* 1 (7), p. 1800065. DOI: 10.1002/adtp.201800065.

Smith, Ellen S.; Whitty, Eric; Yoo, Byunghee; Moore, Anna; Sempere, Lorenzo F.; Medarova, Zdravka (2022): Clinical Applications of Short Non-Coding RNA-Based Therapies in the Era of Precision Medicine. In *Cancers* 14 (6). DOI: 10.3390/cancers14061588.

Smyth, Mark J.; Teng, Michele Wl (2018): 2018 Nobel Prize in physiology or medicine. In *Clinical & translational immunology* 7 (10), e1041. DOI: 10.1002/cti2.1041.

Spranger, Stefani; Bao, Riyue; Gajewski, Thomas F. (2015): Melanoma-intrinsic β-catenin signalling prevents anti-tumour immunity. In *Nature* 523 (7559), pp. 231–235. DOI: 10.1038/nature14404.

Spranger, Stefani; Gajewski, Thomas F. (2016): Tumor-intrinsic oncogene pathways mediating immune avoidance. In *Oncoimmunology* 5 (3), e1086862. DOI: 10.1080/2162402X.2015.1086862.

Spranger, Stefani; Gajewski, Thomas F. (2018): Impact of oncogenic pathways on evasion of antitumour immune responses. In *Nature reviews. Cancer*, pp. 139–147. DOI: 10.1038/nrc.2017.117.

Staunton, D. E.; Dustin, M. L.; Erickson, H. P.; Springer, T. A. (1990): The arrangement of the immunoglobulin-like domains of ICAM-1 and the binding sites for LFA-1 and rhinovirus. In *Cell* 61 (2), pp. 243–254. DOI: 10.1016/0092-8674(90)90805-o.

Staunton, D. E.; Marlin, S. D.; Stratowa, C.; Dustin, M. L.; Springer, T. A. (1988): Primary structure of ICAM-1 demonstrates interaction between members of the immunoglobulin and integrin supergene families. In *Cell* 52 (6), pp. 925–933. DOI: 10.1016/0092-8674(88)90434-5.

Stephenson, M. L.; Zamecnik, P. C. (1978): Inhibition of Rous sarcoma viral RNA translation by a specific oligodeoxyribonucleotide. In *Proceedings of the National Academy of Sciences of the United States of America* 75 (1), pp. 285–288. DOI: 10.1073/pnas.75.1.285.

Strazza, Marianne; Azoulay-Alfaguter, Inbar; Pedoeem, Ariel; Mor, Adam (2014): Static adhesion assay for the study of integrin activation in T lymphocytes. In *Journal of visualized experiments : JoVE* (88). DOI: 10.3791/51646.

Strazza, Marianne; Azoulay-Alfaguter, Inbar; Peled, Michael; Mor, Adam (2016): Assay of Adhesion Under Shear Stress for the Study of T Lymphocyte-Adhesion Molecule Interactions. In *Journal of visualized experiments : JoVE* (112). DOI: 10.3791/54203.

Syed, Yahiya Y. (2021): Givosiran: A Review in Acute Hepatic Porphyria. In *Drugs* 81 (7), pp. 841–848. DOI: 10.1007/s40265-021-01511-3.

Tan, Evan; Chin, Cara Sze Hui; Lim, Zhi Feng Sherman; Ng, Say Kong (2021): HEK293 Cell Line as a Platform to Produce Recombinant Proteins and Viral Vectors. In *Frontiers in bioengineering and biotechnology* 9, p. 796991. DOI: 10.3389/fbioe.2021.796991.

Tan, Kemin; Casasnovas, Jose M.; Liu, Jin-Huan; Briskin, Michael J.; Springer, Timothy A.; Wang, Jia-Huai (1998): The structure of immunoglobulin superfamily domains 1 and 2 of MAdCAM-1 reveals novel features important for integrin recognition. In *Structure* 6 (6), pp. 793–801. DOI: 10.1016/S0969-2126(98)00080-X.

Tang, Wei; Dodge, Michael; Gundapaneni, Deepika; Michnoff, Carolyn; Roth, Michael; Lum, Lawrence (2008): A genome-wide RNAi screen for Wnt/beta-catenin pathway components identifies unexpected roles for TCF transcription factors in cancer. In *Proceedings of the National Academy of Sciences of the United States of America* 105 (28), pp. 9697–9702. DOI: 10.1073/pnas.0804709105.

Theivendran, Shevanuja; Tang, Jie; Lei, Chang; Yang, Yannan; Song, Hao; Gu, Zhengying et al. (2020): Post translational modification-assisted cancer immunotherapy for effective breast cancer treatment. In *Chemical science* 11 (38), pp. 10421–10430. DOI: 10.1039/d0sc02803g.

Thelen, Marcus (2001): Dancing to the tune of chemokines. In *Nature immunology* 2 (2), pp. 129–134. DOI: 10.1038/84224.

Thiele, Andrea; Nagamine, Yoshikuni; Hauschildt, Sunna; Clevers, Hans (2006): AU-rich elements and alternative splicing in the β-catenin 3′UTR can influence the human β-catenin mRNA stability. In *Experimental cell research* 312 (12), pp. 2367–2378. DOI: 10.1016/j.yexcr.2006.03.029.

Traber, Gavin M.; Yu, Ai-Ming (2023): RNAi-Based Therapeutics and Novel RNA Bioengineering Technologies. In *The Journal of pharmacology and experimental therapeutics* 384 (1), pp. 133–154. DOI: 10.1124/jpet.122.001234.

Treiber, Thomas; Treiber, Nora; Meister, Gunter (2019): Regulation of microRNA biogenesis and its crosstalk with other cellular pathways. In *Nature reviews. Molecular cell biology* 20 (1), pp. 5–20. DOI: 10.1038/s41580-018-0059-1.

Uhlén, Mathias; Fagerberg, Linn; Hallström, Björn M.; Lindskog, Cecilia; Oksvold, Per; Mardinoglu, Adil et al. (2015): Proteomics. Tissue-based map of the human proteome. In *Science (New York, N.Y.)* 347 (6220), p. 1260419. DOI: 10.1126/science.1260419.

van Buul, Jaap D.; Kanters, Edwin; Hordijk, Peter L. (2007): Endothelial signaling by Ig-like cell adhesion molecules. In *Arteriosclerosis, thrombosis, and vascular biology* 27 (9), pp. 1870–1876. DOI: 10.1161/ATVBAHA.107.145821.

van Nostrand, Eric L.; Freese, Peter; Pratt, Gabriel A.; Wang, Xiaofeng; Wei, Xintao; Xiao, Rui et al. (2020): A large-scale binding and functional map of human RNA-binding proteins. In *Nature* 583 (7818), pp. 711–719. DOI: 10.1038/s41586-020-2077-3.

van Rooij, Eva; Purcell, Angela L.; Levin, Arthur A. (2012): Developing microRNA therapeutics. In *Circulation Research* 110 (3), pp. 496–507. DOI: 10.1161/CIRCRESAHA.111.247916.

Vestweber, Dietmar (2015): How leukocytes cross the vascular endothelium. In *Nature Reviews Immunology* 15, 692 EP -. DOI: 10.1038/nri3908.

Walling, Brandon L.; Kim, Minsoo (2018): LFA-1 in T Cell Migration and Differentiation. In *Frontiers in immunology* 9, p. 952. DOI: 10.3389/fimmu.2018.00952.

Wang, Tianhong; Niu, Guilian; Kortylewski, Marcin; Burdelya, Lyudmila; Shain, Kenneth; Zhang, Shumin et al. (2004): Regulation of the innate and adaptive immune responses by Stat-3 signaling in tumor cells. In *Nature Medicine* 10 (1), pp. 48–54. DOI: 10.1038/nm976.

Wei, Chen; Ma, Yichao; Wang, Fei; Liao, Yiqun; Chen, Yuji; Zhao, Bin et al. (2022): Igniting Hope for Tumor Immunotherapy: Promoting the "Hot and Cold" Tumor Transition. In *Clinical Medicine Insights. Oncology* 16, 11795549221120708. DOI: 10.1177/11795549221120708.

Weitz-Schmidt, Gabriele; Chreng, Stéphanie (2012): Cell adhesion assays. In *Methods in molecular biology (Clifton, N.J.)* 757, pp. 15–30. DOI: 10.1007/978-1-61779-166-6_2.

Wen, Lai; Lyu, Qingkang; Ley, Klaus; Goult, Benjamin T. (2022): Structural Basis of β2 Integrin Inside-Out Activation. In *Cells* 11 (19). DOI: 10.3390/cells11193039.

Weng, Yejing; Sui, Zhigang; Shan, Yichu; Jiang, Hao; Zhou, Yuan; Zhu, Xudong et al. (2016): In-Depth Proteomic Quantification of Cell Secretome in Serum-Containing Conditioned Medium. In *Analytical chemistry* 88 (9), pp. 4971–4978. DOI: 10.1021/acs.analchem.6b00910.

Wu, Tongbin; Fu, Xiang-Dong (2015): Genomic functions of U2AF in constitutive and regulated splicing. In *RNA biology* 12 (5), pp. 479–485. DOI: 10.1080/15476286.2015.1020272.

Wu, Yuze; Yi, Ming; Zhu, Shuangli; Wang, Haiyong; Wu, Kongming (2021): Recent advances and challenges of bispecific antibodies in solid tumors. In *Experimental hematology & oncology* 10 (1), p. 56. DOI: 10.1186/s40164-021-00250-1.

Xu, Chunxiao; Fillmore, Christine M.; Koyama, Shohei; Wu, Hongbo; Zhao, Yanqiu; Chen, Zhao et al. (2014): Loss of Lkb1 and Pten leads to lung squamous cell carcinoma with elevated PD-L1 expression. In *Cancer cell* 25 (5), pp. 590–604. DOI: 10.1016/j.ccr.2014.03.033.

Xu, Nan; Ren, Yunpeng; Bao, Yufang; Shen, Xianfeng; Kang, Jiahui; Wang, Ning et al. (2023): PUF60 promotes cell cycle and lung cancer progression by regulating alternative splicing of CDC25C. In *Cell reports* 42 (9), p. 113041. DOI: 10.1016/j.celrep.2023.113041.

Xue, Junli; Yu, Xuetao; Xue, Liqiong; Ge, Xiaoxiao; Zhao, Wei; Peng, Wei (2019): Intrinsic β-catenin signaling suppresses CD8+ T-cell infiltration in colorectal cancer. In *Biomedicine & Pharmacotherapy* 115, p. 108921. DOI: 10.1016/j.biopha.2019.108921.

Yang, Jinbo; Liao, Xudong; Agarwal, Mukesh K.; Barnes, Laura; Auron, Philip E.; Stark, George R. (2007): Unphosphorylated STAT3 accumulates in response to IL-6 and activates transcription by binding to NFkappaB. In *Genes & development* 21 (11), pp. 1396–1408. DOI: 10.1101/gad.1553707.

Yang, Li; Li, Aitian; Lei, Qingyang; Zhang, Yi (2019): Tumor-intrinsic signaling pathways: key roles in the regulation of the immunosuppressive tumor microenvironment. In *Journal of Hematology & Oncology* 12 (1), p. 125. DOI: 10.1186/s13045-019-0804-8.

Yang, Yuting; Jun, Chang-Duk; Liu, Jin-Huan; Zhang, Rongguang; Joachimiak, Andrzej; Springer, Timothy A.; Wang, Jia-Huai (2004): Structural basis for dimerization of ICAM-1 on the cell surface. In *Molecular cell* 14 (2), pp. 269–276.

Yi, Ming; Jiao, Dechao; Xu, Hanxiao; Liu, Qian; Zhao, Weiheng; Han, Xinwei; Wu, Kongming (2018): Biomarkers for predicting efficacy of PD-1/PD-L1 inhibitors. In *Molecular cancer* 17 (1), p. 129. DOI: 10.1186/s12943-018-0864-3.

Yu, Hua; Pardoll, Drew; Jove, Richard (2009): STATs in cancer inflammation and immunity: a leading role for STAT3. In *Nature Reviews Cancer* 9 (11), pp. 798–809. DOI: 10.1038/nrc2734.

Zhang, Tao; Ma, Chao; Zhang, Zhiqiang; Zhang, Huiyuan; Hu, Hongbo (2021): NF-κB signaling in inflammation and cancer. In *MedComm* 2 (4), pp. 618–653. DOI: 10.1002/mco2.104.

Zhao, Jonathan; Li, Xingyao; Guo, Mingxiong; Yu, Jindan; Yan, Chunhong (2016): The common stress responsive transcription factor ATF3 binds genomic sites enriched with p300 and H3K27ac for transcriptional regulation. In *BMC genomics* 17, p. 335. DOI: 10.1186/s12864-016-2664-8.

Zhou, Zhongguo; Tao, Can; Li, Jianting; Tang, Johnny Cheuk-On; Chan, Albert Sun-Chi; Zhou, Yuanyuan (2022): Chimeric antigen receptor T cells applied to solid tumors. In *Frontiers in immunology* 13, p. 984864. DOI: 10.3389/fimmu.2022.984864.

8 Acknowledgments

First and foremost, I want to thank Gunter Meister for giving me the opportunity to do my PhD in his lab. Thank you for experimental freedom, enthusiasm and ideas to get the project going. Thank you for the trust and support to work on this completely new (and challenging) project outside of our RNA comfort zone. I am grateful for working in your lab and giving me the chance to learn a lot during my time here.

Secondly, I want to thank Michael Hannus from siTOOLs Biotech GmbH, starting from providing us with the siPOOL library up to great discussions, ideas and support during my PhD. Without your help and enthusiasm, the project wouldn't be at the point, which we reached until now.

Of course, I also want to thank Reinhard Sterner, Gunhild Sommer, Stephan Schneuwly and Remco Sprangers for being part of my thesis examination committee.

I also want to thank my collaboration partner and mentor Jörg Wischhusen for the constant support during my PhD and for his immunologic expertise. Our discussions were always inspiring and motivating. Additionally, a big thank you goes to the members of the lab Birgitt Fischer, Beatrice Haack, Florian Wedekink and Vincent Tiehmann for all the help and nice collaboration.

Moreover, I want to thank the RNA family at Biochemistry I. Our three angels Sigrun Ammon, Corinna Friederich and Birgit Clemens. Without you the lab wouldn't be working and we all would be lost. Thanks to our engineers Robert Hett, Gerhard Lehmann and Norbert Eichner, making instruments and computers work again with their magic hands and answering tons of questions while always staying patient. A special thank you goes to all my PhD colleagues, the Biochemistry Lovers & Partybeasts. Working here with you was beautiful amaaaazing. I am deeply thankful for the tremendous support and the help through difficult times. Thank you for great discussions but also with gossiping, beer hours, parties and events outside the lab! Magnificent friendships were started and will last!

A big big thank you goes also to my friends. First of all, my biochemicker and friends Tommy, Domi, Georg, Simon, Julia and Kevin for all the support, fun at cooking and movie nights, BBW sessions, boardgame events and so much more. Secondly, my Pfignstnaaa gang Sandra, Stephie, Basti, Naddl, Markus, Maki, Lichde, Mina, Chiara and

Martin who always were there for me even when I wasn't there that much. Thank you for always having my back and many amazing trips, adventures and Charly nights! Lastly, I want to say thank you to also our Naxler gang and the Krisenrat Jojo, Bina, Kevin, Rich and Franzbert for great holidays, gossiping, pöbeln, complaining about whatsoever and having fun.

Last but not least, I want to thank my family. Without you all, I wouldn't have been able to do and finish my PhD. I am deeply grateful for all your support and help. Thank you for caring for me, calming me down and motivating me even when times were difficult. I love you!